

In-situ control of the morphology of multiphase latex/clay nanocomposites

Citation for published version (APA):

Mballa Mballa, M. A. (2012). *In-situ control of the morphology of multiphase latex/clay nanocomposites*. [Phd Thesis 1 (Research TU/e / Graduation TU/e), Chemical Engineering and Chemistry]. Technische Universiteit Eindhoven. <https://doi.org/10.6100/IR731231>

DOI:

[10.6100/IR731231](https://doi.org/10.6100/IR731231)

Document status and date:

Published: 01/01/2012

Document Version:

Publisher's PDF, also known as Version of Record (includes final page, issue and volume numbers)

Please check the document version of this publication:

- A submitted manuscript is the version of the article upon submission and before peer-review. There can be important differences between the submitted version and the official published version of record. People interested in the research are advised to contact the author for the final version of the publication, or visit the DOI to the publisher's website.
- The final author version and the galley proof are versions of the publication after peer review.
- The final published version features the final layout of the paper including the volume, issue and page numbers.

[Link to publication](#)

General rights

Copyright and moral rights for the publications made accessible in the public portal are retained by the authors and/or other copyright owners and it is a condition of accessing publications that users recognise and abide by the legal requirements associated with these rights.

- Users may download and print one copy of any publication from the public portal for the purpose of private study or research.
- You may not further distribute the material or use it for any profit-making activity or commercial gain
- You may freely distribute the URL identifying the publication in the public portal.

If the publication is distributed under the terms of Article 25fa of the Dutch Copyright Act, indicated by the "Taverne" license above, please follow below link for the End User Agreement:

www.tue.nl/taverne

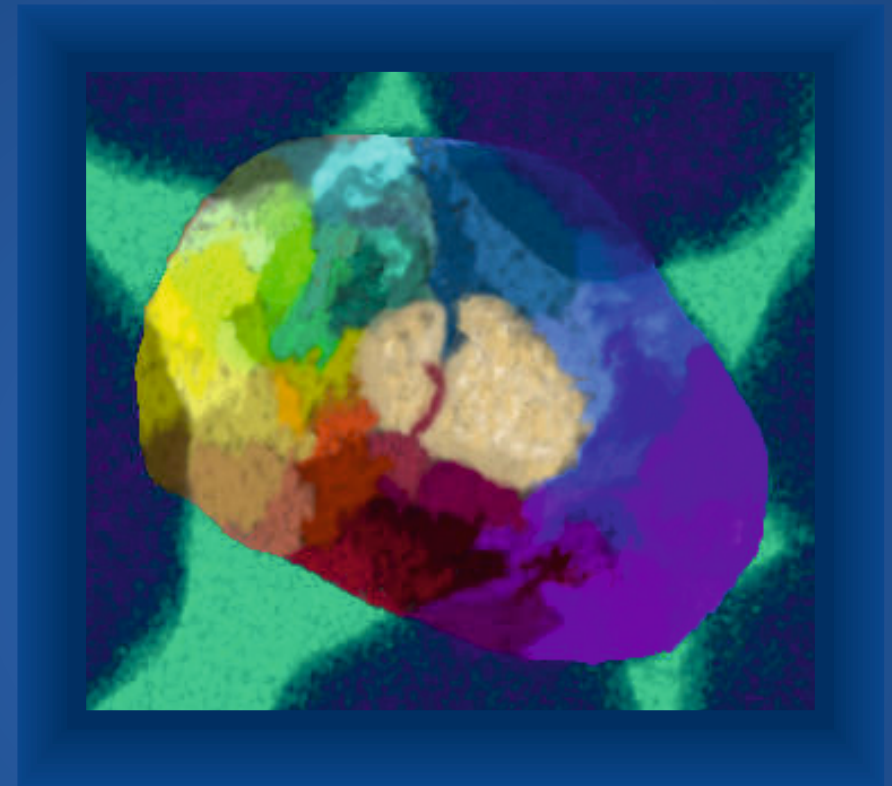
Take down policy

If you believe that this document breaches copyright please contact us at:

openaccess@tue.nl

providing details and we will investigate your claim.

In-situ control of the morphology of multiphase latex/clay nanocomposites



Monique Alexina Mballa Mballa

In-situ control of the morphology of multiphase latex/clay nanocomposites

In-situ Control of the Morphology
of Multiphase Latex/Clay Nanocomposites

Monique Alexina Mballa Mballa

A catalog record is available from the Eindhoven University of Technology Library
ISBN: 978-90-386-3125-7

© 2012, M.A. Mballa Mballa

The research described in this thesis forms part of the research program of the Dutch Polymer Institute(DPI, P.O. Box 902, 5600 MB, Eindhoven, the Netherlands), Technology Area High-throughput Experimentation, DPI project # 621)

Subject headings: latex/clay nanocomposite, control of particle morphology, low-cost low-resolution Raman spectroscopy, high-throughput experimentation

Cover design: Jacques Cuijpers, azoe-art.nl

Printed at Multicopy The Communication Company, Venray

In-situ Control of the Morphology of Multiphase Latex/Clay Nanocomposites

PROEFSCHRIFT

ter verkrijging van de graad van doctor aan de
Technische Universiteit Eindhoven, op gezag van de
rector magnificus, prof.dr.ir. C.J. van Duijn, voor een
commissie aangewezen door het College voor
Promoties in het openbaar te verdedigen
op dinsdag 24 april 2012 om 16.00 uur

door

Monique Alexina Mballa Mballa

geboren te Parijs, Frankrijk

Dit proefschrift is goedgekeurd door de promotor:

prof. dr. A.M. van Herk

Copromotor:

dr. ir. J.P.A. Heuts

“ In whom are hid all the treasures of wisdom and knowledge”

A verse from the Bible, Col 2: 3

Contents

Chapter 1	11
Introduction	
1.1 General introduction	12
1.2 Aims of the study	14
1.3 Outline of the thesis	15
References	17
Chapter 2	19
Theoretical Background	
2.1 Free-radical (co)polymerization	20
2.1.1 Homopolymerization	20
2.1.2 Copolymerization	22
2.2 Emulsion polymerization	23
2.3 Control of particle morphology	24
2.4 Principles of clay encapsulation through emulsion polymerization	28
2.4.1 The structure and physical aspects of montmorillonite	28
2.4.2 General principles of encapsulation	30
2.5 Morphology control of latex/clay nanocomposites	31
References	33
Chapter 3	38
Morphology Control of Two-Phase Latex/Clay Nanocomposites	
3.1 Introduction	39
3.2 Experimental	42
3.2.1 Chemicals	42
3.2.2 Organic modification of MMT	43
3.2.3 Dialysis treatment	43
3.2.4 Emulsion (co)polymerization in the presence of clay	44

Contents

3.2.5 Systematic study of the effects of clay loading, surfactant concentration and surfactant type on clay/polymer interaction.....	45
3.2.6 Characterization	46
3.3 Stability of the organoclays towards hydrolysis	48
3.3.1 Surface modification of the clay.....	48
3.3.2 Amphiphilic character of the organoclay.....	54
3.3.3 Hydrolytic stability	55
3.4 Effect of experimental parameters on the LCN morphology.....	58
3.4.1 Effect of the organic modification.....	58
3.4.2 Effect of monomer feed composition.....	61
3.4.3 Effect of process type	64
3.4.4 Mechanism of the clay encapsulation.....	66
3.4.5 Effect of surfactant type, surfactant concentration and clay loading on the clay/polymer interaction of the synthesized LCN	68
3.5 Orientation of the clay platelets in the LCN films.....	71
3.6 Concluding remarks.....	72
References	74
Chapter 4	78
The Morphology of Three-Phase PS/PMMA/MMT Clay/Latex Particles	
4.1 Introduction	79
4.2 Experimental.....	80
4.2.1 Chemicals.....	80
4.2.2 Preparation of the seed polymers.....	80
4.2.3 Second stage polymerization of styrene.....	83
4.2.4 Characteristics	85
4.3 Case study 1: semi-batch addition of styrene, large seed.....	85
4.4 Case study 2: semi-batch addition of styrene, small seed	89
4.5 Case study 3: batch addition of styrene, large seed	91
4.6 Case study 4: batch addition of styrene, small seed.....	92
4.7 Concluding remarks.....	93
References	95

Contents

Chapter 5	96
The Potential of High-Throughput Experimentation and Raman Spectroscopy for The On-line Monitoring of Emulsion (Co)polymerizations	
5.1 Introduction.....	97
5.2 Theoretical background.....	98
5.3 Experimentals	101
5.3.1 Chemicals.....	101
5.3.2 Conventional emulsion polymerizations.....	101
5.3.3 Automated emulsion polymerizations	105
5.3.4 Characterizations	108
5.4 Optimization of the automated reactions.....	111
5.5 Reproducibility of the automated reactions	114
5.6 Batch emulsion copolymerization: comparison between automated and conventional operations	127
5.7 On-line monitoring of PMMA-seeded emulsion homopolymerizations of styrene using a low-cost low-resolution Raman spectrometer	133
5.8 On-line monitoring of PMMA-seeded emulsion copolymerizations of styrene and butyl acrylate using a low-cost low-resolution Raman spectrometer	135
5.9 Effect of clay on Raman spectra.....	139
5.10 Concluding remarks.....	140
References	141
Summary.....	144
Epilogue	146
Appendices	148
Abbreviations	158
Acknowledgements.....	160
Curriculum vitae	162

Chapter 1

Introduction

1.1 GENERAL INTRODUCTION

Since the mid 1980s, latex/clay nanocomposites (LCN) have emerged as one of the most promising classes of hybrid inorganic polymers from which to design new materials with enhanced properties, mainly in water-based coating and adhesive applications.¹⁻⁶ Indeed, the incorporation of clay particles within a polymer matrix offers unique opportunities for significant improvements in thermal stability, gas barrier or mechanical properties as compared to the unfilled polymer.⁷⁻¹² A good dispersion and an alignment of the clay layers as single platelets into the polymer matrix are the prerequisites for the largest property enhancement as indicated by some mathematical models.¹⁰⁻¹² Such requirements have been the driving force for the development of many LCN synthetic routes.

For the preparation of latex/clay nanocomposites, conventional emulsion polymerization has gained much attention both from an academic⁴⁻⁶ and an industrial point of view.^{13, 14} Indeed, besides being highly versatile and industrially relevant, the emulsion approach can allow a direct encapsulation of the clay particles (generally organically modified) at a nanoscopic scale, which in turn should be beneficial in achieving good dispersion of the inorganic matter in a polymer film.

The clay-containing latex particles synthesized via emulsion polymerization can exhibit all kinds of morphologies including the armored-,¹⁵⁻²¹ the dumb-bell-²² or the corn-flake morphology.²³ The morphology of the LCNs will be reflected in the microstructure of the resulting LCN film and, therefore, affects its end-use properties.^{8, 24} So, it is important to be able to control the LCN morphology, which is actually far from being a straightforward task.

The morphology control of the LCN requires both thermodynamic and kinetic considerations as illustrated in Figure 1.1. Indeed, on the one hand, thermodynamics will dictate the development of the equilibrium morphology corresponding to the minimum Gibbs free energy of the latex system. On the other hand, kinetics will determine whether the thermodynamically-stable morphology will be attained in a reasonable time.

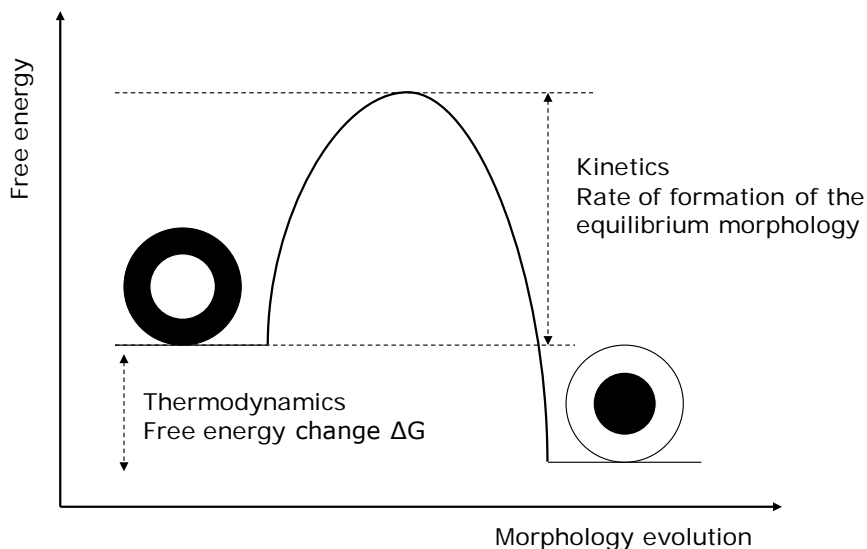


Figure 1.1 Schematic representation of the evolution of latex particles morphology as an interplay between thermodynamics and kinetics.

1.2 AIMS OF THE STUDY

A significant step towards a better understanding of the morphology control of latex/clay nanocomposites will be achieved by elucidating the role of experimental parameters and conditions in the encapsulation process.

In this thesis, conventional emulsion polymerizations are employed exclusively for the encapsulation of clay particles keeping procedures and chemicals simple and industrially applicable. Natural clay montmorillonite (MMT) particles are used as the type of inorganic fillers. The primary goal of this study is to make a start in fine tuning the dispersion and orientation of the clay into the polymer matrix by controlling the morphology of two-phase latex/clay nanocomposites. Furthermore, it is attempted to gain more insight into the effect of clay in the development of multiphase latex particles.

A very large number of experimental parameters and conditions exists that need to be investigated in order to get full insight in the morphology control of clay-

Chapter 1

containing multiphase latex particles. Systematic studies of these factors would be extremely time-consuming if one solely uses lab scale reactors. High-throughput experimentation should overcome this issue as will be shown in the last chapter of this study.

Finally, in order to quantitatively determine the thermodynamic and kinetic factors that come into play in the encapsulation process, the viscosity and the composition of the latex particle phases (mainly related to the level of unreacted monomers) must be known during the course of the reaction as fast as possible. For the on-line monitoring of monomer conversion, the work described in this thesis explores the possibility of using a low-cost low-resolution portable Raman spectrometer.

The aims of this thesis are schematically summarized in Figure 1.2

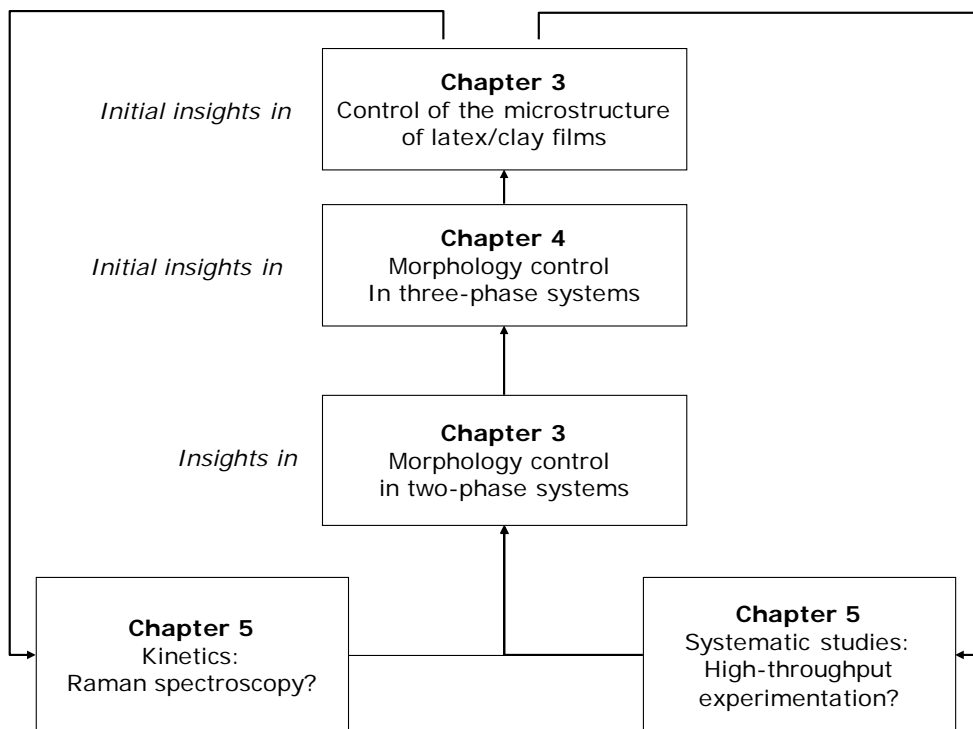


Figure 1.2 Schematic representation of the aims of this thesis to gain more insight in the control of the morphology of latex/clay nanocomposites. The separate elements should be iterated a few times to obtain optimum results. In this thesis, each element is investigated in a preliminary way to set the path to successful iterations.

1.3 OUTLINE OF THE THESIS

Chapter 2 gives the fundamental aspects of free-radical polymerization in combination with emulsion polymerization. Also, the structure of the montmorillonite clay platelets used in this study is described followed by an overview of the basic principles of morphology control of latex/clay particles.

Chapter 3, first, deals with a study of the hydrolytic stability of organically modified clays which will be further used to synthesize some LCNs. Then, the actual emulsion polymerization in the presence of (hydrophobized) clay particles is

Chapter 1

described. The morphology of the hybrid particles is characterized via (cryogenic) transmission and scanning electron microscopy. The effect of organic modification, monomer feed composition and process mode on the morphology of the LCNs synthesized is discussed. Furthermore, a systematic study of the effect of clay loading, surfactant concentration and surfactant type on the polymer/clay interaction is performed. Finally, the orientation of clays in LCN films is investigated.

Chapter 4 describes the morphology of three-phase polystyrene (PS)/poly(methyl methacrylate) (PMMA)/MMT latex particles synthesized via seeded emulsion polymerizations. The interpretation of the results obtained is based on the application of existing theories which explain the development of the morphology of two-phase conventional (purely polymeric) latex particles.

Chapter 5 describes a method for carrying out batch emulsion copolymerizations using an automated synthesizer. The monomer conversion-time histories obtained by gas chromatography demonstrate the reproducibility of the robotic platform but also reveal some specific problems that can occur with this type of equipment. In addition, this chapter proposes to evaluate the potential of Raman spectroscopy in giving reliable kinetic data from batch emulsion (co)polymerization experiments. A portable and compact Raman instrument has been used which could easily be integrated with high-throughput equipment. Monomer conversion-time histories determined with the Raman instrument are compared with the ones obtained by gas chromatography and gravimetry.

The epilogue addresses the question of how this thesis contributes to a better understanding of the morphology control of latex/clay nanocomposites. Future developments of this current research topic are put into perspective.

Part of the work described in this thesis has been published.²⁵ Part of the work in chapter 3 has been accepted for publication in *Polymer international*. Other parts of chapters 3 and 4 are in preparation for publication in *Colloid and Polymer Science*.

REFERENCES

1. Lee D.C.; Jang L.W. *J. Appl. Polym. Sci.* 61: 117 (1996).
2. Giannelis E. P. *Adv. Mater.* 8: 29 (1996).
3. Noh M.W.; Lee D.C. *Polym. Bull.* 42: 619 (1999).
4. Bourgeat-Lami E.; Duguet E. *Polymer Encapsulation of Inorganic Particles*, in Functional Coatings. WILEY-VCH Verlag GmbH & Co. KGaA Weinheim, pp: 85 – 152 (2006).
5. Bourgeat-Lami E.; Lansalot M. *Adv. Polym. Sci.* 233: 95 – 102 (2010).
6. Van Herk A.M.; Landfester K. *Hybrid Latex Particles: Preparation with (mini)Emulsion Polymerization*. Springer-Verlag Berlin Heidelberg, 287 pages (2010).
7. Kim T.H.; Jang L.W.; Lee D.C.; Choi H.J.; Jhon M.S. *Macromol. Rapid Commun.* 23: 191 (2002).
8. Negrete-Herrera N.; Puteaux J.; David L.; de Haas F.; Bourgeat-Lami E. *Macromol. Rapid Comm.* 28 : 1567 (2007).
9. Beall G.W.; Powell C.E. *Fundamentals of Polymer–Clay Nanocomposites*. Cambridge University Press, New York (2011).
10. Nielsen N.E. *J. Macromol. Sci. A1* 5: 929 (1967).
11. Bharadwaj R. *Macromolecules* 34: 9189 (2001).
12. Fornes T.D.; Paul D.R. *Polymer* 44: 4993 (2003).
13. Xue Z.; Wiese H. U.S. patent US7094830B2 (2006).
14. Tiarks F.; Leuninger J.; Wagner O.; Jahns E.; Wiese H. *Surf. Coat. Intern.* 90: 221 (2007).
15. Ashby N.P.; Binks B.P. *Chem. Phys.* 2: 5640 (2000).

Chapter 1

16. Negrete-Herrera N.; Letoffe J.-M.; Putaux J.-L.; David L.; Bourgeat-Lami E. *Langmuir* 20: 1564 (2004).
17. Negrete-Herrera N.; Letoffe J.-M.; Reymond J.-P.; Bourgeat-Lami E. *J. Mater. Chem.* 15: 863 (2005).
18. Negrete-Herrera N.; Putaux J.-L.; Bourgeat-Lami E. *Prog. Solid State Chem.* 34: 121 (2006).
19. Voorn D.-J.; Ming W.; van Herk A.M. *Macromolecules* 39: 4654 (2006).
20. Bourgeat-Lami E.; Negrete Herrera N. ; Putaux J.-L.; Perro A. ; Reculosa S. ; Ravaine S. ; Duguet E. *Macromol. Symp.* 248: 213 (2007).
21. Zhang J.; Chen K.; Zhao H. *J. Polym. Sci. Part A: Polym. Chem.* 46: 2632 (2008).
22. Voorn D.-J.; Ming W.; van Herk A.M. *Macromol. Sym.* 245: 584 (2006).
23. Ali S.I. *Colloidal Templating : A Route Towards Controlled Synthesis of Functional Polymeric Nanoparticles*. Eindhoven University of Technology, PhD thesis (2010).
24. Greesh N.; Hartmann P.C.; Cloete V.; Sanderson R.D. *J. Polym. Sci. Part A: Polym. Chem.* 46: 3619 (2008).
25. Mballa Mballa M.; Schubert U.S.; Heuts J.P.A; van Herk A.M. *J. Polym. Sci. Part A: Polym. Chem.* 49: 314 (2011).

Chapter 2

Theoretical Background

2.1 FREE-RADICAL (CO)POLYMERIZATION

This section briefly introduces the mechanism and kinetics of free-radical polymerization, which requires vinyl monomers to prepare polymers. Detailed descriptions can be found in an excellent handbook written by Matyjaszewski and Davis.¹

2.1.1 Homopolymerization

The polymerization basically proceeds into four distinct steps: (1) primary radical formation, (2) initiation, (3) propagation and (4) bimolecular termination.

(1) *Primary radical formation.* Primary free radicals ($R\bullet$) are produced via photochemical, electrochemical or thermal initiator decomposition. Most commonly used initiators (I) are peroxide ($-O-O-$) or azo ($-N=N-$) compounds. The radical formation step can be schematically represented by the following equation:

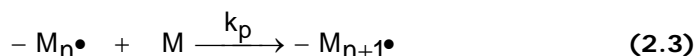


The radicals produced may further initiate the polymerization or may undergo side reactions (such as recombination of initiator molecules) which cause a loss of radicals. The rate of radical production will therefore depend on the so-called efficiency factor f defined as the ratio of the radicals which actually initiate the polymerization to the radicals produced by the initiator decomposition.

(2) *Initiation.* The primary radicals $R\bullet$ react with the first monomer molecule M according to the following equation:

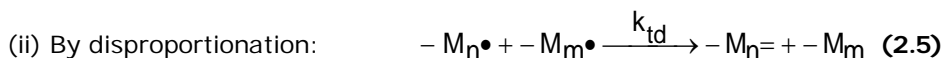
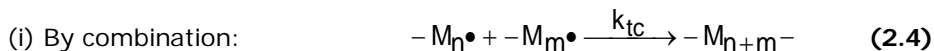


(3) *Propagation.* This process consists of sequential additions of one molecule of monomer to radicals containing n monomeric units as follows:



Chapter 2

(4) *Termination*. In this process, two radicals terminate to form one (by combination) or two dead polymers (by disproportionation). Depending on the termination mode, the reaction between two growing polymer chains is as follows:



The chain growth can also be stopped by chain transfer reactions, where the active radical centre is transferred to another molecule X (solvent, monomer, other polymer chains, etc):



The overall rate of polymerization R_p can generally be expressed as:

$$R_p \propto [M][I]^{\frac{1}{2}} \quad (2.7)$$

with the assumption of a steady state in free radical concentration (the rate of production of radicals equals the rate of disappearance); and chain length dependence of the rate coefficient is neglected.

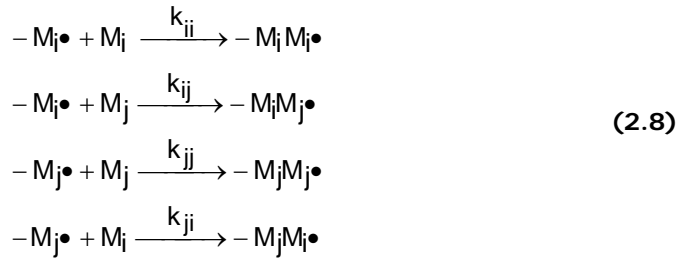
It should be noted that certain substances such as oxygen can react with radicals to produce species which do not or slowly reinitiate polymerization. This is the reason why radical polymerizations are generally performed in an inert atmosphere.

2.1.2 Copolymerization

Most polymerization processes involve at least two monomer types to form copolymers. This section aims to introduce a classical kinetic model for radical copolymerization, called the terminal (or the Mayo-Lewis) model.^{2,3} In this model,

Chapter 2

it is assumed that the reactivity of the radical only depends on the nature of the last monomer unit of the propagating chain and not on the penultimate unit. In general, this is sufficient for an adequate description for the composition, but for a description of the kinetics, the more complicated penultimate model should be used. In this model, only four different steps of the propagation should be considered:



with the monomer reactivity ratios defined as :

$$\begin{aligned} r_i &= \frac{k_{ii}}{k_{ij}} \\ r_j &= \frac{k_{jj}}{k_{ji}} \end{aligned} \quad (2.9)$$

Assuming a steady-state for the concentration of the two monomer radicals, the mole fractions F_i and F_j of monomers M_i and M_j in the instantaneously formed copolymer can be expressed as a function of the mole fractions f_i and f_j of monomers M_i and M_j in the feed:

$$\frac{F_i}{F_j} = \frac{f_i(r_i f_i + f_j)}{f_j(r_j f_j + f_i)} \quad (2.10)$$

2.2 EMULSION POLYMERIZATION

Emulsion polymerization is a heterogeneous free – radical polymerization process. Besides being environmentally friendly, this polymerization technique offers the advantage of producing high molar mass polymers at high rates of

Chapter 2

polymerization. Emulsion polymerizations are typically employed for the production of paints, coatings, adhesives and carpet backings.^{4, 5}

In emulsion polymerization, a water phase, a polymer phase and a monomer droplet phase coexist. Before polymerization, monomers are generally dispersed in the aqueous phase, and the resulting monomer droplets are stabilized by surfactant molecules. The initiation of the polymerization generally involves water-soluble initiators such as persulfate salts. The polymerization usually takes place inside monomer-swollen micelles present in the aqueous phase when surfactants are used above the critical micelle concentration.

From Harkins theory,⁶ three distinct intervals can be distinguished during the course of the polymerization.

Interval I describes the start of the polymerization, during which latex particles nucleate. Several nucleation mechanisms may exist and may simultaneously operate. The micellar nucleation mechanism, quantified by Smith and Ewart⁷ occurs when micelles are present in the aqueous phase. In homogeneous nucleation, the latex particles are created in the water phase by collisions of precipitates of oligomer radicals which have reached a certain chain length (coil-globule transition).

Interval II begins when latex particles are no longer formed. The monomer-swollen particles, i.e., the loci of polymerization, increase in size while the monomer droplets decrease until complete disappearance. Monomer molecules actually diffuse from the droplets into the latex particles via the aqueous phase.

Interval III is characterized by a consumption of the monomer molecules present in the water phase and the latex particles.

The rate equation of the overall polymerization is:

$$R_p = k_p [M]_p \frac{N_p}{N_{AV}} \bar{n} \frac{\text{mol}}{\text{dm}_w^3 \text{s}} \quad (2.11)$$

Chapter 2

where $[M]_p$ is the monomer concentration within the latex particle, N_p the number of particles per dm_w^3 and the \bar{n} average number of radicals per particle.

Batch and (semi-) continuous processes can be used to prepare latex particles in order to reach the final properties targeted. Semi-continuous processes applying monomer addition strategies are widely employed to control latex particle characteristics such as the particle morphology.⁸

2.3 CONTROL OF PARTICLE MORPHOLOGY

In order to prepare multiphase (hybrid) latex particles, seeded emulsion polymerization is the most commonly used technique. This technique comprises two stages: a first stage in which well-defined polymer or inorganic particles (so-called seeds) are synthesized and a second stage where monomers polymerize in the presence of the seed particles. In the course of the polymerization, phase separation phenomena usually occur within the latex particles leading to a large range of morphological structures such as core-shell, hemispherical, occluded, raspberry morphologies, etc (c.f. Figure 2.1). The composite particles should exhibit synergistic properties combining the qualities of each individual phase.^{9, 10} So, the main interest in controlling the latex particle morphology is to be able to adjust the final properties of the (hybrid) polymer colloid.

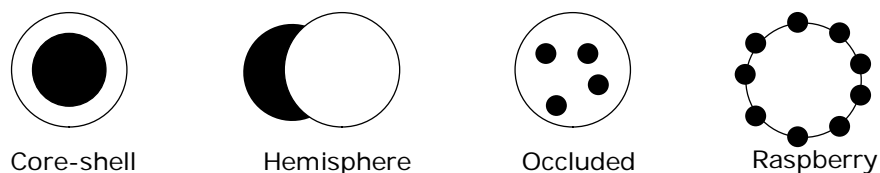


Figure 2.1 Sketch of a few known morphologies of composite latex particles prepared by two-stage emulsion polymerization.

Latex particle morphology is controlled by thermodynamics and kinetics as illustrated in Figure 2.2. For example, according to thermodynamics, polymerization of styrene in the presence of poly(methyl methacrylate) (PMMA) seed latexes should lead to the formation of latex particles where the non-polar polystyrene (PS) resides in the core of the particle surrounded by a polar PMMA shell. In Figure 2.2,

Chapter 2

PS and PMMA are represented by the black and white polymers, respectively. The formation of the PS-core/PMMA-shell morphology must, however, overcome a free energy barrier i.e. a Gibbs free energy of activation as represented by the hump in Figure 2.2. Hence, because of potentially severe kinetic restrictions, the equilibrium morphology may never be obtained.

Since Torza and Mason,¹¹ the morphology control via thermodynamic considerations has been extensively studied by several research groups such as those from Sundberg¹², El-Aasser¹³ and Asua.¹⁴ Their approaches were based on the concept that thermodynamically-controlled (or equilibrium) morphologies are determined by a minimization of the total Gibbs free energy change, which can be expressed as follows:

$$\Delta G_{P,T} = \sum \gamma_{ij} A_{ij} \quad (2.12)$$

where γ_{ij} and A_{ij} are the interfacial tension and the interfacial area between the phases i and j (including the water phase), respectively.

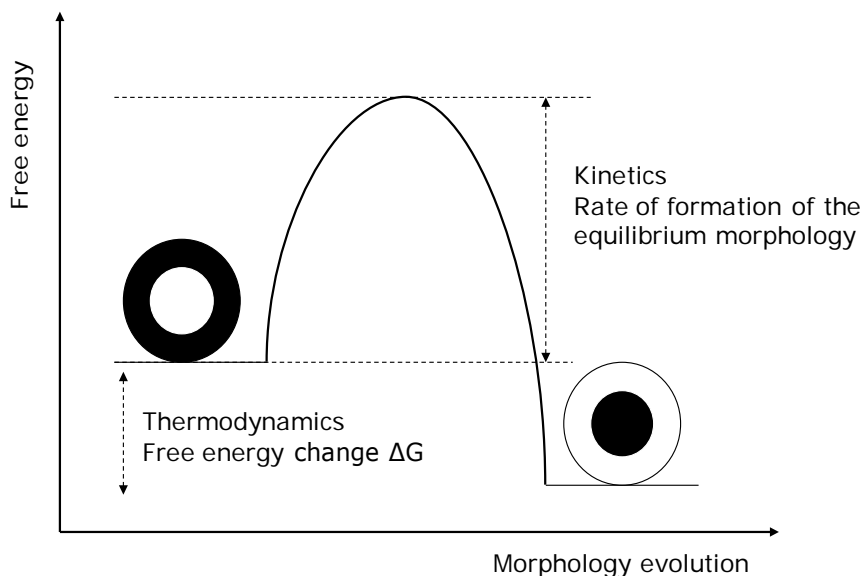


Figure 2.2 Schematic representation of the evolution of latex particle morphology as interplay between thermodynamics and kinetics.

From a kinetic point of view, both reaction and diffusion rates of polymer species within the latex particle are the controlling parameters.^{15 - 23} As seen in section 2.2, the polymerization rate will in general be affected by the concentrations of reacting species (monomer molecules and polymeric radicals) within the latex particle and the propagation, termination, radicals entry and radicals exit rate coefficients. Concerning the diffusivity of the polymer species, the molar mass and molecular structure of the polymers chain, and the intraparticle viscosity are important factors.

Thermodynamics and kinetics must be treated together, and not separately, in order to understand the evolution of the particle morphology. González-Ortiz and Asua developed a dynamic mechanistic model describing the evolution of the particle morphology based on the migration of clusters (or polymer nanodomains).^{14, 18, 19} The nucleation of a cluster corresponds to a phase separation between freshly formed polymers and a host polymer matrix. The motion of the clusters towards their equilibrium state is due to a balance of van der Waals attraction (closely related to interfacial energies)²⁴ and viscous forces.

Chapter 2

Although thermodynamics must not be ignored, kinetic factors have definitely been proven to be predominant for controlling the particle morphology.²⁵ According to Stubbs and Sundberg, the morphology development of a composite latex particle depends on the extent of penetration of the oligomers formed in the aqueous phase into the particle.²⁰ The extent of such penetration will depend on the glass transition temperature (T_g) of the host latex particle: the oligomer radicals will easily penetrate in a “soft” polymer particle having a T_g which is around 20 °C below the reaction temperature. Subsequent phase separation occurs as long as polymer chain diffusion is permitted.^{26, 27} The last stage of the morphology formation is a so-called phase consolidation or growth, when the particle phases rearrange themselves in order to reduce the interfacial free energy of the latex system.²⁷

Stubbs et al. have elegantly summarized the different steps of morphology development by the design of a general framework represented in Figure 2.3.²⁷ This “decision tree flow chart” could be the basis for understanding and interpreting the morphology development of other latex systems such as hybrid organic-inorganic latex particles.

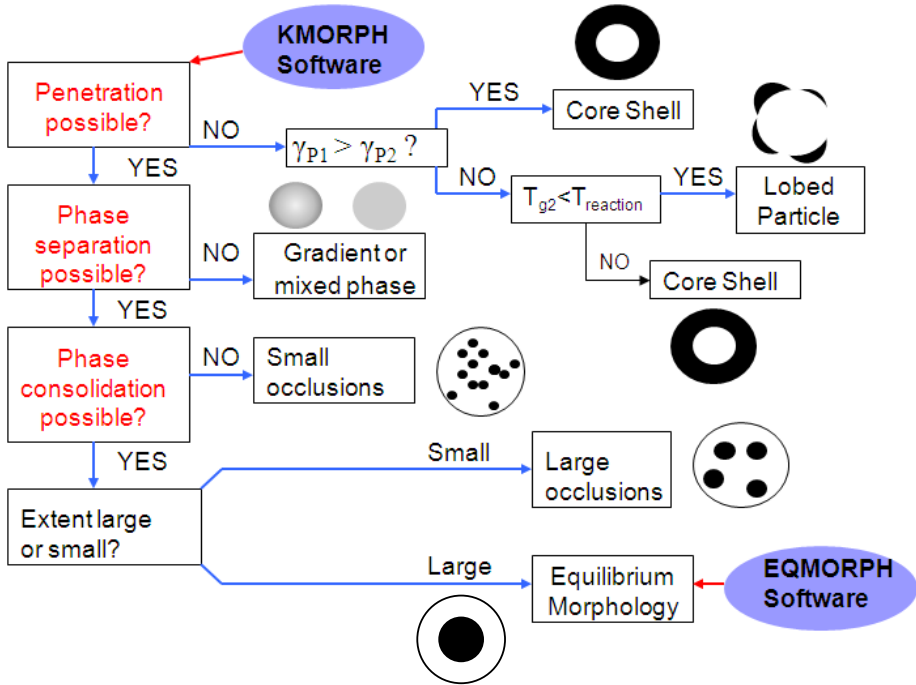


Figure 2.3 Decision tree flow chart for predicting morphology development in multiphase latex particles designed by Stubbs et al. [see Ref. 27]. The second stage polymer (black) is more hydrophobic than the seed polymer.

2.4 PRINCIPLES OF CLAY ENCAPSULATION THROUGH EMULSION POLYMERIZATION

2.4.1 The structure and physical aspects of montmorillonite

Montmorillonite clays are the particles to be encapsulated in the work described in this thesis. The smectite mineral has two tetrahedral sheets containing Si^{4+} ions sandwiching an Al-octahedral sheet (c.f. Figure 2.4). The permanent negative charge of the clay structure is due to isomorphous substitutions for Si^{4+} by Al^{3+} in the tetrahedral sheets, and for Al^{3+} by Mg^{2+} in the octahedral sheet. The clay crystal is therefore neutralized by hydrated cations (Ca^{2+} , Na^{+}) adsorbed to the surface of the sheets. These cations are weakly bound to the clay surface in a wet environment and are easily exchangeable. Hence, water and various ions are attracted to the interlayer space between sheets causing significant expansion of

Chapter 2

the clay. In addition to interlayer charges, hydroxyl sites, mainly octahedral Al-OH and tetrahedral Si-OH, are located at the broken edges of the crystal and are pH-dependent.^{28, 29}

Typically, montmorillonite particles (consisting of several layers) are plate-like, flat disks. The layers have a thickness of around 1 nm with a width varying from a few to several hundreds of nanometers.

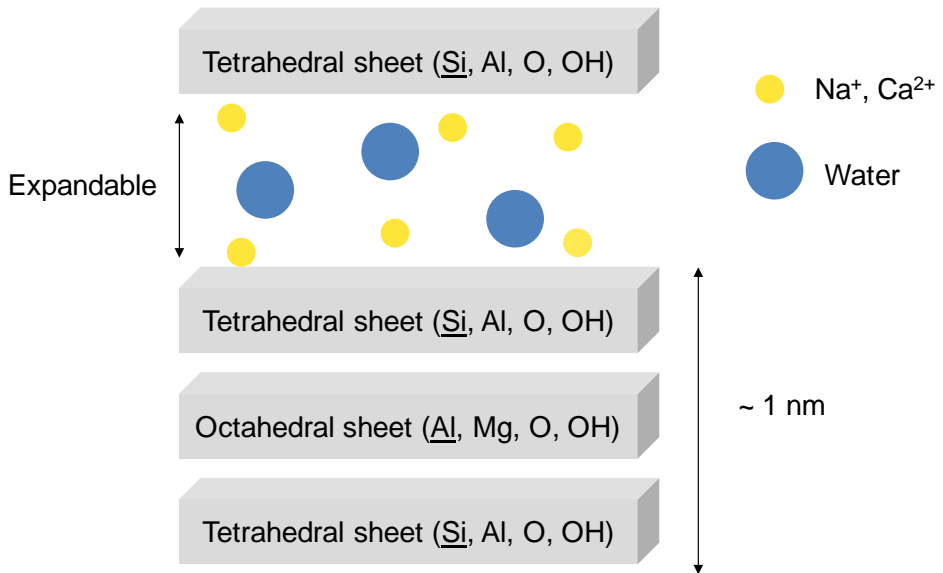


Figure 2.4 Schematic representation of a montmorillonite clay layer.

2.4.2 General principles of encapsulation

In the emulsion approach, the encapsulation of clay is generally preceded by an organic modification of the inorganic moiety. Indeed, a clay particle, intrinsically very hydrophilic, must be rendered partially hydrophobic in order to be more compatible with the encapsulating monomer/polymer. The organic modification of clay can be done via adsorption of (macro) molecules (e.g. surfactant, RAFT copolymers, etc.), ion exchange with an organic cation (e.g. alkyl ammonium) and/or covalent bonding using typically silane or titanate coupling agents.³⁰⁻³⁸ The “hydrophobized” clays are thereafter dispersed in an aqueous solution of surfactants generally using high-shear mixers. A good dispersion stability of the clay particles, ideally consisting of a very few layers, is actually an important parameter for a uniform and effective control of the morphology of the clay-containing latex particle.³⁵ The actual encapsulation of clay particles can take place via a hemimicellar or a precipitation mechanisms as represented in Figure 2.5.^{39, 40}

The hemimicellar encapsulation begins by adsorptions of emulsifier molecules at the inorganic surface forming hemi- or admicelles. Such adsorptions occur through electrostatic interactions, ion-dipole interactions and/or hydrogen bonding.⁴¹⁻⁴⁴ Then monomers are solubilized within the hemimicelles allowing further polymerization in the surrounding of the inorganic surface.

The precipitation encapsulation is characterized by adsorption of aggregates of polymer chains formed in the aqueous phase onto the inorganic surface. These aggregates swollen with monomers are the loci for further polymerization.

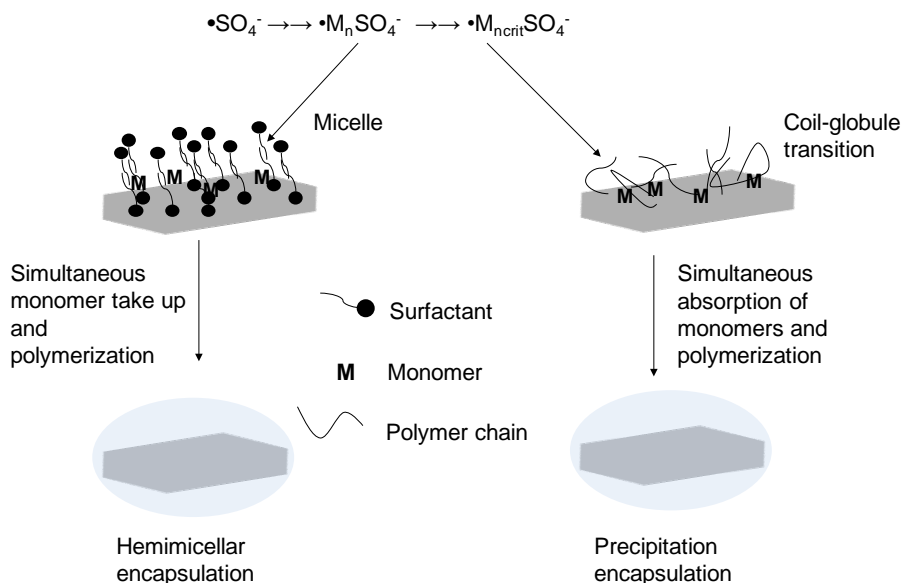


Figure 2.5 Schematic representation of the encapsulation mechanisms of clay particles via emulsion polymerization.

2.5 MORPHOLOGY CONTROL OF LATEX/CLAY NANOCOMPOSITES

Most studies aimed at controlling the morphology of latex/clay nanocomposite (LCN) by tuning the compatibility between the clay particle and the polymer matrix.^{32, 36, 45 - 51} Such compatibility is generally controlled by using organic modifiers which should strongly interact with the clay particle. The concentration, the type or even the mode of functionalization of the organic modifier should have a direct effect on the clay/polymer compatibility. For instance, in a recent work, Negrete-Herrera et al. studied the influence of clay modification level (as a percentage of organic modifiers attached to the clay) on the morphology of Laponite/latex composites.⁴⁷ Laponite particles, belonging to the synthetic smectite-type clay family, were functionalized by cation exchange with the azo initiator 2,2-azobis(2-methylpropionamide) hydrochloride (AIBA). They found that the higher the amount of AIBA molecules attached to the clay, the more diversified the particle morphology was. Negrete-Herrera et al. also studied the effect of clay modifier type

Chapter 2

on the LCN morphology.⁴⁶ Laponite particles were modified either by edge-modification via a mono- or trifunctional silane coupling agents or by ion exchange via a cationic initiator or monomer. The clay particle modified with the trifunctional silane did not lead to the formation of any hybrid particles. Armored LCNs, where the clay platelets are located in the outside of the latex particles, were obtained only with the other types of organically modified clay.

Most of the morphologies of LCN as reported in the literature are armored-like where the clay particles act like (Pickering) stabilizers for the synthesized LCN.^{49, 52-54} In fact, the armored morphology can also be obtained by physical blending of (modified) clay with latex without involving any chemistry.⁵⁵ In contrast, a total encapsulation of clay by latex particles can only be obtained via *in-situ* incorporation of the inorganic moiety in the LCN synthesis. In the past, our group showed that clay encapsulation can be successfully achieved by using special edge-modified clay particles.⁵⁰ Later on, clay encapsulation was achieved by adsorption of stabilizing copolymers containing a RAFT group followed by a seeded emulsion polymerization.^{32, 56} In the work described in his thesis,⁵⁶ Ali performed the organic modification of montmorillonite particles via the adsorption of cationic random RAFT copolymers on the surface of the inorganic compound. The RAFT-copolymers were further chain extended by the addition of monomers and initiator to form a polymeric shell around the clay. Beside conventional emulsion polymerization, miniemulsion polymerization can be a good alternative for successful clay encapsulation as indicated by several authors.^{57, 58}

Similarly to purely polymeric particles, the LCN morphology control should be studied by both considering thermodynamics and kinetics.⁵¹ As far as our knowledge is concerned, the kinetics control of the LCN morphology has barely been investigated experimentally. Most kinetic studies were performed for the main purpose of understanding the overall mechanism of the LCN synthesis and not the intra-particle events leading to phase separation.^{49, 59}

Chapter 2

REFERENCES

1. Matyjaszewski K.; Davis T.P. *Handbook of Radical Polymerization*. John Wiley and Sons Ltd, Hoboken (2002).
2. Lewis F.M.; Mayo F.R. *J. Am. Chem. Soc.* 66: 1594 (1944).
3. Alfrey T.; Goldlinger G. *J. Chem. Phys.* 12: 205 (1944).
4. Van Herk A.M. *Chemistry and Technology of Emulsion Polymerization*. Blackwell Publishing Ltd, Oxford (2005).
5. Gilbert R.G. *Emulsion Polymerization: A Mechanistic Approach*. Academic Press, London (1995).
6. Blackley D.C. *Emulsion Polymerization*. Applied Science Publishers Ltd, London (1975).
7. Smith W.V.; Ewart R.H. *J. Chem. Phys.* 16: 592 (1948).
8. Sundberg D.S.; Durant I.G. *Thermodynamic and Kinetic Aspects for Particle Morphology Control*, in *Polymeric Dispersions: Principles and Applications*, ed. Asua J.M.; Kluwer Academic Publishers, Dordrecht, p: 177 (1997).
9. Eliseeva V.I. *Prog. Org. Coat.* 13: 195 (1985).
10. Devon M.J.; Gardon J.L.; Roberts G.; Rudin A. *J. Appl. Polym. Sci.* 39: 2119 (1990).
11. Torza S.; Mason S.G. *J. Colloid Interface Sci.* 33: 67 (1970).
12. Sundberg D.C.; Casassa A.P.; Pantazopoulos J.; Muscato M.R.; Kronberg B.; Berg J. *J. Appl. Polym. Sci.* 47: 1425 (1990).
13. Chen Y.C.; Dimonie V.; El-Aasser M.S. *Macromolecules* 24: 3779 (1991).
14. González-Ortiz L.J.; Asua J.M. *Macromolecules* 28: 3135 (1995).

Chapter 2

15. Chen Y.C. ; Dimonie V.L. ; El-Aasser M. S. *Pure Appl. Chem* 64: 1691 (1992).
16. Jönsson J.-E. L. ; Hassander H. ; Jansson L. H. ; Törnell B. *Macromolecules* 24: 126 (1991).
17. Lee S. ; Rudin A. *J. Polym. Sci. Part A: Polym. Chem.* 30: 2211 (1992).
18. González–Ortiz L.J. ; Asua J.M. *Macromolecules* 29: 383 (1996).
19. González–Ortiz L.J. ; Asua J.M. *Macromolecules* 29: 4520 (1996).
20. Stubbs J.; Karlsson O.; Jönsson J.-E.; Sundberg E.; Durant Y.; Sundberg D. *Colloids Surf. A* 153: 255 (1999).
21. Karlsson L.E.; Karlsson O.J.; Sundberg D.C. *J. Appl. Polym. Sci.* 90: 905 (2003).
22. Sundberg D.C.; Durant Y.G. *Polym. React. Eng.* 11: 379 (2003).
23. Stubbs J.; Sundberg D.C. *J. Appl. Polym. Sci.* 102: 945 (2006).
24. Van Oss C.J.; Chaudhury M.K.; Good R.J. *Chem. Rev.* 88: 927 (1988).
25. Stubbs J.; Tsavalas J.; Carrier R.; Sundberg D. *Macromol. React. Eng.* 4: 424 (2010).
26. Stubbs J.M.; Durant Y.G.; Sundberg D.C. *C.R. Chimie* 6: 1217 (2006).
27. Stubbs J.M.; Sundberg D.C. *Prog. Org. Coat.* 61: 156 (2008).
28. Lagaly G.; Ziesmer S. *Adv. Colloid Interface Sci.* 102: 105 (2003).
29. Tombácz E.; Szekeres M. *Appl. Clay Sci.* 27: 75 (2004).
30. Carrado K.A.; Xu L.; Csencstits R.; Muntean J.V. *Chem. Mat.* 13: 3766 (2001).

Chapter 2

31. de Paiva L.B.; Morales A.R.; Díaz F.R.V. *Appl Clay Sci* 42: 8 (2008).
32. Ali S.I.; Hawkett B.S.; Heuts J.P.A.; van Herk A.M. *Langmuir* 25: 10523 (2009).
33. Xi Y.; Frost R.L.; He H. *J. Colloid Interface Sci.* 305: 150 (2007).
34. Parulekar Y.; Mohanty A.K. *J. Nanosci. Nanotechnol.* 5: 2138 (2005).
35. Negrete-Herrera N.; Letoffe J.-M.; Puteaux J.-L.; David L.; Bourgeat-Lami E. *Langmuir* 20: 1564 (2004).
36. Voorn D.-J.; Ming W.; van Herk A.M. *Macromol. Symp.* 245: 584 (2006).
37. He H.; Duchet J.; Galy J.; Gerard J-F. *J. Colloid Interface Sci.* 288: 171 (2005).
38. Tiwari R.R.; Khilar K.C.; Natarajan U. *Appl. Clay Sci.* 38: 203 (2008).
39. Bourgeat-Lami E.; Duguet E. *Polymer Encapsulation of Inorganic Particles*, in Functional Coatings. WILEY-VCH Verlag GmbH & Co. KGaA Weinheim, 85 (2006).
40. Van Herk A.M.; Landfester K. *Hybrid Latex Particles: Preparation with (mini)Emulsion Polymerization*. Springer-Verlag Berlin Heidelberg (2010).
41. Hower W. F. *Clays Clay Miner.* 18: 97 (1970).
42. Shalaby M. N.; *Polym. Av. Technol.* 15: 533 (2004).
43. Yang K.; Zhu L.; Xing B. *Environ. Pollut.* 145: 571 (2007).
44. Sánchez-Martín M. J.; Dorado M. C.; del Hoyo C.; Rodríguez-Cruz M. S.; *J. Hazard. Mater.* 150: 115 (2008).
45. Qutubuddin S.; Fu X.; Tajuddin Y. *Polym. Bull.* 48: 143 (2002).

Chapter 2

46. Negrete-Herrera N.; Puteaux J.; Bourgeat-Lami E. *Prog. Solid State Chem.* 34: 121 (2006).
47. Negrete-Herrera N.; Puteaux J.; David L.; Bourgeat-Lami E. *Macromolecules* 39: 9177 (2006).
48. Negrete-Herrera N.; Puteaux J.; David L.; de Haas F.; Bourgeat-Lami E. *Macromol. Rapid Comm.* 28: 1567 (2007).
49. Sheibat-Othman N.; Cenacchi-Pereira A.M.; Dos Santos A.M.; Bourgeat-Lami E. *J. Polym. Sci. Part A: Polym. Chem.* 49: 4771 (2011).
50. Voorn D.-J. *Polymer/platelet nanocomposite particles: encapsulation of platelets by physical and chemical approaches*. Eindhoven University of Technology. PhD Thesis (2006).
51. Reyes Y.; Asua J.M. *Polymer* 48: 2579 (2010).
52. Cauvin S.; Colver P. J.; Bon S.A.F. *Macromolecules* 38: 7887 (2005).
53. Bon S. A. F. ; Colver P. J. *Langmuir* 23: 8316 (2007).
54. Bourgeat-Lami E. ; Negrete Herrera N. ; Puteaux J.-L. ; Perro A. ; Reculosa S. ; Ravaine S. ; Duguet E. *Macromol. Symp.* 248: 213 (2007).
55. Binks B.P.; Lumsdon S.O. *Langmuir* 16: 2539 (2000).
56. Ali S.I. *Colloidal templating: a route towards controlled synthesis of functional polymeric nanoparticles*. Eindhoven University of Technology. PhD thesis (2010).
57. Mičušík M. ; Bonnefond A.; Reyes Y.; Bogner A.; Chazeau L.; Plummer C.; Paulis M., Leiza J.R. *Macromol. React. Eng.* 4: 432 (2010).
58. Faucheu J. ; Gauthier C. ; Chazeau L. ; Cavailié J.-Y. ; Mellon V. ; Bourgeat-Lami E. *Polymer* 51: 6 (2010).

Chapter 2

59. Chern C.-S. ; Lin J.-J. ; Lin Y.-L. ; Lai S.-Z. *Eur. Polym. J.* 42: 1033 (2006).

Chapter 3

Morphology Control of Two-Phase Latex/Clay Nanocomposites

Abstract: This chapter is divided into two main parts. The first part deals with a study of the hydrolytic stability of clays organically modified (organoclays) with two kinds of titanate coupling agents, titanium IV, (2-propanolato)tris(2-propanoata-O), 2-(2-methoxyethoxy) ethanol (unsaturated) and titanium IV, 2-propanolato, tris isooctadecanoato-O (saturated) which are subsequently used for the synthesis of latex/clay nanocomposites (LCN) via conventional emulsion polymerization. It was found that the surface modification on the clays were highly sensitive towards hydrolysis as evidenced via Fourier transform infrared and thermal gravimetry analyses. In the second part of this chapter, we report about the influence of organic modification of clay, monomer feed composition, i.e. monomer mixtures consisting of different weight ratios methyl methacrylate/ butyl acrylate, and process type on the morphology of two-phase LCN. The morphologies of the LCN obtained were analyzed using cryogenic transmission electron microscopy and scanning electron microscopy. Successful clay encapsulations were evidenced by the presence of anisotropic dumb-bell-like LCN morphologies. Surprisingly, the organic modification of the clay particles was found to be unnecessary to achieve good encapsulations. In contrast, the monomer feed composition and the process type strongly impacted the LCN morphology. Based on the results obtained, a mechanism for the clay encapsulation was proposed, where the clay particle act as a seed for the polymerization. Then, the analysis of variance of a 2³ full factorial design of experiments showed that the clay loading, the surfactant concentration and type have a significant effect on clay/polymer interaction as evidenced by the results of glass transition temperatures of dried LCN powders. The last part of this chapter describes investigations on the orientation of clay particles in dried LCN films.

3.1 INTRODUCTION

As seen in Chapter 2, clay platelets involved in an encapsulation process via conventional emulsion polymerization are supposedly seed particles and should therefore be well dispersed in the aqueous phase before polymerization. It is generally not desirable to have very hydrophobic clay particles (organoclays) which may phase separate stacking again in aqueous media without a large addition of surfactant and intensive shear mixing. So, in order to “moderately” hydrophobize the clay particles, silanes and titanates have attracted particular attention.^{1, 2} The coupling agent reacts with the hydroxyl groups of the clay particles located on the edges and/or the interlayer space of the crystalline structure. These reactive hydroxides represent only a small fraction of the total surface area of the inorganic particle still exposing the faces of the clay as to the favourable interaction with water.^{3, 4}

It is often preferred to utilize titanates for the hydrophobization of the clay particles due to the fact that the grafting reactions do not necessarily require the presence of water and form a monomolecular layer at the inorganic surface.⁵ In contrast, silanes exclusively operate via hydrolysis and a condensation mechanism and can generate multipolymeric layers.^{6, 7} The formation of such layers can render the control of the grafting reaction difficult.

According to the literature, another interesting feature of the titanates is their good stability towards hydrolysis even at elevated temperature. Indeed, previous works in our group by Caris et al.⁸ have shown that titanium dioxide spherical particles modified with the saturated titanate coupling agent titanium IV, 2-propanolato, tris isooctadecanoato-O (KRTTS) could exhibit a “self-protecting effect” against hydrolysis at 60 °C if the titanate contents were above 0.7 wt-% (based on the loading of TiO₂ particles). The so-called self-protecting effect was attributed to steric hindrance by uniformly distributed large alkyl chains of the organo-functional groups of the titanate. However, the findings of Caris cannot be generalized to all cases because the chemistry involved in the titanate coupling mechanism might greatly depend on the structure and morphology of the inorganic

particle.^{9, 10} Also, non-uniform modification of the clay particles by the titanate coupling agent might lead to the loss of this self-protecting effect.

In the first part of this chapter, the hydrolytic stability of organoclays is investigated. The modification of the clay particles is performed using KRTTS and titanium IV (2-propanolato)tris(2-propenoata-O), 2-(2-methoxyethoxy)ethanol (KR39DS), where the former is saturated and the second has unsaturated alkyl groups. The structures of these titanates are represented in Figure 3.1. The modification of the clay particles is qualitatively verified via FT-infrared spectroscopy (FT-IR) and X-ray diffraction (XRD) analysis. In addition, some thermogravimetric analyses (TGA) allow to quantitatively estimate the efficiency of the modification process. The surface active properties of aqueous suspensions of the organoclays are also studied in order to check whether the inorganic moieties exhibit amphiphilic-like character which may result from the presence of hydrophobic molecules in their crystalline structure as shown by previous studies.¹ In order to investigate the stability of the organoclays towards hydrolysis, dialysis treatments of 1 wt-% aqueous suspension of the organoclays are performed either at room temperature or at 80 °C. The dried dialyzed clay particles are subsequently characterized by FT-IR and TGA in order to evaluate the presence of titanates on the inorganic surface after treatment.

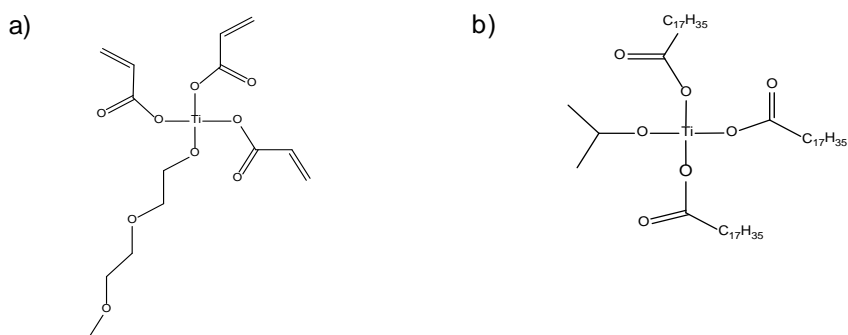


Figure 3.1 Structure of the titanate coupling agents (a) KR39DS and (b) KRTTS.

Chapter 3

The second part of this chapter proposes to elucidate the effect of several experimental parameters which can have an influence on the LCN morphology from both a thermodynamic and a kinetic point of view. Targeting the core/shell morphology (where a single clay platelet is surrounded by a polymeric shell), some starved-feed semi-batch emulsion (co)polymerizations in the presence of clay are performed. Native or organically modified clay particles synthesized in the first part of this chapter are used. First, the effect of organic modification of the clay on the LCN morphology is investigated. Then, the effects of monomer feed composition on the morphology control are studied. It is known that, depending on the monomer composition, the interfacial energy and the glass transition temperature (T_g) of the latex/clay system can vary.^{11 - 13} A change of the interfacial energy and the T_g can play an important role on the mobility of the particle phases. Finally, the influence of process type on the morphology control is addressed. The process type determines the monomer concentration within a particle during the course of the reaction; in a batch process the monomer concentration can considerably fluctuate whereas in a semi-batch reaction the monomer concentration can be kept constant. The presence of monomer in the reaction locus can have an influence on the polymer/water interfacial tension and on the mobility of the phases.^{13, 14} Cryo-TEM and SEM were used for the characterizations of the LCN morphologies.

In addition, this part deals with a systematic study of the effects of clay loading, surfactant concentration and surfactant type on the clay/polymer interaction which can be qualitatively determined by analyzing the glass transition temperature (T_g) of dried powders of the LCN synthesized. This qualitative method to assess the clay/polymer interaction is based on the fact that clay platelets in good contact with the polymer matrix will restrict the mobility of the polymeric chains during a thermal transition, as often expressed by an increase in the T_g .^{15 - 19}

It is generally believed that a control of the morphology of latex/clay nanocomposites will allow a good control of the orientation of the clay platelets within a polymeric film²⁰ which in turn greatly influences the final properties (e.g. barriers properties) of the composite latex coating.^{3, 16, 17, 19, 21} The longer path length for molecules diffusing through a film containing clay platelets and the reduced mobility of the polymeric chains in contact with the clay surface can affect

the diffusion of liquids and gas through the polymer films strongly. Bharadwaj explains the prevention of gas diffusion into a polymer-clay nanocomposite by a model schematically represented in Figure 3.2.²¹ According to this model, the relative permeability of the nanocomposite will be maximal or minimal if the clay platelets align perpendicular or parallel to the substrate, respectively. The question is whether the orientation of the clay platelets can be achieved by simply drying the LCN synthesized in our study.

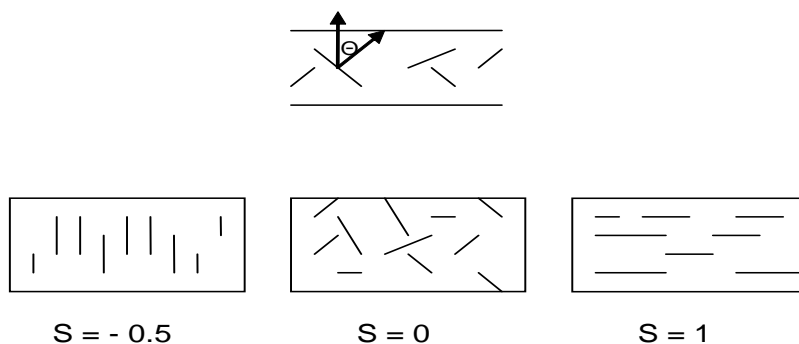


Figure 3.2 Schematic representation of the angle θ between the normal to the substrate and the normal to the clay platelet (after ref 17). S is the orientation factor defined as $S = \frac{1}{2} (3 \cos^2\theta - 1)$.²¹

3.2 EXPERIMENTAL

3.2.1 Chemicals

The sodium montmorillonite (MMT) used in this study was Cloisite® Na⁺ kindly provided by Southern Clay Products Inc. (Texas, USA). According to the supplier, the exchange capacity of the clay was 92 mequiv per 100 g of clay. Inhibitors were removed from the monomers methyl methacrylate (MMA, 99% Aldrich) and butyl acrylate (BA, 99%, Aldrich) by slowly passing through a basic aluminum oxide column (Sigma-Aldrich). The water-soluble initiator 2,2'-azobis[2-methyl-N-(2-hydroxyethyl) propionamide] (VA-086, Wako Chemicals GmbH, see Figure 3.3), the non-ionic detergent Triton X-100 (TX-100, Sigma-Aldrich), the anionic

surfactant sodium dodecylbenzenesulfonate (SDBS, technical grade Sigma- Aldrich) and toluene (P.A. grade, Biosolve) were used as received. The water used was demineralized. The titanate modifiers titanium IV (2-propanolato)tris(2-propenoata-O), 2-(2-methoxy, ethoxy) ethanol (KR39DS) and titanium IV, 2-propanolato, tris isooctadecanoato-O (KRTTS) were used as provided by Kenrich Petrochemicals, Inc. (New-Jersey, USA).

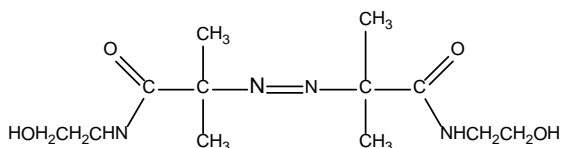


Figure 3.3 Structure of the water-soluble initiator 2,2'-azobis[2-methyl-N-(2-hydroxyethyl) propionamide] (VA-086) used to synthesize latex/clay nanocomposites.

3.2.2 Organic modification of MMT

The organic modification of clay was performed as follows. First, 10 g of MMT particles were slowly added to a solution of titanate coupling agent in toluene (0.2 % w/w) mixed at 11,500 rpm using the Ultra Turax T25 (Ika). The ratio MMT/titanate was fixed at 0.07 w/w. The reaction took place in 3 hours at ambient temperature. After modification, a centrifugation was done twice at 2500 rpm for 10 minutes to remove the excess of titanate molecules which did not react with the clay particles. A filtration of the modified clay was done, followed by intensive washing with toluene. The organically modified clay (organoclay) particles were dried overnight in a vacuum oven at 60 °C.

3.2.3 Dialysis treatment

The dialysis of the clay particles was performed with Visking membranes (12,500 molecular weight cut off), which are able to retain clay particles at the retentate side of the membrane while dissolved molecules permeate the membrane. The membrane was filled with around 100 mL of water/clay suspension at a 1 % w/w ratio and sealed. Once filled, the membrane was immersed in 2 L demineralized water for 2 hours at ambient temperature or at 80 °C. The dialyzed

samples were centrifuged twice at 30,000 rpm and dried overnight in vacuum oven at 60 °C for subsequent analysis.

3.2.4 Emulsion (co)polymerization in the presence of clay

The organoclay was dispersed ultrasonically with the ultrasound device UP400S (from Hielscher with a tip diameter of 22 mm and an energy output of 393 W s mL⁻¹) in a surfactant solution (below CMC; the CMCs of the surfactants as determined via a surface tension titrator (Data Physics) were 0.13 g L⁻¹ and 0.6 g L⁻¹ for the mixed surfactant system TX-100: SDBS (with a weight ratio of 6: 1) and pure SDBS, respectively). It should be noted that the interfacial properties (hydrophilicity) of the clay particle will greatly depend on the type of surfactant used due to the fact that Triton X-100 and SDBS adsorb on the clay particle surface via different adsorption mechanisms.²²⁻²⁵ Triton X-100 surfactant molecules can be adsorbed in the interlayer space of the clay particles;²³ whereas SDSB is hardly capable of intercalating the inorganic compound.^{24, 25} The use of a mixed surfactant system may offer certain interfacial properties which may not be obtained by the adsorption of a single surfactant. The organoclay dispersion was centrifuged at 2500 rpm for 10 minutes to remove any possible clay aggregates. The initiator was added to the clay dispersion in one pulse after an elevation of the temperature to 80 °C, after which the reaction medium was allowed to stir for 10 minutes (the half-life of VA-086 is around 10 hours at 80 °C). Then, monomers were slowly added to the reaction mixture with a feeding rate of 17 μL min⁻¹ by a syringe pump (New Era NE-1000). Before polymerization, all reactants were de-oxygenated by purging with argon for around 20 minutes. A small pressure of argon was maintained over the reaction medium during the polymerization to avoid oxygen inhibition. Typical recipes of the reactions are given in Table 3.1.

Table 3.1 Recipes used for the clay encapsulation

Ingredients	E-0 ^{a, c}	E-1 ^{a, d}	E-1b ^{a, d}	E-1c ^{d, e}	E-2 ^{a, d}	E-3 ^{a, d}	E-4 ^{a, d}
Water (g)	100	100	100	100	100	100	100
MMA (g)	7.05	7.05	7.05	7.05	4.23	5.29	-
BA (g)	-	-	-	-	2.82	1.76	7.05
VA-086 (wt-%) ^b	2	2	2	2	2	2	2
MMT (wt-%) ^b	-	3.5	5.5	3.5	3.5	3.5	3.5
[Surfactant] (x CMC)	0.9	0.9	0.5	0.9	0.9	0.9	0.9

a) Total monomer feed rate = 16 mg min⁻¹

b) Based on monomer weight

c) TX-100: SDBS (6:1) used as surfactant

d) SDBS used as surfactant

e) Batch addition of the monomer

3.2.5 Systematic study of the effects of clay loading, surfactant concentration and surfactant type on clay/polymer interaction

A 2³ full factorial statistical design of experiment (DOE) was applied by varying the clay loading, the surfactant type and concentration, all the other parameters remaining constant. The investigated responses of this DOE were the difference between the T_g of the dried final products of each experiment and the T_g (110 °C) of a film of PMMA latex particles prepared using the recipe E-0. All the statistics were done with the software Statgraphics Centurion XVI (version 16.0.05, StatPoint Technologies).

3.2.6. Characterization

FT-Infrared spectroscopy

Fourier-transformed infrared (FTIR) spectra were recorded with a FTS 6000 spectrometer (Bio-Rad). The final spectrum was an average of 200 scans at a resolution of 4 cm^{-1} . Analyses of the spectra were done with the software Varian Resolutions Pro version 4.0.5.009.

Thermogravimetric analysis

Thermogravimetric analysis (TGA) was performed using a high resolution TA-Q500 instrument under nitrogen flow at 50 ml min^{-1} . A scanning rate of $10 \text{ }^\circ\text{C min}^{-1}$ was used. TGA was used to determine the amount of titanate molecules which have coupled with the montmorillonite type clay Cloisite[®] Na⁺ (coupled Ti) using Equation 3.1 from the weight loss (corrected from the weight loss of pure MMT) between $120 \text{ }^\circ\text{C}$ and $500 \text{ }^\circ\text{C}$, $W_{120-500}$ (%), corresponding to titanate degradation.

$$\text{Coupled Ti } (\mu \text{ equiv g}_{\text{clay}}^{-1}) = \frac{10^6 W_{120-500}}{(100 - W_{120-500}) \times M} \quad (3.1)$$

where M (g mol^{-1}) is the molecular weight of the grafted titanate molecules. It was assumed that the organic modification took place as in Equation 3.3

The organic modification yield (%) defined as the percentage of titanate that has effectively reacted during the organic modification was determined using Equation 3.2

$$\text{Modification yield} = \text{coupled Ti} \times \frac{100}{[\text{Ti}]} \quad (3.2)$$

where $[\text{Ti}]$ ($\mu\text{equiv g}^{-1}$) is the initial concentration of titanate.

X-ray Diffraction

The X-ray diffraction patterns were obtained from a Rigaku Geigerflex Bragg-Brentano Powder Diffractometer, with a copper tube at 40 kV and 30 mA. The samples were measured using a step scan from 1.3 till 10 degrees 2-theta with a step size of 0.02 and a counting time of 10 seconds. The X-ray (powder) diffraction patterns were analysed using a Cu K α_1 radiation, wavelength 1.54056 Angstrom. A graphite monochromator on the diffracted site eliminates the K β_2 radiation, resulting in only the Cu K α_1 , while the K α_2 is stripped by profile fitting.

Differential Scanning Calorimetry

Differential scanning calorimetry (DSC) measurements were performed on a TA Instruments Advanced Q100. The temperature gradient was $-20\text{ }^\circ\text{C}$ to $150\text{ }^\circ\text{C}$ at a rate of $20\text{ }^\circ\text{C min}^{-1}$. The glass transition temperatures were determined from the second heating run.

Electron Microscopy

Cryogenic transmission electron microscopy (cryo-TEM) measurements were performed on a FEI Tecnai 20, type Sphera TEM instrument (with a LaB₆ filament, operating voltage = 200 kV). The sample vitrification procedure was performed using an automated vitrification robot (FEI Vitrobot Mark III). A 3 μL sample was applied to a Quantifoil grid (R 2/2, Quantifoil Micro Tools GmbH; freshly glow discharged for 40 seconds just prior to use) within the environmental chamber of the Vitrobot and the excess liquid was blotted away. The thin film thus formed was shot into melting ethane. The grid containing the vitrified film was immediately transferred to a cryoholder (Gatan 626) and observed under low dose conditions at $-170\text{ }^\circ\text{C}$.

For TEM ultramicrotomy, ultrathin sections (70 nm) of dried LCNs were obtained at room temperature using a Reichert-Jung Ultracut E microtome equipped with a Diatome knife. The sections were put on a 200 mesh copper grid with a carbon support layer. The sections were also examined with the Sphera instrument

Scanning electron microscopy (SEM) of dried LCN samples was performed using a FEI Company XL30 SEM running at 10 kV. Before scanning, the SEM samples were mounted onto stubs and sputter coated with gold.

3.3 STABILITY OF THE ORGANOCLOYS TOWARDS HYDROLYSIS

According to the literature, the modification of the clay particles takes place via the following mechanism.⁵



where (OX) and (OY) represent the monoalkoxy group and the organo-functional fragments of the titanate coupling agent, respectively. HO-M represents the reactive hydroxyl groups located on the broken edges and/or the interlayer space of the clay particles.

3.3.1 Surface modification of the clay

(i) FTIR and XRD analysis

Figure 3.4 shows the typical infrared spectra of KR39DS (Ti_1), the unsaturated titanate coupling agent, the native and KR39DS-modified clay ($M-Ti_1$). The stretching carbonyl vibration ($\nu_{str}(C=O)$) at 1724.8 cm^{-1} , belonging to the characteristic peaks of KR39DS, seems to be shifted to a lower value around 1718 cm^{-1} in the spectrum of $M-Ti_1$. The deformation vibration of OH groups, $\delta(OH)$, belonging to water bound on the clay surface, also shifted to a lower value after modification. These changes of $\nu_{str}(C=O)$ and $\delta(OH)$ show that some kind of interaction between the titanate molecules and the clay particle has been created during the modification process. The coupling of the titanates is also evidenced by the presence, though very slight, of the asymmetric vibration of the ester groups linked to the titanium atom of the coupling agent ($\nu_{asym}(COOTi)$) around 1540 cm^{-1} . A broad band around 2935.6 cm^{-1} , corresponding to stretching vibrations of aliphatic groups ($\nu_{str}(C-H)$), also proves a successful coupling of the titanate.

Similarly, Figure 3.5 shows that, for KRTTS-modified clay (M-Ti₂), $\delta(\text{OH})$ is shifted to lower value whereas a set of three bands characteristic of a $\nu_{\text{str}}(\text{C-H})$ is shifted to higher wavenumbers. These last observations are, again, evidence of an existing interaction between the titanate molecules and the clay surface. However, $\nu_{\text{str}}(\text{C=O})$ at 1735 cm^{-1} , present in the spectrum of KRTTS, completely disappears in the spectrum of M-Ti₂. In fact, $\nu_{\text{str}}(\text{C=O})$ might be attributed to the carbonyl groups of free isostearic acid likely present in the solution of KRTTS. Previously, Caris²⁶ has shown that the solution of KRTTS, as supplied by Kenrich Petrochemicals, was actually a mixture of 72 % of diisopropyl diisostearoyl titanate and 28 % isostearic acid. Furthermore, in the LC/MS profile of KRTTS (c.f. Figure 3.6), the peak at 283.15 might be due to a loss of H⁺ of isostearic acid molecules whose molecular weight is 284.48 g mol^{-1} . So, after the modification process, the isostearic acid molecules have probably been extracted during the intensive washing of the organoclays with toluene.

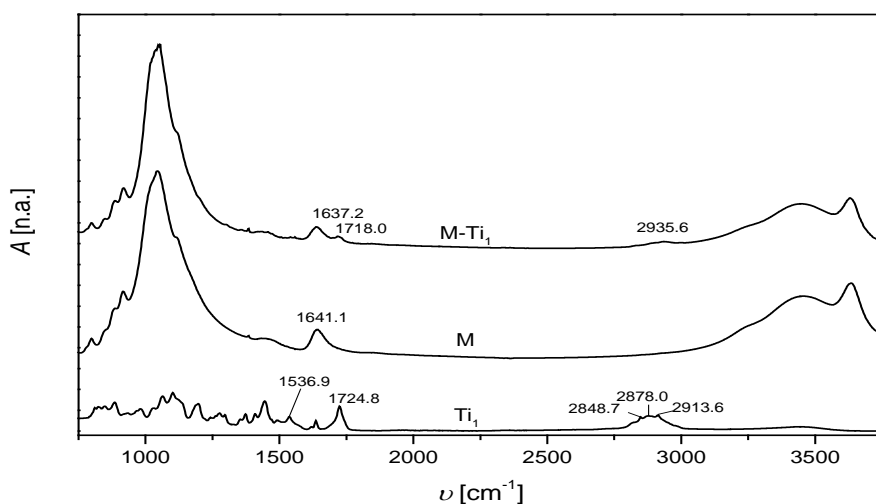


Figure 3.4 Typical FT-IR spectra of KR39DS (Ti₁), the unsaturated titanate coupling agent, (M) native and KR39DS – modified MMT (M-Ti₁).

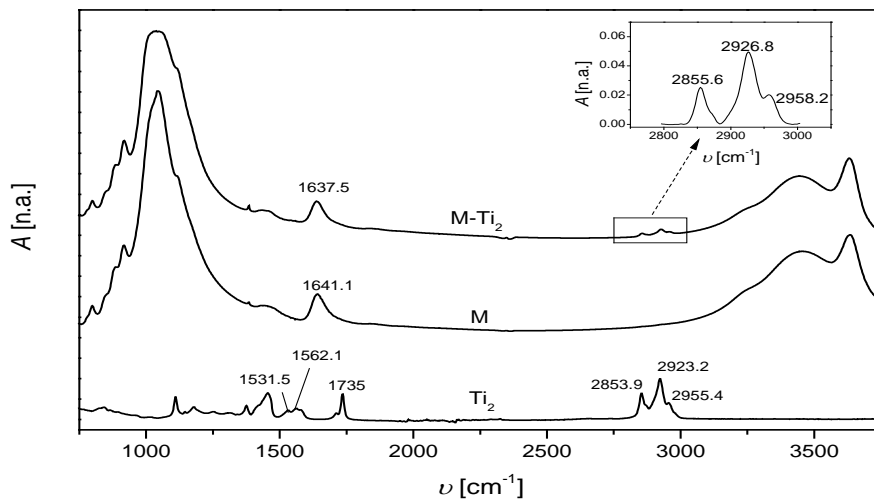


Figure 3.5 Typical FT-IR spectra of KRTTS (Ti_2), the saturated titanate coupling agent, (M) native and KRTTS- modified MMT (M-Ti_2).

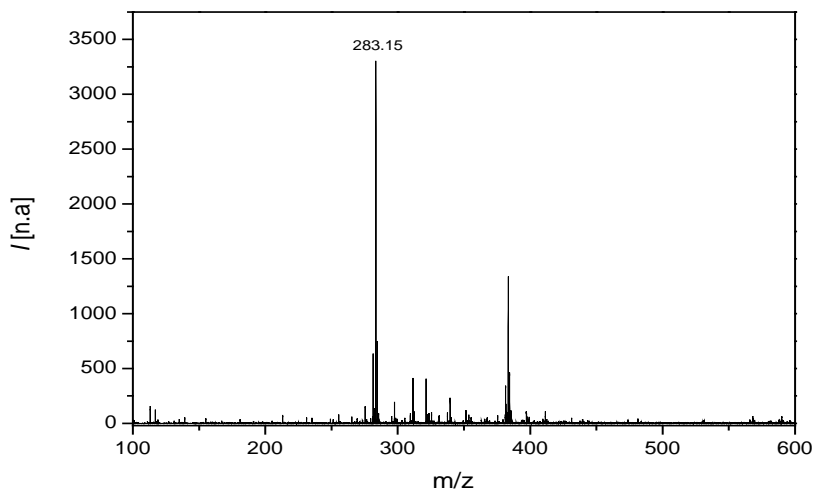


Figure 3.6 The LC-MS spectrum of a solution of KRTTS in THF ($\sim 1 \text{ mg mL}^{-1}$).

Figure 3.7 shows the XRD patterns of native, KR39DS- and KRTTS- modified clay particles. Apparently, the modification process did not seem to have a significant effect on the basal spacing (d_{001}) of the clay particles: just a very slight increase of d_{001} values is noticeable for both modified clays. However, the higher intensities of the d_{001} peaks of M-Ti₁ and M-Ti₂ might indicate a better ordering of the lamellar stacking of the clay layers compared to the native clay sheets.²⁷

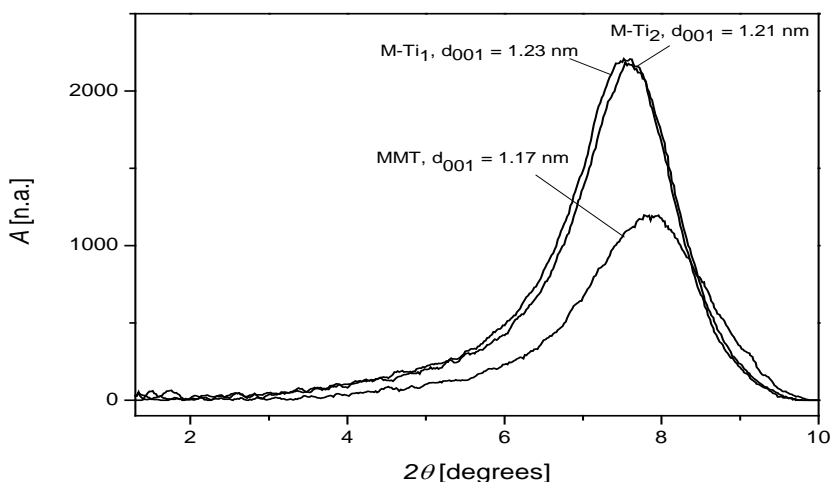


Figure 3.7 Typical X-ray diffraction patterns of native (MMT), KR39DS- (M-Ti₁) and KRTTS- modified MMT (M-Ti₂) clay particles. The indicated values d_{001} correspond to the basal spacing (001)

(ii) TGA analysis

The typical TGA curves of MMT, M-Ti₁ and M-Ti₂ particle show several decomposition steps as can be seen in Figure 3.8. For all cases, the mass loss from 30 °C to 120 °C corresponds to the release of free water physisorbed on the surface and located in the interlayer space of the clay particle. Over 500 °C, the structural hydroxyl groups of the clay dehydrate. Weight losses between 120 °C and 500 °C can be attributed to the degradation of organic moieties.^{27,28} In this temperature range, for KR39DS, two main decomposition steps, at 198 °C and 320 °C, and a slight bump around 455 °C can be distinguished. Concerning KRTTS,

most of the organic moieties degrade around 412 °C. The amounts of titanate molecules attached to the clay surface and the yields of the modification processes are given in Table 3.2. We observe that the modification yield depends on the nature of the titanate coupling agent used: the unsaturated coupling agent (M-Ti₁, KR39DS) leads to a higher modification efficiency.

Apparently, different thermal degradation mechanisms can take place depending on the titanate coupling agent used. This suggests that several interaction types between the titanate molecules and the clay particle might exist. Indeed, similarly to silane, grafting reactions of the titanate might take place on the external surface (via hydrophobic interactions), on the broken edges and/or in the interlayer space (via covalent and/or hydrogen bonding) of the clay particle.^{1, 9, 29} From the results obtained above, it is difficult to clearly depict the different possible grafting mechanisms partly due to the fact that such chemistries are poorly documented in the open literature. In addition, the titanates might have different configurations than the ones proposed by Kenrich Petrochemicals as found by other authors.^{26, 30} In Figure 3.9, the TGA profiles of the titanate as supplied show several thermal degradation steps corresponding to the decomposition of the organofunctional groups of the titanate coupling agents. The fact that the decomposition of these groups takes place through different thermal mechanisms suggests a complex structure of the coupling agents which may considerably differ from the ones depicted in Figure 3.1.

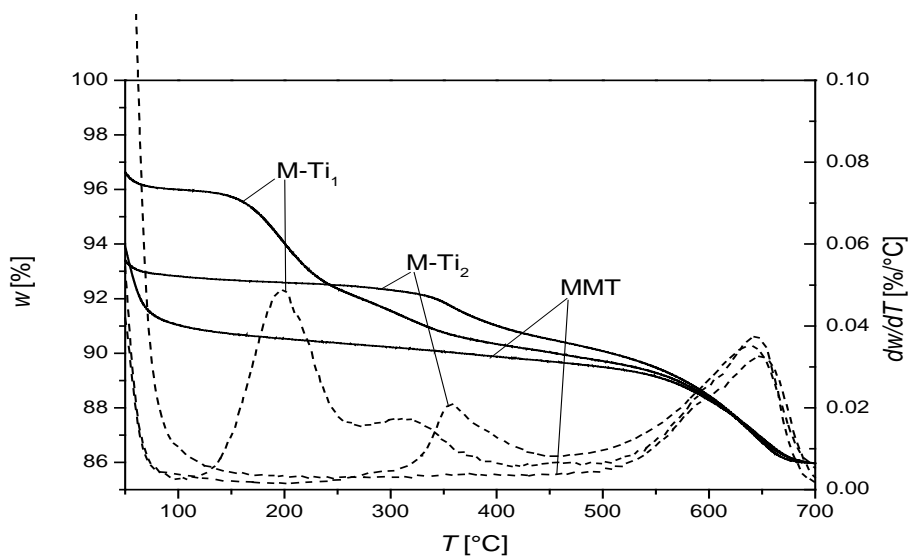


Figure 3.7 Typical TGA curves of (M-Ti₁) KR39DS-modified, (M-Ti₂) KRTTS - modified and native MMT.

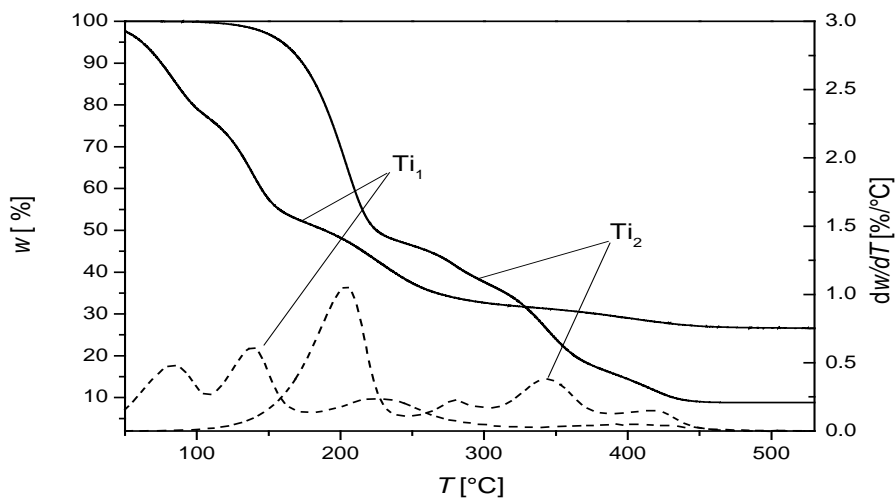


Figure 3.8 TGA curves of (Ti₁) the unsaturated KR39DS and (Ti₂) the saturated KRTTS titanate coupling agents.

3.3.2 Amphiphilic character of the organoclay

Previous studies have shown that silane-grafted clay particles could self-associate in specific configurations showing some amphiphilic character.¹ It was therefore interesting to see whether the titanate-containing organoclays synthesized in our study would also exhibit some amphiphilicity.

Figure 3.9 shows the results of surface tension titrations of clay-containing aqueous suspensions. In contrast to native and KR39DS-modified clay particles, organoclays functionalized with KRTTS seem, at first, to possess some surface active properties.

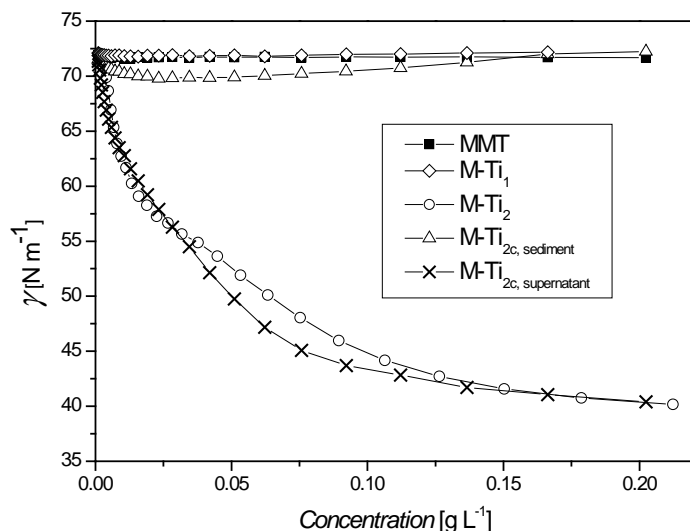


Figure 3.9 Surface tension as a function of the concentration of (■) native (MMT), (◇) KR39DS- (M-Ti₁) and (○) KRTTS-modified (M-Ti₂) MMT clay suspensions. (X) and (△) correspond to the supernatant (M-Ti_{2c, supernatant}) and sediment (M-Ti_{2c, sediment}) of a centrifugation at 30 000 rpm of the KRTTS-modified clay suspension, respectively. For all cases, the initial concentration of the clay suspensions was arbitrarily set at 1 g L⁻¹ on the titrator software.

Such surface activity of the KRTTS-modified clay particles may simply be due to the desorption of molecules physically attached to the clay surface. A simple experiment was carried out in order to check whether the surface activity observed in Figure 3.9 was inherent in the organoclays or whether it arose from desorption of molecules from the clay surface. An aqueous suspension of KRTTS-modified clays (0.01 w/w) was centrifuged at 30 000 rpm. Surface tension titrations were performed for the extracted supernatant (around 100 mL) and the sediment which was redispersed in 100 mL of water. In Figure 3.9, it can be seen that the supernatant is surface active whereas the sediment has little surface activity. So, it becomes obvious that the surface activities observed for the KRTTS-modified clays suspensions arose from desorption of molecules from the clay surface.

3.3.3 Hydrolytic stability

From the previous section, it seems that the organoclays synthesized can easily release some water soluble molecules when suspended in water. This section addresses the question whether these molecules represent the titanate molecules which were initially attached to the clay.

According to the literature,⁵ the alkoxy group of the titanate agent should readily react with any free hydroxyl groups and/or water molecules bound to the clay surface. Only the reaction with the free OH groups of the clay should permit a covalent bonding between the titanate and the inorganic moiety. The native clays used in this study could contain up to 10 % of physisorbed water as estimated from thermogravimetric analysis. This small amount of water might have initiated important hydrolysis of the titanate during the modification process. Some hydrolysates thus created might just have physically adsorbed on the clay surface. As a consequence, a chemical grafting between the titanate and the clay must have been, at least partially, prevented.

In fact, the possible interactions (via chemical grafting or adsorption) between the coupling agent and the clay will not be subject to further discussion in this section. We rather attempt to simply answer the question whether the organoclays synthesized will resist to hydrolysis. According to Table 3.2, important losses of titanates are observed after any dialysis treatment. However, one could argue that,

before dialysis, the organoclay suspensions were exposed to powerful ultrasounds which might have somehow significantly contributed to the hydrolytic instability of the inorganic moieties.³² In order to check the validity of this argument, a simple experiment was carried out where the organoclays were suspended in water using the high-shear mixer T25 Ultra-turrax[®] (IKA). The organoclays suspensions were further dialyzed either at room temperature or at 80 °C for two hours. FT-IR and TGA data showed that all the dialyzed samples, with one exception, seemed void of titanates. Only the room-temperature dialyzed KRTTS-modified clays seemed to have relatively good stability. Indeed, the percentage of titanates still attached to the clay was estimated to be around 0.8 % (corrected from the weight loss of the native clays).

So, the results obtained clearly suggest a problem with the hydrolytic instability of the organoclays synthesized under ultrasonication and/or at elevated temperature. Stable sites between the coupling agent and the clay might, however, still occupy just a small fraction of the total surface area of the inorganic. The characterization techniques used might not have been sensitive enough to detect such trace amounts of titanate molecules.

Table 3.2 The yield of the organic modification of clay depending on the nature of the titanate coupling agent and the dialysis treatment at room temperature and at 80 °C

Samples	Weight loss ^{a)}	Corrected weight loss ^{b)}	Coupled Ti ^{c)}	Modification yield ^{c)}
	%	%	$\mu\text{equiv g}^{-1}_{\text{clay}}$	%
MMT	1.57	-	-	-
M-Ti ₁ ^d	6.48	4.91	199	73.8
M-Ti _{1,dia} ^e	1.78	0.21	8	3.0
M-Ti _{1,dia, Δ} ^f	1.55	~ 0	~ 0	~ 0
M-Ti ₂ ^d	3.23	1.66	19	24.1
M-Ti _{2,dia} ^e	1.57	~ 0	~ 0	~ 0
M-Ti _{2,dia, Δ} ^f	1.73	~ 0	~ 0	~ 0

a) The weight loss was taken between 120 °C and 500 °C

b) The corrected weight loss is the weight loss of the samples minus the weight loss of MMT between 120 °C and 500 °C (i.e. 1.57 %).

c) The grafted amount and yield were respectively determined using Equations 3.1 and 3.2

d) M-Ti₁ and M-Ti₂ stand respectively for organically modified Cloisite Na⁺ with KR39DS and KRTTS.

e) M-Ti_{1,dia} and M-Ti_{2,dia} correspond to the dried samples of M-Ti₁ and M-Ti₂ which were dialyzed at room temperature for 2 hours and subsequently centrifuged twice at 30 000 rpm.

f) M-Ti_{1,dia, Δ} and M-Ti_{2,dia, Δ} correspond to the dried samples of M-Ti₁ and M-Ti₂ which were dialyzed at 80 °C for 2 hours and subsequently centrifuged twice at 30 000 rpm.

3.4 EFFECT OF EXPERIMENTAL PARAMETERS ON THE LCN MORPHOLOGY

3.4.1 Effect of the organic modification

Emulsion polymerizations were carried out with native and organoclays to see whether the modification step, though insignificant, has an influence on the morphology of the LCNs. All reactions were performed according to the recipe E-1a of Table 3.1. The final solid content was around 6 %. Figure 3.10 shows the typical cryo-TEM of the synthesized LCNs that we observed. Strikingly, the morphologies of the LCN were the same for each type of clay particles used, including the native ones. In Figure 3.11, we can see a large distribution of irregular-shaped latex particles suggesting successful encapsulation of the clay platelets. The clay platelets could easily be seen when they were oriented parallel to the electron beam. For instance, a better estimation of the number of clay platelets encapsulated in the samples shown in Figure 3.12 can be done by simply tilting the stage of the microscope at a certain angle.

In fact, the results found in this section clearly disprove the argument that successful encapsulation necessarily requires an edge-modification of the clay by a saturated or unsaturated titanate coupling agent, as concluded in earlier work from our group.² Most likely the hydrolysis of the titanate was overlooked at that time.

In fact, the success of the encapsulation process might also be due to the fact that the organoclay particles used, not being amphiphilic (as demonstrated in section 3.3.2) and hardly hydrophobic, could be well dispersed in the aqueous phase before polymerization. Indeed, Negrete-Herrera et al. have shown that severe aggregation states of organoclay particles before polymerization would very likely lead to partial encapsulation of the inorganic moiety.³¹ This is due to the fact that the clay particles, modified in their interlayer space, tend to agglomerate when dispersed in water due to long-range van der Waals interactions.²⁹ High shear stirring and the addition of a large amount of surfactants are often used to break down the clay aggregates.^{31, 33} However such solutions can severely compromise an efficient encapsulation process as will be discussed in section 3.4.5.

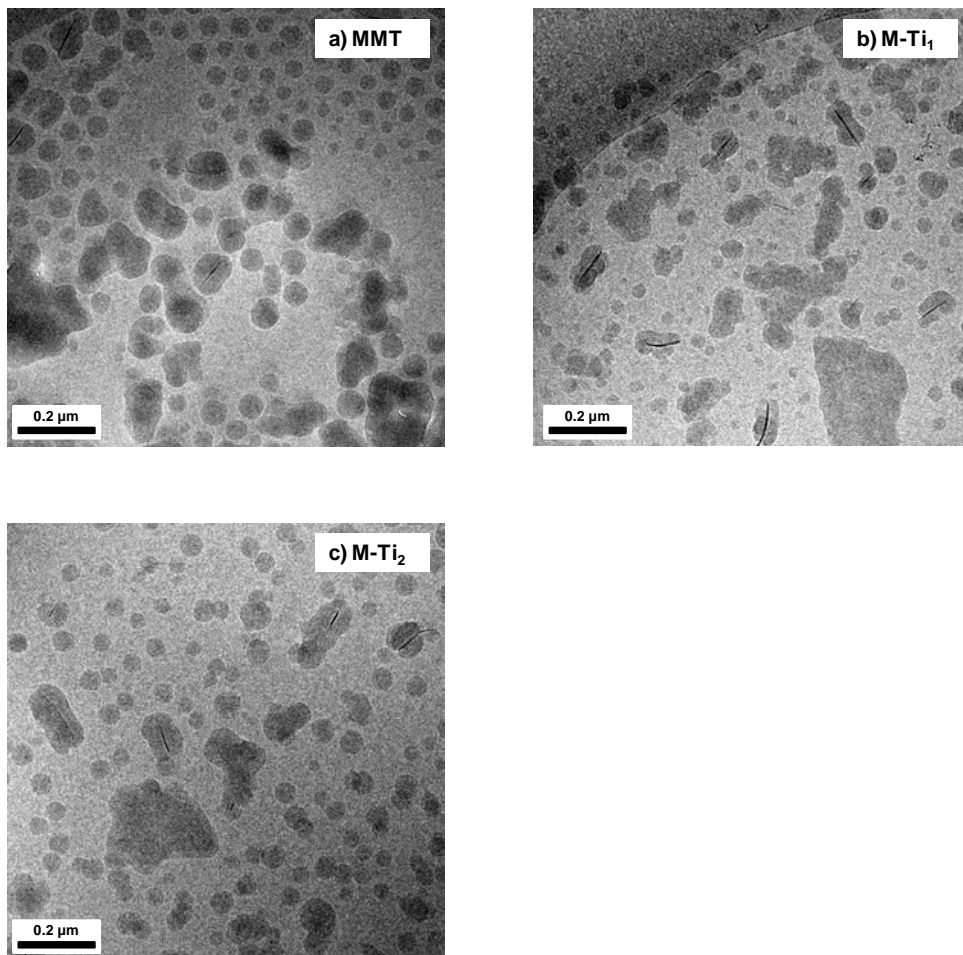


Figure 3.10 Cryo-TEM pictures of the latex/clay nanocomposites synthesized from (a) native (MMT), (b) KR39DS- (M-Ti₁) and (c) KRTTS- (M-Ti₂) modified clay particles using the following experimental conditions: H₂O (100 g), MMA (7.05 g), VA-086 (0.14 g), clay loading (3.5 wt-% based on monomer), SDBS (0.056 g) a monomer feed rate of 16 mg min⁻¹ and a reaction temperature of around 80 °C.

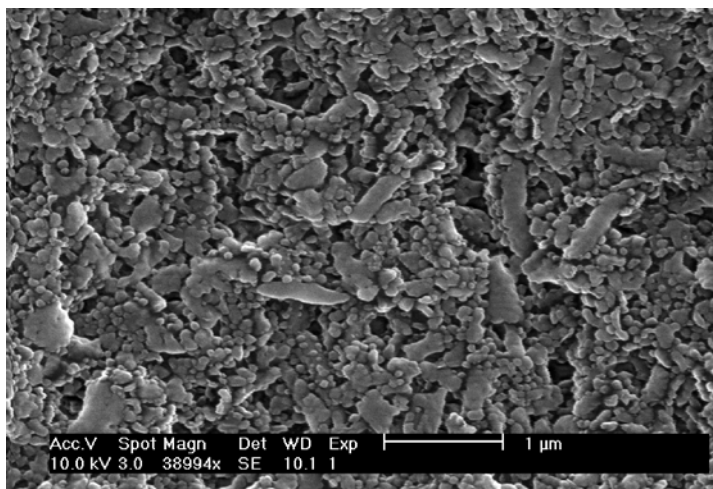


Figure 3.11 Typical SEM picture of the synthesized latex/clay nanocomposites prepared using the following experimental conditions: H₂O (100 g), MMA (7.05 g), VA-086 (0.14 g), clay loading (3.5 wt-% based on monomer), SDBS (0.056 g) a monomer feed rate of 16 mg min⁻¹ and a reaction temperature of around 80 °C

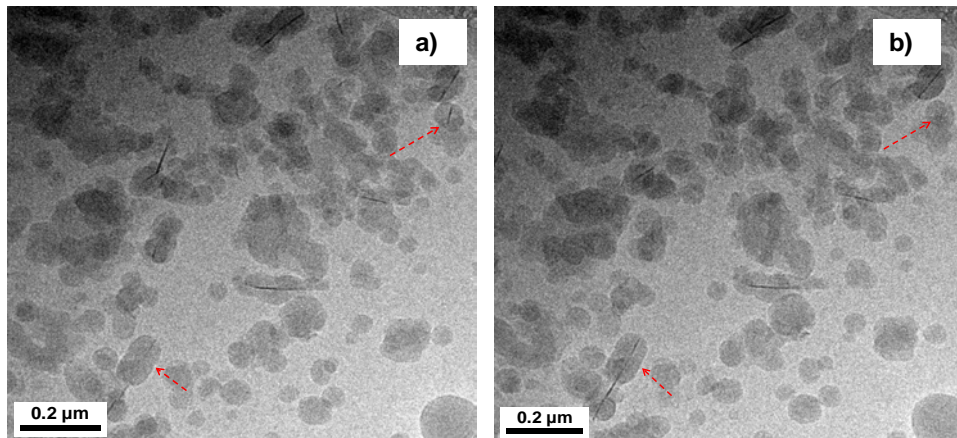


Figure 3.12 Effect of the cryoTEM tilting angle on image analyses of the LCN synthesized. The arrows in red point some latex particles where the visibility of the clay particle changes depending on the tilting angle: (a) 0 °C and (b) 12 °C. The LCN shown in these pictures were synthesized according to the recipe E-1 of Table 3.1.

3.4.2 Effect of monomer feed composition

From a thermodynamic point of view, it was very surprising that native clay particles, which are initially very hydrophilic, were found well confined in a hydrophobic polymeric shell. Indeed, hydrophilic clay would tend to minimize its contact with a hydrophobic polymeric phase in order to achieve the lowest interfacial energy. In this case, partial or even no encapsulation would be achieved. So, the encapsulation of the clay particle must be due to some other important experimental parameters which needed to be identified.

In this section, the effect of the monomer feed composition on the morphology of the LCN is reported. The recipes used for this study are described in Table 3.1 (Entries E-1a, E-2 – E.4). In Figure 3.13, we can see that the armored-morphology was obtained with the addition of butyl acrylate to the monomer feed: latex particles covered by one or a couple of layers of clay particles can clearly be observed. Also, several latex particles seem to be adsorbed onto the surface of the largest clay platelets.

The differences of the morphologies observed for the BA-MMA copolymers and the MMA homopolymer might be due to the differences in the T_g s of the encapsulating polymers. It seems that the clay platelets want to be on the surface of the latex particle but can only do this when the T_g of the encapsulating polymer is low. Indeed, if the monomer concentration is low in the locus of the polymerization and the T_g of the reacting polymer is lower than the reaction temperature, the composite phases will have high mobility as indicated by several authors.^{12, 13} Similar observations were reported by Ali et al.²⁰ who worked in the latex encapsulation of gibbsite (γ -Al(OH)₃) platelets. In their studies, the migration of the inorganic compounds towards the surface of latex particles was also favored by an increase of BA content in the encapsulating copolymer composition. It should be noted that, on the right hand side of Figure 3.13b, the dumb-bell like morphology of a LCN looks like two spherical latex particles physisorbed on both sides of the same clay platelet. Such a dumb-bell-like morphology, where the clay platelet is clearly not encapsulated, has previously been observed by several authors.^{34, 35}

So, in our experimental conditions, the LCN morphology apparently depends to a large extent on kinetic forces which more or less limit the mobility of the inorganic filler.

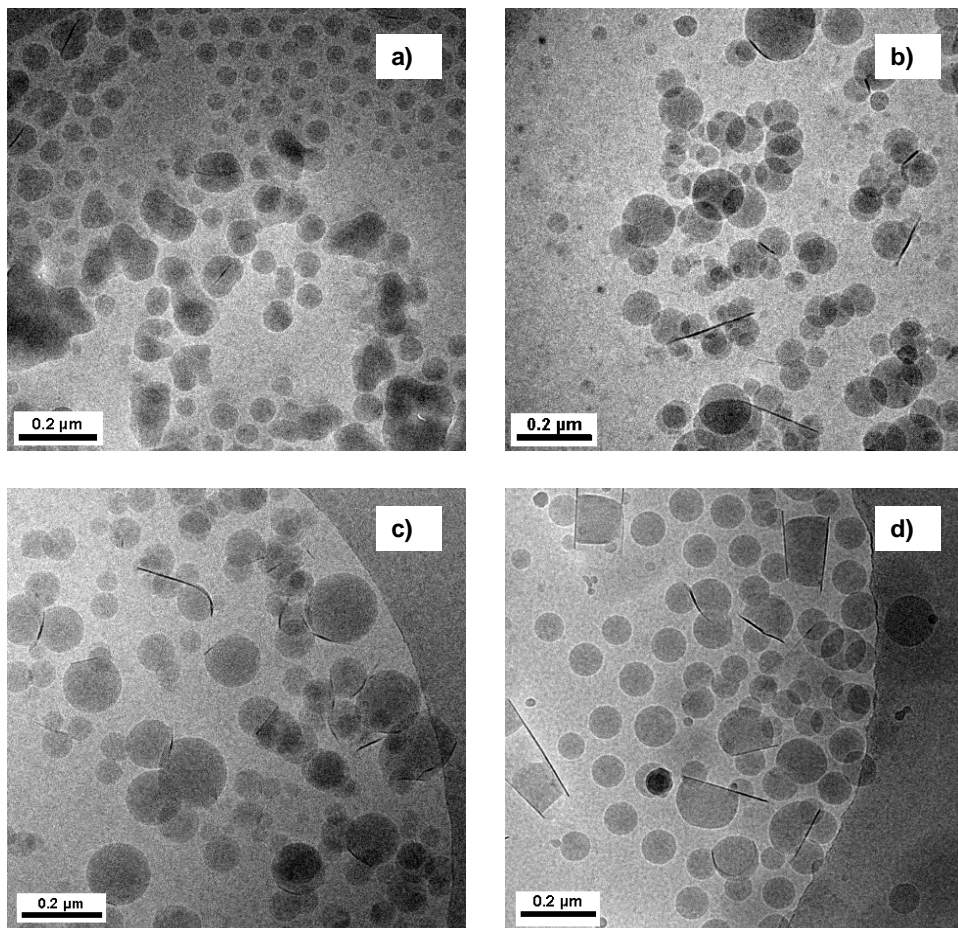


Figure 3.13 CryoTEM pictures of the latex/clay nanocomposites synthesized by varying the monomer feed composition ratio (by weigh) as such: (a) MMA:BA (1:0), (b) MMA:BA (3:1), (c) MMA:BA (3:2) and (d) MMA:BA (0:1). Experimental conditions: H₂O (100 g), monomer (7.05 g), VA-086 (0.14 g), clay loading (3.5 wt-% based on monomer), SDBS (0.056 g), a monomer feed rate of 16 mg min⁻¹ and a reaction temperature of 80 °C.

3.4.3 Effect of process type

Figure 3.14 shows the typical instantaneous monomer conversion-time profiles of the PMMA-latex encapsulation. It seems that the polymerization kinetics did not depend on the surfactant used for the encapsulation process. The polymerizations reached a final conversion within around 150 minutes after the start of the polymerization. Since the solubility of MMA in water is around 0.15 mol dm^{-3} at 20°C ³⁶ and the feed rate was about $0.16 \text{ mmol min}^{-1}$ (the total amount of monomer and water can be seen in Table 3.1), monomer molecules were barely present inside the latex particle during the entire course of the polymerization. So, as the clay encapsulations were successful under starved feed conditions, it was important to check whether it would have been otherwise in a batch process.

So, a batch, instead of a semi-batch, emulsion polymerization of MMA was performed using the recipe E-1c in Table 3.1. In Figure 3.15a we can see that most of the latex particles look spherical, suggesting no encapsulation of the clay platelets. However, few particles exhibit the armored morphology and larger aggregates of clay platelets can also be observed (c.f. Figure 3.15b). In batch conditions, the concentration of monomers in the latex particles is very high, lowering the effective T_g of the polymer.³⁷ Because of this plasticizing effect, the polymer/clay system can easily phase separate completely or partially as respectively evidenced by the presence of clusters of clay platelets and armored-like latex particles.

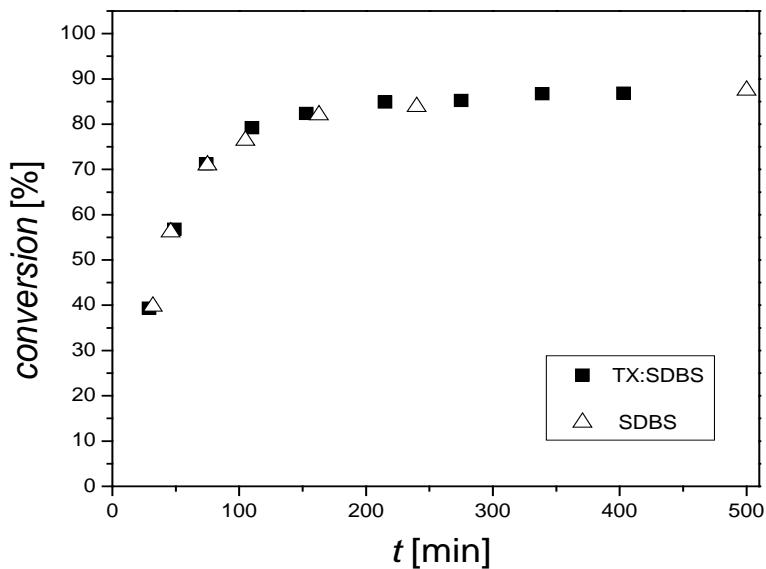


Figure 3.14 Typical instantaneous monomer conversion-time profiles of the semi-batch emulsion homopolymerization of MMA in the presence of clay. Experimental conditions: H₂O (100 g), MMA (7.05 g), VA-086 (0.14 g), clay loading (3.5 wt-% based on monomer), SDBS (0.056 g), a monomer feed rate of 16 mg min⁻¹ and a reaction temperature of 80 °C.

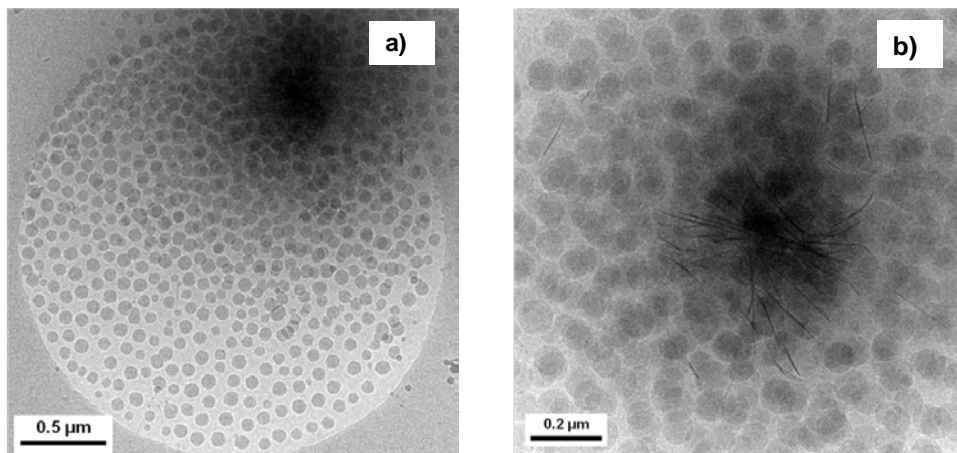


Figure 3.15 CryoTEM picture at (a) 6.5×10^3 and (b) 14.5×10^3 magnification of latex/clay nanocomposite synthesized via a batch emulsion polymerization of MMA using the following recipe: H₂O (100 g), monomer (7.05 g), VA-086 (0.14 g), clay loading (3.5 wt-% based on monomer), SDBS (0.056 g) and a reaction temperature of 80 °C.

3.4.4 Mechanism of the clay encapsulation

From the results obtained, a mechanism for the clay encapsulation can be proposed. Initially, the reaction medium consists of the dispersion of MMT particles in an aqueous solution of surfactant and initiator at 80 °C. The polymerization starts by the slow addition of monomers. At the early stage of the reaction, oligomers, uncharged in our recipes, are formed and may adsorb onto the clay surface by hydrogen bonding or dipole/dipole interactions (interactions between the carbonyl groups of the oligomers and the silicon oxide of the clay).^{38, 39} The MMT adsorbed oligomers become the locus of further polymerization: a seeded-like emulsion polymerization takes place. The evolution of the LCN morphology will strongly depend on the mobility of the inorganic phase inside the polymer matrix. When using MMA as the polymerizing monomer, the migration of MMT particles towards the latex particle surface becomes difficult as the conversion of the reaction increases. Indeed, PMMA is in its glassy state under the starved reaction conditions since its T_g is around 110 °C which is higher than the reaction temperature. The reaction was performed under starved conditions where the

polymer particles contain hardly any monomer which would otherwise lead to a strong T_g depression.³⁷ In other words, the success of the encapsulation process might have been due to diffusion restrictions of the clay platelets not being able to migrate to the polymer/water interface of the latex particles. The anisotropic morphologies observed could therefore be referred to as kinetically-controlled morphologies.

On the contrary when the comonomers BA-MMA were used, the migration of the clay towards the polymer/water interface easily occurred due to the softness of the latex particles (T_g s of the copolymers were lower than the reaction temperature). In this case, it seems that the armored-morphology, being the equilibrium morphology, can be reached.

The fact that the encapsulation might be kinetically controlled was confirmed by a simple experiment. A LCN emulsion was using the recipe of E-1b in Table 3.1 was stored in an oven for around 20 hours at 130 °C. This heat treatment was applied to soften the glassy PMMA-latex particles and therefore to facilitate the mobility of the inorganic phase. The results in Figure 3.16 demonstrate that all the LCN particles which were initially anisotropic as in Figure 3.16a exhibit, after heat treatment, the armored morphology (c.f. Figure 3.16b).

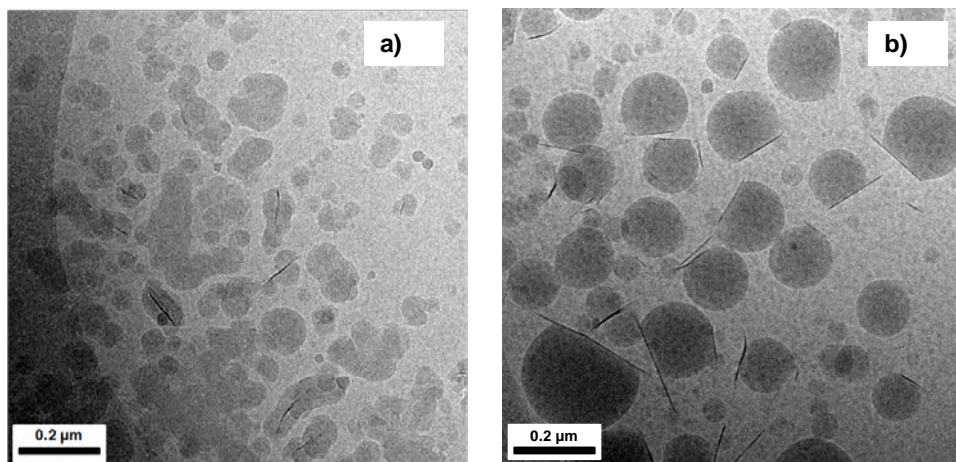


Figure 3.16 Cryo-TEM pictures of PMMA- latex/clay nanocomposites (a) before and (b) after heat treatment at 130 °C for ~ 20 hours. The experimental conditions used to synthesize the LCN are: H₂O (100 g), monomer (7.05 g), VA-086 (0.14 g), clay loading (3.5 wt-% based on monomer), SDBS (0.056 g), a monomer feed rate of 16 mg min⁻¹ and a reaction temperature of 80 °C.

3.4.5 Effects of surfactant type, surfactant concentration and clay loading on the clay/polymer interaction of the LCN synthesized

A set of LCNs were prepared using a two-level full factorial designs of experiment by varying the surfactant type, the surfactant concentration and the clay loading, all the other parameters remaining constant (c.f. Table 3.3). Table 3.4 shows the difference ΔT_g between the T_g of dried powders of the LCN synthesized and of a reference PMMA (110 °C). The analysis of variance (ANOVA) was used to estimate the main and the interaction effect of the variables (c.f Table I.1 in Appendix I).

Table 3.3 Definition of process variables and levels of the 2³ design of experiments

Variables	Notations	Levels	
		-	+
Surfactant type	A	TX-100:SDBS ^{a)}	SDBS
[Surfactant](x CMC)	B	0.5	0.9
Clay loading (wt- %) ^{b)}	C	3.5	5.5

^{a)} Mixture of TX-100:SDBS with a weight ratio 6:1

^{b)} Based on the total amount of monomer

Table 3.4 The results of the 2³ design of experiments applied in this study

Dried LCN	Factors			ΔT_g ^{a)}
	Surfactant type	[Surfactant]	Clay loading	°C
1	-	+	+	11
2	+	-	+	3
3	-	-	+	11
4	-	+	-	0
5	+	-	-	11
6	+	+	-	-4
7	+	+	+	2
8	-	-	-	11

^{a)} Difference between the T_g s of the dried LCN and of a reference PMMA (110 °C)

Chapter 3

According to Table I.1 in Appendix I the surfactant type (A), the surfactant concentration (B), the clay loading (C), the interactions AC and BC seem to have significant effect on ΔT_g at confidence levels between 80 % and 90 %. The interaction AB seems to have the least influence at 75 % confidence level.

Apparently, an increase of the surfactant concentration will negatively impact the encapsulation process. From section 3.4.4, two nucleation mechanisms may compete. Indeed, the latex particle nucleation might take place onto the surface of the inorganic filler or in the aqueous phase via a homogeneous mechanism (since there are no micelles and monomer droplets present in the reaction medium).⁴⁰ The polymerization on the surface of the clay particles should be favored by a low concentration of surfactants in the continuous phase as demonstrated by Chern et al..⁴¹ The homogeneous mechanism will lead to the formation of latex particles that do not contain clay platelets, decreasing the encapsulation efficiency. The number of "empty" latex particles thus created will increase with the concentration of surfactant in excess in the aqueous phase. This result in a decrease of the amount of polymers which are effectively in contact with the inorganic particle in the LCN film and, therefore, a decrease of the T_g as well. Such effect of the surfactant concentration, however, strongly depends on the clay loading (c.f. Figure II.b in Appendix II). Indeed, in contrast with a clay loading of 3.5 wt-%, the T_g remains almost constant, independent of the surfactant concentration with a clay loading of 5.5 wt-%. Some explanations can be found for this last observation. Indeed, as the clay is supposedly a site of polymerization, the total number of LCN particles should increase with the concentration of the inorganic compound. The concentration of surfactant dissolved in the aqueous phase should decrease as more surfactant molecules are necessary for the LCN particle stabilization. The homogenous nucleation being therefore limited, the polymerization essentially takes place on the surface of the clay particle. So, for a clay loading of 5.5 wt-%, the surfactant may have been used mainly for the LCN particle stabilization. In this case, the total polymer/clay interfacial area has not really changed by varying the surfactant concentration: the T_g kept a nearly constant value.

Also, according to Figure II.a (c.f. Appendix II), the mixed surfactant system clearly leads to higher increase of ΔT_g than the anionic one. The non-ionic

surfactants Triton X-100 can strongly adsorb on the surface of the clay particle^{22, 23} whereas SDBS is known to have little sorption on the inorganic moiety.²⁵ The use of the mixed surfactant system (TX-100 representing 85 % of the surfactant formulation) might have enhanced the solubilization of monomers around the clay particles. The surface coverage of the inorganic moiety by the encapsulating polymers might therefore be more important when using the mixed surfactant system instead of the anionic one, resulting to higher clay/polymer interfacial area in the LCN film.

Another interesting result is that the effect of clay loading on ΔT_g depends on the surfactant type (c.f. Figure II.c). Indeed, the clay loading will have little effect on ΔT_g when the anionic surfactant is used at a certain concentration. In contrast, a higher clay loading will markedly increase the ΔT_g of the LCN synthesized with the mixed surfactant system. This result supports the idea that nucleation of the latex particles in the aqueous phase, instead on the surface of the clay particle, might be favored when using the anionic surfactant. Again, this may affect the total clay/polymer interfacial area in the LCN film.

In summary, one can conclude that a good clay/polymer interaction should be obtained when using the mixed surfactant system at half its critical micelle concentration and with a clay loading of 5.5 wt-%.

3.5 ORIENTATION OF THE CLAY PLATELETS IN THE LCN FILMS

The drying of the LCN was obtained by slow evaporation of water at room temperature. At the beginning of the drying process, the particles move freely and randomly in the aqueous phase (Brownian motion). The particle motion becomes more restricted as water evaporates and stops when the individual latex particles irreversibly coalesce. The Brownian motion may explain the random orientation of the clay platelets in the polymeric films in Figure 3.17, despite the anisotropy of the LCN synthesized.

In fact, applying external forces at high viscosity of the drying coating layer might induce more orientation of the clay platelets because the Brownian motion is no

longer operative.⁴² Another option is to use the pseudoplastic behavior of polymers.⁴³

The LCN synthesized should, however, exhibit improved barrier properties as compared to the corresponding unfilled polymer film. Indeed, according to Figure 3.2, the relative permeability will be lower than for the pure polymer even in case of a random orientation of the clay sheets. In addition, Diaconu et al. have recently shown that LCN films with exfoliated structure exhibited improved barrier properties.^{16, 17} The mechanical properties such as the relative modulus should also increase due to the high aspect ratio of MMT.^{3, 16, 17}

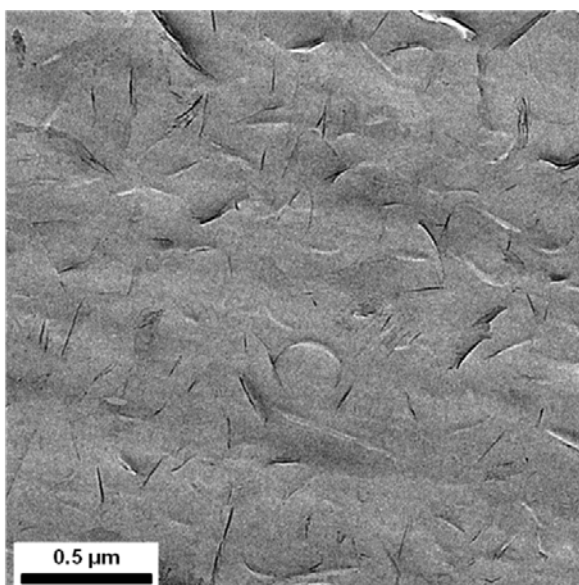


Figure 3.17 Typical TEM picture of cross-sectioned films of the latex/clay nanocomposite synthesized using the following recipe: H₂O (100 g), monomer (7.05 g), VA-086 (0.14 g), clay loading (3.5 wt-% based on monomer), SDBS (0.056 g), a monomer feed rate of 16 mg min⁻¹ and a reaction temperature of 80 °C.

3.6 CONCLUDING REMARKS

Single clay platelets have been successfully encapsulated via starved-feed emulsion polymerization of MMA. It was found that the organic modification was not stable in the emulsion conditions but also not necessary in order to successfully achieve clay encapsulation. The most important result is that the monomer feed composition strongly influenced the morphology of the LCN. Indeed, when the T_g of the encapsulating (co)polymer was well above the reaction temperature (hard polymer), anisotropic latex particles containing single clay platelets were mainly observed. In contrast, the use of a soft encapsulating polymer led to armored-like latex particles. Furthermore, only starved-feed monomer addition led to successful encapsulation: a batch process generated important aggregates of clay particles and only a few armored-like latex particles. A heat treatment of the LCN synthesized showed that the clay encapsulation process was mainly kinetically controlled. A mechanism of encapsulation has been proposed, where the clay particles act as seed in the process (polymerization carried out from the surface of the inorganic particle). Concerning the clay/polymer interaction, the clay loading, the surfactant concentration and type were all found to have significant effects. According to the statistical model developed via a 2^3 factorial design of experiment, a good clay/polymer encapsulation should be achieved by using the mixed surfactant system Triton X-100: SDBS (weight ratio 6:1), at half its critical micelle concentration and with a clay loading of 5.5 wt-%.

In summary, the experimental parameters which led to successful clay encapsulations have been clearly identified and could be easily controllable. Under these conditions, the primary size and shape distributions of the clay particles, serving as templates in the reaction, might be the key parameters controlling the development of the LCN morphology. Such parameters can be fine-tuned by using numerous fractionation techniques commercially available (ultracentrifugation, field flow separation, etc.).

REFERENCES

1. Negrete-Herrera N.; Letoffe J.-M.; Puteaux J.-L.; David L.; Bourgeat-Lami E. *Langmuir* 20: 1564 (2004).
2. Voorn D.-J.; Ming W.; van Herk A.M. *Macromol. Symposia* 245: 584 (2006).
3. Beall G.W.; Powell C.E. *Fundamentals of Polymer-Clay Nanocomposites*. Cambridge University Press, New York (2011).
4. Bourgeat-Lami E.; Duguet E. *Polymer encapsulation of inorganic particles*, in *Functional Coatings*, ed by Ghosh S. K.. WILEY-VCH Verlag GmbH & Co. KGaA Weinheim, 85 – 152 (2006).
5. Monte S.J. ; Sugerman G. *Polym Eng Sci* 24 : 1369 (1984).
6. Miyatake K.; Ohama O.; Kawahara Y.; Urano A.; Kimura A. *Sei Technical Review* 65 : 21 (2007).
7. Yu-Song P. *Micro Nano Lett* 6 : 129 (2011).
8. Caris C.H.M.; Kuijpers R.P.M.; van Herk A.M.; German A.L. *Macromol. Symp.* 35/36 : 535 (1990).
9. He H.; Duchet J.; Galy J.; Gerard J.-F. *J. Colloid Interface Sci.* 288 : 171 (2005).
10. Wang Z.-W.; Wang T.-J. *J. Colloid Interface Sci.* 304 : 152 (2006).
11. Reyes Y.; Asua J.M. *Polymer* 48 : 2579 (2010).
12. Karlsson L.E.; Karlsson O.J.; Sundberg D.C. *J. Appl. Polym. Sci.* 90 : 905 (2003).
13. Sundberg D.C.; Durant Y. *Polym. React. Eng.* 11 : 379 (2003).
14. González-Ortiz L.J.; Asua J.M. *Macromolecules* 29 : 4520 (1996).

Chapter 3

15. Negrete-Herrera N.; Puteaux J.; David L.; de Haas F.; Bourgeat-Lami E. *Macromol. Rapid Comm.* 28 : 1567 (2007).
16. Diaconu G.; Asua J.M.; Paulis M.; Leiza J.R. *Macromol. Symp.* 259 : 305 (2007).
17. Diaconu G. ; Paulis M. ; Leiza J.R. *Polymer* 49 : 2444 (2008).
18. Greesh N.; Hartmann P.C.; Cloete V.; Sanderson R.D. *Polymer* 46 : 3619 (2008).
19. Greesh N.; Hartmann P.C.; Cloete V.; Sanderson R.D. *Macromolecular Mat. Eng.* 294 : 206 (2009).
20. Ali S.I.; Heuts J.P.A.; Hawket B.S.; van Herk A.M. *Langmuir* 25 : 10523 (2009).
21. Bharadwaj R. *Macromolecules* 34 : 9189 (2001).
22. Paria S.; Khilar K. *Adv. Colloid Interface Sci.* 110 : 75 (2004).
23. Sánchez-Martín M.J.; Dorado M.C.; del Hoyo C.; Rodríguez-Cruz M.S. *J. Hazard. Mater.* 150 : 115 (2008).
24. Lin K.-J.; Jeng U.S.; Lin K.-F. *Mater. Chem. Phys.* 131 : 120 (2011).
25. Yang K. ; Zhu L. ; Xing B. *Environ. Pollut.* 145 : 571 (2007).
26. Caris C.H.M. *Polymer encapsulation of inorganic submicron particles in aqueous dispersion*. Eindhoven University of Technology, PhD thesis, 28 – 39 (1990).
27. Tiwari R.R.; Khilar K.C.; Natarajan U. *Appl. Clay Sci.* 38 : 203 (2008).
28. Xie W.; Gao Z.; Liu K.; Pan W.-P.; Vaia R.; Hunter D.; Singh A. *Thermochim. Acta* 367: 339 (2001).

Chapter 3

29. De Paiva L.B. ; Morales A.R. ; Díaz F.R.V. *Appl. Clay Sci.* 42 : 8 (2008).
30. Schubert U. *J. Mater. Chem.* 15 : 3701 (2005).
31. Negrete-Herrera N.; Puteaux J.; David L.; Bourgeat-Lami E. *Macromolecules* 39: 9177 (2006).
32. Hielscher T. *Ultrasonic Production of Nano-Size Dispersions and Emulsions*, in Proceedings of European Nanosystems Conference ENS'05 (2005).
33. Negrete-Herrera N.; Puteaux J.; Bourgeat-Lami E. *Prog. Solid State Chem.* 34 : 121 (2006).
34. Faucheu J. ; Gauthier C. ; Chazeau L. ; Cavaillé J.-Y. ; Mellon V. ; Bourgeat-Lami E. *Polymer* 51 : 6 (2010).
35. Mičušík M. ; Bonnefond A. ; Reyes Y. ; Bogner A. ; Chazeau L. ; Plummer C. ; Paulis M. ; Leiza J.R. *Macromol. React. Eng.* 4 : 432 (2010).
36. Sajjadi S.; Yianneskis M. *Polym React Eng* 11 : 715 (2003).
37. Schoonbrood H. *Emulsion co- and terpolymerization Monomer partitioning, kinetics and Control of Microstructure and Mechanical Properties*. Eindhoven University of Technology, PhD thesis, 151 – 152 (1994).
38. Choi Y.; Ham H.; Chung I. *Chem. Mater.* 16 : 2522 (2004).
39. Sheibat-Othman N.; Cenacchi-Pereira A.M.; Dos Santos A.M.; Bourgeat-Lami E. *J. Polym. Sci. Part A: Polym. Chem.* 49: 4771 (2011).
40. Van Herk A.M. *Chemistry and technology of emulsion polymerization*. Blackwell Publishing Ltd, Oxford (2005).
41. Chern C.-S. ; Lin J.-J. ; Lin Y.-L. ; Lai S.-Z. *Eur. Polym. J.* 42 : 1033 (2006).
42. Malwitz M.M.; Lin-Gibson S.; Hobbie E.K.; Butler P.D.; Schmidt G. *J. Polym. Sci. Part B Polym. Phys.* 41 : 3237 (2003).

Chapter 3

43. Malwitz M.M.; Schmidt G. *Polymer* 8 : 103 (2003).

Chapter 4

The Morphology of Three-Phase PS/PMMA/MMT Clay/Latex Particles

Abstract: This chapter describes the synthesis of three-phase PMMA/PS/MMT latex particles from clay-containing PMMA seeds via (semi-)batch emulsion polymerization of styrene. The morphology of the particles was analyzed via transmission electron microscopy. For the interpretations of the results obtained, the theories established to understand the morphology development of two-phase latex particles could be applied. An interesting observation was that clay platelets might act as physical barriers against diffusion of polymeric phases within the seed polymer.

4.1 INTRODUCTION

In order to understand the effect of experimental parameters i.e. recipe and operation on particle morphology, it is of utmost importance to correctly characterize and interpret the morphology obtained.

In this chapter, we propose to study the morphology of three-phase PS/PMMA/MMT hybrid latex particles. Facing a lack of theoretical background for an understanding of the morphology development of hybrid systems, our main aim is to obtain reliable experimental data and give sound interpretations of the results obtained.

For our investigations, PMMA-seeded emulsion polymerizations of styrene are carried out in the presence of native clay particles. The clay particles are introduced in the preparation of the PMMA seed polymers using the same experimental strategy as in Chapter 3 (c.f. section 3.2.4). The synthesis of the hybrid particles are such that kinetics (i.e. polymer radicals' transport) limits the development of the equilibrium morphology which should be an inverted core-shell as polystyrene is much more hydrophobic than PMMA.¹⁻⁴ Also, from a thermodynamic point of view, the clay platelets should be situated at the surface of the latex particles due to their high hydrophilicity.⁵⁻⁷ The relative size of the seed latexes and the mode of operation (batch vs. semi-batch) of the second stage monomer styrene are varied in order to lower the transport resistance operating against the evolution of the equilibrium morphology. Some experiments are performed in the absence of clay (blank experiments) in order to better understand the role of the inorganic moiety in the development of the morphologies obtained. Four case studies, classified according to the monomer addition and the relative size of the seed, are described through this chapter. For the interpretations of the results, the theories explaining the morphology development of two-phase latex systems are used (see Chapter 2).

The morphologies of the hybrid PS/PMMA/MMT latex particles are analyzed via TEM. Some TEM samples are stained with ruthenium tetroxide to enhance the contrast between the phases. The PS-rich regions, selectively stained by RuO₄ due to the aromatic structure of PS, should appear much darker than the PMMA-rich

regions in the TEM picture. TEM imaging of ultramicrotomed sections are made in order to gain more insight into the internal structure of the latex particles.

4.2 EXPERIMENTAL

4.2.1 Chemicals

Styrene (Sty, Aldrich >99%), methyl methacrylate (MMA, Aldrich 99 %) and butyl acrylate (BA, Aldrich >99%) were purified from inhibitors by passing them through a column filled with basic aluminum oxide. Apart from the monomers, all chemicals were used as received. Potassium persulfate (KPS, Aldrich > 99 %) and ammonium persulfate (APS, Aldrich > 99 %) were used as initiators. Sodium dodecyl sulfate (SDS, Merck, p.a), sodium dodecyl benzenesulfonate (SDBS, Aldrich) and Triton X-100 (TX-100, Aldrich) were used as surfactants and sodium bicarbonate (NaHCO_3 , Merck, p.a) as a pH buffer. Water was deionized using the Super Q reverse osmosis (Millipore) set up. The other chemicals, N,N,N',N' tetramethylethylenediamine (TMEDA, Aldrich ~ 99%) and potassium hydroxide (KOH, Sigma-Aldrich 90 %) were used as received.

4.2.2 Preparation of the seed polymers

All the following reactions were performed in flat – bottomed glass reactors with baffles, equipped with a mechanical stirrer (45° pitched downflow six-bladed impeller), a temperature indicator, a reflux condenser and an inert gas inlet. The system was heated by circulating water through the cylinder-jacket of the reactor.

The seed latex sp-1 was prepared via a typical batch emulsion polymerization as follows. The reactor (250 mL) was initially loaded with 163 g of distilled water and de-aerated with argon for a period of 30 minutes. After addition of a mixture of surfactants (0.24 g of SDBS and 2.71 g of TX-100), the argon flow was reduced to avoid foam formation. 90 g of MMA was charged dropwise into the reactor while purging with argon and stirring at a rate of 320 rpm. The reaction temperature (T_r) was slowly raised to 75 °C, and after temperature stabilization, 0.44 g of KPS

Chapter 4

(having a half-life $t_{1/2}$ of about 4 hours at T_r) were added. The reaction time was about 2.5 hours.

A semi-batch surfactant-free emulsion polymerization was performed to prepare sp-2. The reactor was initially charged with 187 g of distilled water and thereafter heated at 80 °C. After addition of 0.47 g of APS ($t_{1/2} \approx 4$ h), the reaction medium was allowed to stir for 10 minutes. Thereafter, 66 g of MMA were fed into the reactor at a rate of 0.5 mL min⁻¹ using a titrator 776 Dosimat (Metrohm AG). After monomer feeding, the reaction was carried out for an additional two hours.

The PMMA and the PMMA/clay latexes, named sp-3 and c-sp-1, respectively, were synthesized as described in Chapter 3 section 3.2.4 using the recipes E-0 and E-1 in Table 3.1 (TX-100:SDBS was used as surfactant at 0.5 times its CMC concentration) respectively. The seed c-sp-2 corresponds to a growth of the seed c-sp-1 via a semi-batch emulsion homopolymerization performed as follows. The initial reactor was charged with 103 g of water, 1 g of seeds c-sp-1, 0.02 g of NaHCO₃ and 0.02 g of SDBS. 11.9 g of MMA and an aqueous solution of KPS (around 2.5 mL at a concentration approximating 0.1 M) were fed simultaneously in the reaction medium using two syringe pumps (NE-1000, New Era Pump systems Inc) for three hours. The stirring rate and the reaction temperature were 300 rpm and 75 °C respectively. All the PMMA/MMT latex particles thus produced exhibited anisotropic morphologies (c.f Figure 4.1).

The characteristics of the seed polymers are given in Table 4.1.

Table 4.1 Characteristics of the (hybrid) PMMA seeds used

Seed names	sp-1	sp-2	sp-3	c-sp-1	c-sp-2
D_z (nm)	220	598	392	200	176
PDI	0.017	0.003	0.004	0.123	0.305
MMT loading (%)				3.5	0.5
Solid content (%)	35.6	25.5	5.7	6.1	8.4
T_g (°C)	107	106	114	117	113

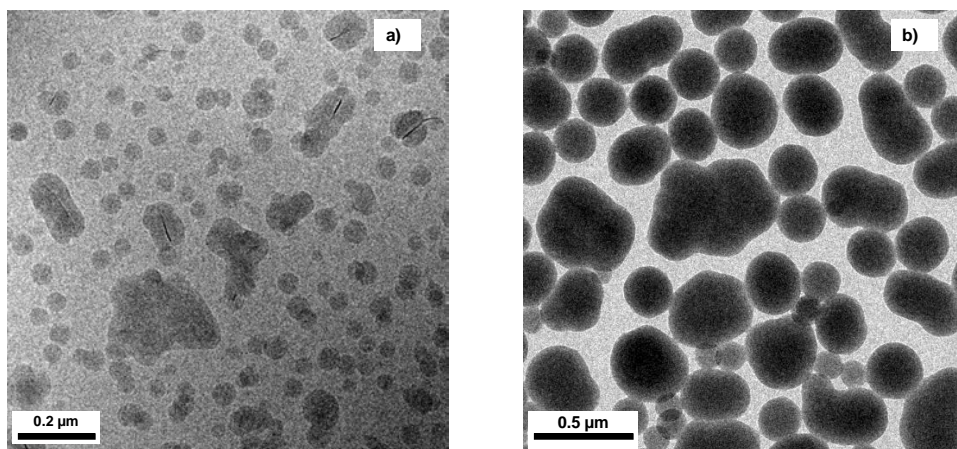


Figure 4.1 (Cryo-)TEM pictures of the following seeds: (a) c-sp-1 prepared using recipe E-1a (see chapter 3) and (b) c-sp-2 prepared using 11.9 g MMA, 0.06 g KPS, 0.02 g NaHCO_3 , 0.02 g SDBS and 1 g of c-sp-1 seeds. The monomer and an aqueous solution of initiators (~ 0.1 M) were fed simultaneously in the reaction medium for 3 h.

4.2.3 Second stage polymerization of styrene

Semi-batch process

The initial reactor loading consisted of distilled water, surfactant and the seed latex. After warming up the reaction medium to 80 °C, KPS initiator ($t_{1/2} \approx 4\text{h}$), was added to the reactor at once. Subsequently, styrene was fed at a rate of 3 mmol min⁻¹ (based on the total amount of monomer). Stirring and heating of the reaction was kept for three hours.

Batch process

This second stage polymerization was initiated by a redox system KPS (oxidant)/ TMEDA (reductant). The reactor was initially charged with distilled water, the surfactant, the buffer and the seed emulsion. The reaction medium was heated up to 40 °C. After stabilization of the temperature, the total amount of monomer was added at once followed immediately by the addition of an aqueous solution of TMEDA and then of KPS.

The recipes used for the reactions performed are given in Table 4.2.

Table 4.2 Recipes used for the synthesis of the multiphase latex particles and their characteristics

Case studies	1		2		3		4	
Experiment	EP-1	EP-2	EP-3	EP-4	EP-5	EP-6	EP-7	EP-8
Seed name	sp-2	c-sp-2	sp-1	c-sp-1	sp-2	c-sp-2	sp-3	c-sp-1
Water (g)	202.3	98.6	170.2	68.2	212	60.6	59.7	58.9
Seed latex (g)	7.6	2.3	7.5	2.2	11	2.5	1.7	2.2
Sty (g)	7.6	6.1	19.9	6.4	11	3.1	3.4	3.7
KPS (g)	0.17	0.15	0.15	0.14	0.05	0.008	0.012	0.011
TMEDA (g)					0.02	0.004	0.01	0.007
NaHCO ₃ (g)					0.13	0.11	0.1	0.12
SDBS (g)	0.03	0.02		0.002	0.03	0.05	0.04	
TX-100 (g)	0.12	0.1		0.08				
Sty feed rate (mmol min ⁻¹)	3	3	3	3				
Characteristics								
D _z	731		362	235.8	731		281	0.142
PDI	0.03		0.06	0.142	0.08		0.271	0.183
Solid content (%)	6.8	7.7	9.5	11.8	8.8	7.8	8.3	8.6

4.2.4 Characteristics

Average particle diameters

The determination of the average particle diameters was performed by the use of a Malvern Zetasizer Nano ZS dynamic light scattering apparatus, with a He-Ne laser as the light source (at a fixed wavelength of 633 nm). This apparatus was used at a scattering angle of 173 °C and at a temperature of 25 °C. The measurements were done after dilution of the samples with deionized water. An indication of the particle size distribution (PSD) was determined with the same equipment. The analysis of the PSD was based on the intensity distribution pattern generated by DLS, assuming that the particles are spherical in shape.

Ultramicrotomy

The dried samples were embedded at room temperature in an epoxy resin (Epofix). Ultrathin sections (70 nm) were obtained at room temperature using a Reichert-Jung Ultracut E ultramicrotome equipped with a diamond knife. The sections were put on a 200 mesh copper grid with a carbon support layer. The sections were also examined with the Sphera TEM instrument (FEI Company).

The DSC measurements and the TEM characterizations are performed as described in Chapter 3 section 3.2.

4.3 CASE STUDY 1: SEMI-BATCH ADDITION OF STYRENE, LARGE SEED

In this case study, large-sized seed latexes are used and a semi-batch addition of the second stage styrene monomers is performed in order to force the second stage polymerization in the outer region of the host polymers.

Figures 4.2a, 4.3a and 4.4 show the morphology of the latex particles synthesized for this case study. Some similarities between the conventional and the hybrid latex systems can easily be observed from these images. The latex particles exhibit outer regions composed of several PS domains with a well-defined PMMA-rich core. Obviously, the expected equilibrium morphology which should be an inverted core-shell, has not been reached for both types of latex particles.¹⁻⁴ From

these observations, it seems that the second stage monomer preferentially reacted in the outer regions of the latex particles indicating that the penetration of oligomer radicals has been quite restricted during the course of the polymerization.^{8,9} This is actually further evidenced by the observation of similar shape between the resulting multiphase latex particle and the host polymer acting as a morphological template. However, the presence of small occlusions of PS in the interior of the particles also reveals that some reacting species could substantially penetrate in the interior of the seed polymer and that phase separation took place (c.f. Figure 4.4). This might have occurred at the early stage of the polymerization due to the initial presence of monomer molecules within the seed polymer. Indeed, the local concentration of monomer, which acts as a plasticizer, was probably quite high initially due to the fast feeding rate applied for these experiments. This plasticizing effect must have promoted the diffusion of the oligomer radicals. However, the seed polymers were completely depleted of monomer quite rapidly: almost the complete amount of styrene monomer was consumed within 20 minutes of reaction as determined by gravimetric measurements. Consequently, the host polymer matrix must have quickly recovered its glassy state (its T_g being well above the reaction temperature which was around 80 °C) forcing further formation of second stage polymers around its external regions. The phase consolidation (or phase growth), which should occur at the late stage of the reaction have been kinetically inhibited due to the glassy nature of both polymers (the T_g of PS should be around 90 and 110 °C).

In contrast to the conventional latex particles, a split of the PMMA core into two regions can sometimes be observed for the hybrid systems (c.f. Figure 4.3a). This unusual configuration, particularly visible for dumb-bell-like hybrid latex particles, might be due to the presence of clay platelets within the polymer matrix. Despite the impossibility to see the inorganic phase in Figure 4.3a, the dumb-bell like morphology observed suggests that the clay platelets are located between the two PMMA regions as can be seen in Figure 4.1. TEM analysis of ultramicrotomed sections of the hybrid particles was performed in order to see the orientation of the inorganic moieties within the polymer matrix (c.f. Figure 4.4b). Surprisingly, a split of the core of the latex particles could not be observed in the TEM picture of the microtomed sections. Such an observation cannot be conclusive because the sample photographed in Figure 4.4b may not be representative of the "true"

morphological features of the hybrid latex particles: only a few tens of latex particles, cut at random positions, are represented.

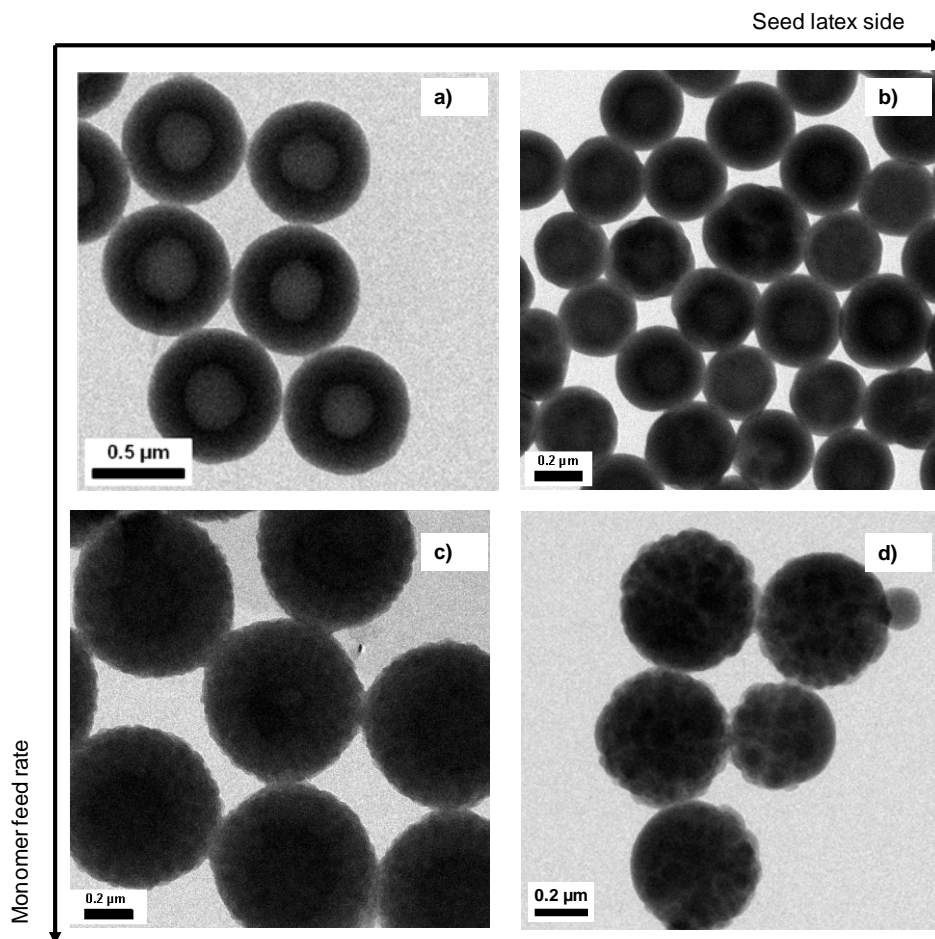


Figure 4.2 TEM pictures of two-phase PMMA/PS latex particles prepared using the recipe (a) EP-1 (case study 1), (b) EP-3 (case study 2), (c) EP-5 (case study 3) and (d) EP-7 (case study 4).

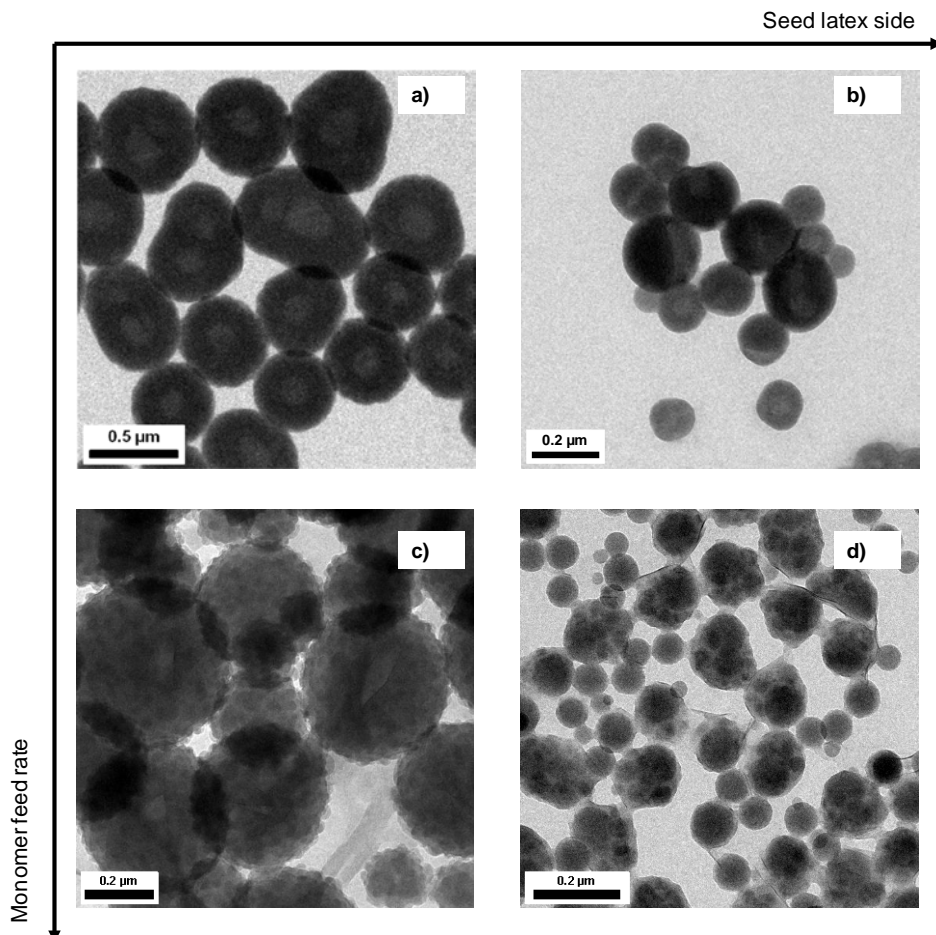


Figure 4.3 TEM pictures of multiphase hybrid PMMA/PS/MMT latex particles prepared using the recipe (a) EP-2 (case study 1), (b) EP-4 (case study 2), (c) EP-6 (case study 3) and (d) EP-8 (case study 4).

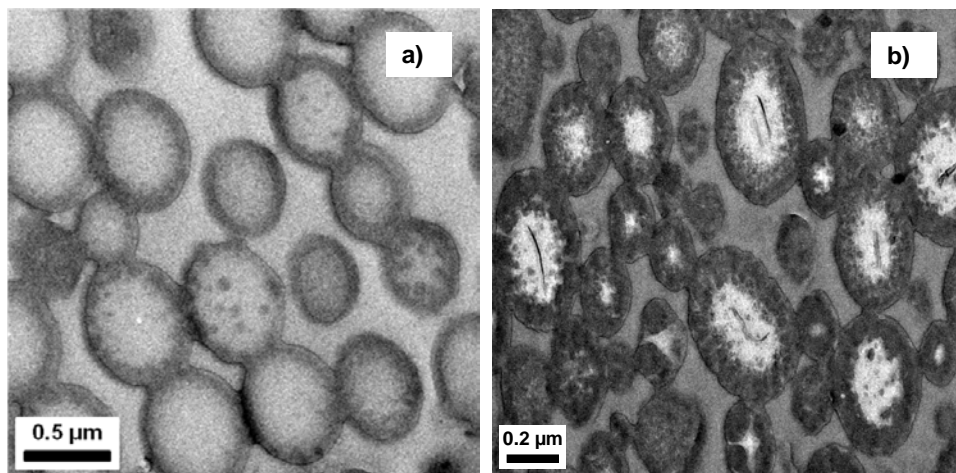


Figure 4.4 TEM pictures of cross- sections of (a) two-phase PMMA/PS and (b) multiphase hybrid PS/PMMA/MMT latex particles prepared using the recipes EP-1 and EP-2 respectively (case study 1).

4.4 CASE STUDY 2: SEMI – BATCH ADDITION OF STYRENE, SMALL SEED

Similarly to the previous section, the second-stage emulsion polymerization is operated via a semi-batch addition of styrene. The seed latexes used in this case are, however, smaller than the ones of the preceding study. During reaction, styrene oligomer radicals formed in the aqueous phase penetrate into the host polymer matrix. The extent of penetration of the oligomer radicals depends on the diffusion and the termination frequencies of the radical species. Both parameters will be affected by the local monomer concentration, the rate of radical production and the size of the latex seed.⁸ The smaller the size of the latex seed, the deeper the penetration of the second stage polymer within the host polymer should be.

Figure 4.2b shows different kinds of morphology for the conventional latex particles. Indeed, some particles seem to have adopted a spherical onion-like morphology composed of a thin black PS-rich region sandwiched between two dark gray regions which probably consist of a mixture of PMMA- and PS-rich polymers; while other particles have a bumpy appearance with larger PS-rich domains in the interior of the particle and a thin PMMA shell.

Chapter 4

The observation of different kinds of morphology in one single latex emulsion is typical for experiments where the morphologies develop under kinetic control.^{1,10} Although phase separation and phase consolidation have obviously been very limited; the particle structures are apparently closer to the equilibrium state expected for this kind of system. This is due to the fact that the particle phases were allowed to diffuse to a higher extent as evidenced by a deeper penetration of the second stage polymers.

In Figure 4.3b, similar morphological characteristics can be observed for the hybrid particles. The position of the clay platelets within the latex particle can also be seen in Figure 4.5. It can be observed that the clay platelets, which were initially in the core of the particle, seem to have shifted towards the surface of the latex particle. This observation shows that the inorganic particles were quite mobile during synthesis and tried to be in contact with the aqueous phase. The position of the clay particles on the latex particle surface is indeed thermodynamically favorable because of the high hydrophilicity of the inorganic.

In contrast to the blank experiment, the synthesis of the hybrid particles seems to have produced a fair number of secondary PS particles as observed in Figure 4.3b and 4.5. The formation of secondary particles might have been promoted by the presence of clay platelets, the only missing parameters in the blank experiment. In this case, the clay platelets seem to have actually acted as physical barriers against polymerization within the seed polymer. An explanation of this last result could be that clay particles, more or less situated on the surface of the latex particles, might have prevented penetration of hydrophobic polymer radicals because of their high hydrophilicity, high aspect ratio and impenetrability.

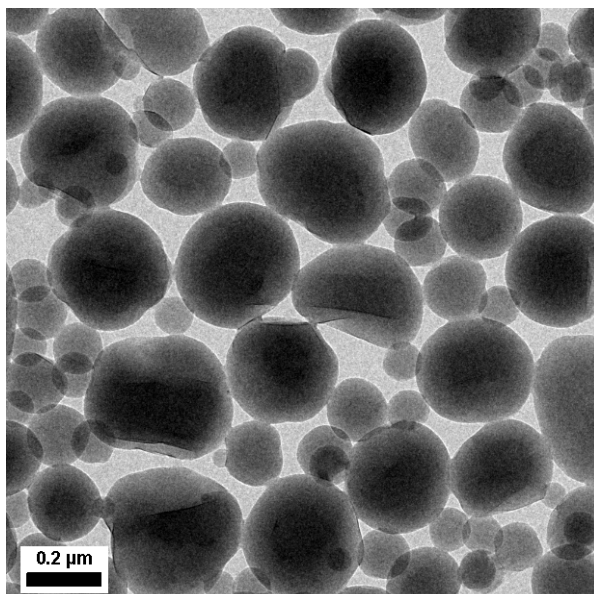


Figure 4.5 A TEM picture of unstained multiphase hybrid PS/PMMA/MMT latex particles prepared using the recipe EP-4.

4.5 CASE STUDY 3: BATCH ADDITION OF STYRENE, LARGE SEED

For this case study, a batch addition of styrene, instead of a feed, was performed in order to obtain a high concentration of monomers within the seed polymers which should allow a good mobility of the particle phases.

From Figures 4.2c and 4.3c it can be seen that both the conventional and the hybrid latex particles have a spherical-like shape with a rough surface. They seem to be filled with many PS domains mixed with the PMMA phase. This observation shows that the second-stage polymers were allowed to significantly penetrate the host polymer particle. This fact is actually further evidenced by a loss of the anisotropic character of the morphology of the hybrid particles, implying that polymerization took place throughout the particle. From these images, however, it is difficult to qualitatively estimate the extent of phase separation due to poor contrast between the particle phases.

An interesting feature is that some hybrid particles display a PMMA core somehow decorated by several clay platelets exhibiting a core-shell-like morphology. This morphology seems to be the result of limited diffusion of the clay platelets towards the surface of the particle. Although the seed polymers must have been initially plasticized, the short timeframe between monomer and initiators addition coupled with a probably fast reaction might have prevented full migration of the inorganic compound.

For this case study, the clay particles seem to act as rigid barriers preventing penetration of the second stage polymers in the core of the particle.

4.6 CASE STUDY 4: BATCH ADDITION OF STYRENE, SMALL SEED

Smaller sizes of the seed latexes combined with a batch addition of styrene were used in order to achieve further penetration of the second stage polymers as compared to the previous cases.

For this case study, the conventional latex particles exhibit an original cauliflower-like morphology (c.f. Figure 4.2d). The particles exhibit a rounded part (bud) with a homogeneous PS-rich phase. The flower-like part seems to be composed of small occluded PS domains within a PMMA matrix. In contrast to the case study 3, it appears that the morphology obtained is closer to its equilibrium state which would have probably been hemispherical-like. Indeed, we can see that the "bud" of the particle seems to adopt a convex configuration tending to minimize its contact with water.

In Figure 4.3d, the morphology of the hybrid latex particles displays large occlusions of PS domains apparently well-phase separated from a PMMA phase. These morphological characteristics, however, look quite different from the conventional ones. It can also be observed that the clay platelets are situated on the surface of all particles suggesting that the particle phases were highly mobile during polymerization.

Similarly to case study 2, the clay platelets might have acted as physical barriers against polymerization within the seed polymers because a high number of

secondary particles can also be observed. This effect of the clay seems actually more obvious here, probably because the migration of the clay platelets towards the surface of the latex particle completely occurred for all particles; whereas in case study 2 this migration was incomplete in many instances.

In fact, the clay platelet, bearing a permanent negative charge on its surface and having a high aspect ratio, might prevent the diffusion of polymeric radicals in the polymerization locus probably partly because of electrostatic and/or hydrophobic repulsions as previously observed for silica particles.¹¹ Indeed, Sheibat-Othman et al. have shown in a recent work that hydrophilic silica particles present on a latex particle could restrict the absorption of styrene oligomer radicals due to their negative charge and their strong incompatibility with the hydrophobic radicals.¹¹

Also, in this case study, it becomes obvious that the effect of the clay platelet on the morphology of the LCN depends on the inorganic filler transport during synthesis. The results obtained here could complement other research works which focus the effect of inorganic compounds in the morphology development of hybrid latex particles by calculation of interfacial tensions.⁵⁻⁷

4.7 CONCLUDING REMARKS

In this chapter, three-phase PMMA/PS/MMT particles were synthesized from clay-containing PMMA-seed latexes via (semi)-batch emulsion polymerizations of styrene. It was attempted to apply some theories established for the understanding of the development of the morphology of two-phase conventional latex particles in order to interpret the morphologies obtained.

Predominantly under kinetic control, all the morphologies observed could be fairly understood in terms of diffusivity of the polymeric and the inorganic phases. It was found that a reaction where the clay platelets are frozen in the core of the seed can naturally lead to hybrid systems with similar morphology as the conventional ones. In contrast, the reactions involving a noticeable displacement of the clay particles highlighted an important effect of the inorganic compound on morphology formation. Indeed, it was found that clay platelets impenetrable

Chapter 4

interfacial layers within the latex particles could act as a physical barrier preventing diffusion of second stage polymers within the host polymer. This effect of the clay promoted the formation of secondary particles.

The characterization of the morphology of the particles obtained was very challenging in itself. Such characterization was solely performed using TEM and gave mainly insight into the whole particle shape and to the internal structure when ultramicrotomy was applied. However, in order to completely determine the morphology, one needs to quantify the composition of the surface and the internal structure of the particle. Such information cannot obviously be provided by the microscopic techniques.

REFERENCES

1. Chen Y.-C.; Dimonie V.; El-Aasser M. S. *Macromolecules* 24: 3779 (1991).
2. González–Ortiz L.J.; Asua J.M. *Macromolecules* 28: 3135 (1996).
3. González–Ortiz L.J.; Asua J.M. *Macromolecules* 29: 4520 (1996).
4. Sundberg D.C.; Durant Y. *Polym React Eng* 11: 379 (2003).
5. Reyes Y.; Asua J.M. *Polymer* 48: 2579 (2010).
6. Reyes Y.; Paulis M.; Leiza J.R. *J. Colloid Interface Sci.* 352: 359 (2010).
7. Mičušík M.; Bonnefond A.; Reyes Y.; Bogner A.; Chazeau L.; Plummer C.; Paulis M.; Leiza J.R. *Macromol. React. Eng.* 4: 432 (2010).
8. Stubbs J.; Karlsson O.; Jönsson J.-E.; Sundberg E.; Durant Y.; Sundberg D. *Colloid Surf., A* 153: 255 (1999).
9. Stubbs J.M.; Sundberg D.C. *Prog. Org. Coat.* 61: 155 (2008).
10. Huo D.; Liu D. *Polym. Int.* 51: 585 (2002).
11. Sheibat-Othman N.; Bourgeat-Lami E. *Langmuir* 25: 10121 (2009).

Chapter 5

The Potential of High-Throughput Experimentation and Low-Cost Low-Resolution Raman Spectroscopy for The On-line Monitoring of Emulsion (Co)polymerization

Abstract: This chapter is divided into two main parts. The first part describes a method for carrying out emulsion copolymerization using an automated synthesizer. For this purpose, batch emulsion copolymerizations of styrene and butyl acrylate were investigated. The optimization of the polymerization system required tuning the liquid transfer method, sufficient oxygen removal from the reaction medium and setting a proper sampling procedure. The monomer conversion-time plots obtained with gas chromatography revealed a good reproducibility of the kinetics of the automated reactions. Furthermore, the particle size distributions and the molar mass distributions were found to be highly reproducible. The performance of the automated reactions was subsequently compared with the conventional ones: similar reproducibility of either synthetic method was observed. In the second part, the possibility of using a low-cost low-resolution portable (LCLR-P) Raman spectrometer in combination with partial least square regression methods for the on-line monitoring of seeded batch emulsion (co)polymerizations is studied. The usage of the LCLR-P Raman spectrometer was found to be a reliable tool to monitor homopolymerization reactions. Concerning the copolymerization reactions, the performance of the LCLR-P Raman spectrometer could not be fully assessed due to some experimental errors.

5.1 INTRODUCTION

A full understanding of the control of particle morphology requires the handling of many experimental parameters and conditions. Systematic studies of these factors would be extremely tedious and time-consuming if one solely uses conventional experimental techniques. Automated parallel synthesizers may speed up such systematic studies by enabling the simultaneous variation of several experimental parameters during reactions.

In the past, Voorn et al. studied some automated batch emulsion homopolymerizations of vinyl acetate and styrene.¹ Using a vortex mixing system, the emulsification efficiency of the automatic platform had to be investigated before reactions. The conversion- and particle diameter-time profiles, molecular weight and particle size distributions were comparable for conventional and automated reactions. Although Voorn's conclusions were favorable for the use of an automated approach for carrying out emulsion polymerization, this study also revealed significant limitations of the robotic platform used. For instance, a vortex mixing system might be insufficient to assure a good dispersion of clay particles in water which requires vigorous mechanical mixing. Hence, another type of automated synthesizer, more versatile with a different mixing technology and robust, is necessary to explore the applicability of emulsion polymerization in combinatorial chemistry.

High-throughput experimentation (HTE) techniques should also offer the possibility to perform systematic studies of reaction rates which are of great importance in providing in depth insight into the formation of the morphology of latex particles. Knowledge of reaction rates can be quantitatively assessed by measuring the amount of unreacted monomers during the course of the reaction. These measurements should be performed with instrumental techniques easy to handle, rapid and relatively cheap.

Among these techniques, on-line Raman spectroscopy offers several advantages such as fast analysis time, non-invasiveness and relative insensitivity to water.²⁻⁷ Several research works have clearly demonstrated the potential of Raman spectroscopy for robust on-line monitoring of emulsion (co)polymerizations.^{2,4-7} As

Chapter 5

far as our knowledge is concerned, these studies used traditional high-resolution Raman spectrometers which are barely applicable for industrial processes because of their relatively high cost and bulkiness. The development of low-cost low-resolution portable (LCLR-P) Raman spectrometers is, however, gradually beginning to reverse this situation as demonstrated by previous research works.^{3, 7}

In the first part of this chapter, the efficiency of a new generation of automated synthesizers for carrying out emulsion copolymerizations is studied. Using a mechanical mixing system, automated batch emulsion copolymerizations of styrene and butyl acrylate are investigated. First, the challenges for translating a conventional emulsion copolymerization method to an automated procedure are highlighted. Those challenges include the precision of liquid transfers, inertization of the reaction medium atmosphere and sampling. Second, the reproducibility of the automated reactions is analyzed by discussing the results obtained with off-line characterization techniques. Finally, an attempt is made to compare the reproducibility of automated reactions with conventional ones.

In the second part, the potential of LCLR-P Raman spectrometry in combination with partial least square regression technique in providing reliable kinetics data from conventional seeded emulsion (co)polymerizations is investigated. The profiles of the monomer conversion-time plots determined with the Raman instrument are compared with the ones obtained via gravimetry and gas chromatography. Moreover, the effect of clay on the Raman spectrum of styrene is studied in order to have a glance at the possibilities offered by Raman spectroscopy to monitor encapsulation of clay via emulsion polymerization.

5.2 THEORETICAL BACKGROUND

A Raman signal is based on inelastic scattering of a monochromatic excitation source (a laser) by a molecule. The incident photon energy can excite the vibrational modes of the molecule resulting to scattered photons which are decreased ($\nu_{sc} < \nu_{ex}$ in Figure 5.1) or increased in energy ($\nu_{sc} > \nu_{ex}$ in Figure 5.1). The observed scattering at frequencies below or above the incident frequency is called Stokes or Anti-Stokes lines, respectively.

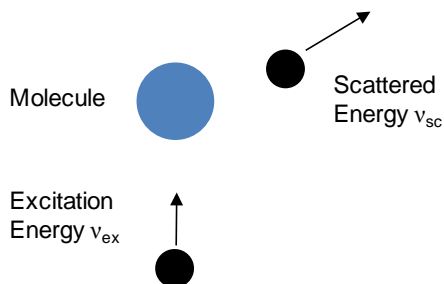


Figure 5.1 Schematic representation of the Raman scattering of a molecule after irradiation by a monochromatic excitation source.

The Raman spectrum is a graph of the intensity of Raman scattered radiation as a function of its frequency difference from the source radiation (Raman shift). Figure 5.2 shows the typical Raman spectra of styrene monomer where some Raman signals are assigned to different groups of the molecule. The intensity of the Raman signals are at most 0.001 % of the intensity of the source, which can make their detection and measurement quite problematic. The intensity of Raman signals depends on the polarizability of the molecule, the intensity of the source and the concentration of the active species.

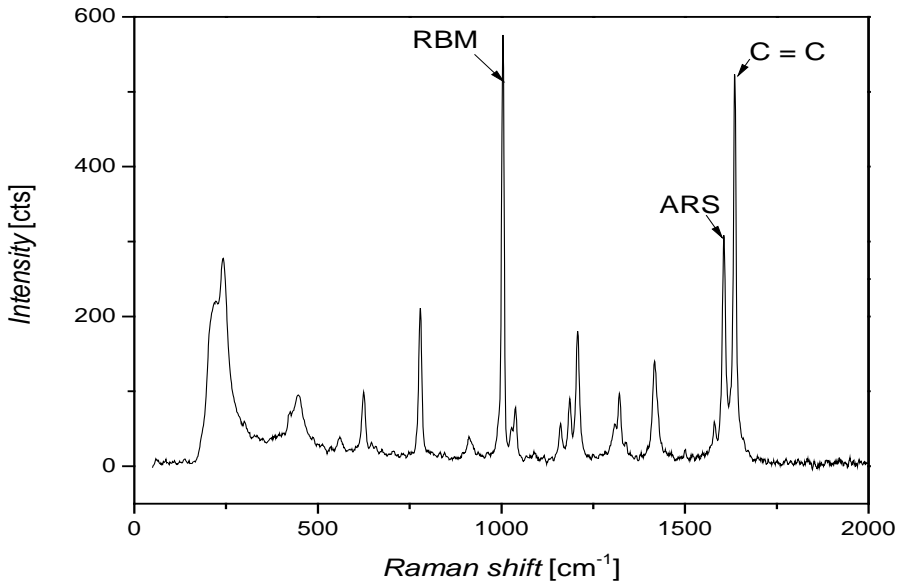


Figure 5.2 Raman spectrum of styrene showing the Raman signals of the (RBM) ring breathing mode, the (ARS) aromatic ring stretch and the (C = C) vinyl stretch vibrations of the monomer molecule.

An interesting approach for estimating the amount of monomers from Raman spectra is to use linear models which try to relate the Raman signals observed with the concentration of the components of interest. Among these methods, partial least square regression (PLSR) technique has been shown to provide good results.

4-7

The partial least square regression (PLSR) can be briefly described as a statistical projection-based method performed in two steps: calibration modeling and test steps. The calibration modeling step tries to relate the properties of interest of a sample (e.g. monomer conversion) to the corresponding spectral data (X-variables) by a multivariate linear model. The calibration model is developed from a training set of n observations (process time points) with m X-variables and p Y-variables. These training data form two matrices \mathbf{X} and \mathbf{Y} , of dimensions $(n \times m)$ and $(n \times p)$ respectively. The model parameters are defined as the regression

coefficients. In the calibration step, **X** and **Y** are known; whereas in the second step, the test step, the Y-variables are unknown and are calculated from the calibration models. For an in-depth description of the statistical aspects of the PLS method, the reader is kindly requested to refer to an excellent tutorial written by Geladi et al.⁸

5.3 EXPERIMENTAL

5.3.1 Chemicals

Styrene (Sty, Aldrich > 99 %), methyl methacrylate (MMA, Aldrich > 99%) and n-butyl acrylate (BA, Aldrich > 99 %) were purified from inhibitor (t-butylcatechol and hydroquinone) by passing them through a column filled with aluminum oxide. All other chemicals were used as received. Potassium persulfate (KPS, Aldrich ≥ 99%) was used as initiator. Sodium dodecyl sulfate (SDS, Merck), sodium dodecylbenzene sulfonate (SDBS, Aldrich) and Triton X-100 (TX-100, Aldrich) were used as surfactants. 1-Dodecanethiol (NDM, Aldrich) was used as chain transfer agent and sodium bicarbonate (NaHCO₃, Merck) as buffer. Distilled water was used in the polymerization.

Other chemicals used are hydroquinone (HQ), n-butyl acetate (BuAc, Merck), tetrahydrofuran (THF containing butylhydroxytoluene, Biosolve) and toluene (Biosolve).

5.3.2 Conventional emulsion polymerizations

All conventional reactions were carried out in flat – bottomed glass reactors with baffles, equipped with a mechanical stirrer (45° pitched downflow six-bladed impeller), a temperature indicator, a reflux condenser and an inert gas inlet. The system was heated by circulating water through the cylinder-jacket of the reactor.

PMMA-seed latex preparation

The PMMA-seed latexes were prepared via batch emulsion polymerizations in an argon atmosphere. All ingredients were de-aerated with argon before introduction into the reaction medium. The reactor was initially loaded with distilled

Chapter 5

water and de-aerated for about 30 minutes. The surfactant solution was added under stirring (120 rpm) and the argon flow was reduced to avoid foam formation. The monomer was added slowly into the reactor under constant stirring (320 rpm) while purging with argon. The reaction temperature was raised to 80 °C, and the initiator solution was introduced as a single pulse after temperature stabilization. After two hours of reaction, the temperature was increased to 90°C for two more hours to totally decompose the remaining initiator. The general composition of the polymerization system is given in table 5.1. The monomer conversion and solid content of the latex obtained were determined by gravimetric measurements.

Table 5.1 Recipe used for the preparation of the PMMA-seed latexes.

Ingredients	Composition (% total mass)
Water	63.4
MMA	35.2
SDBS	0.1
TX-100	1.1
KPS	0.2

Batch PMMA-seeded emulsion homopolymerizations of styrene

The reactor was initially loaded with distilled water and a PMMA seed latex and de-aerated during 30 min. The buffer and surfactant solution was introduced under stirring (120 rpm). The monomer mixture (Sty and NDM) was added slowly into the reactor under constant stirring (320 rpm) while purging with argon. The reaction temperature was raised to 55°C, and the initiator solution was introduced as a single pulse after temperature stabilization. The general composition of the polymerization system is given in table 5.2. Samples were withdrawn from the

Chapter 5

reactor at regular time intervals for off-line analyses, whereas Raman spectra were recorded for on-line monitoring.

Table 5.2 The composition (wt-%) of the recipes used for the PMMA-seeded batch emulsion homopolymerization of styrene

Entry	Water ^a	PMMA latex ^{b,c}	Sty ^a	NDM ^c	SDS ^c	KPS ^c
1 ^c	Variable ^d	100	Variable ^d	1	1.5	Variable ^d
2	69	100	14.6	1	1.5	0.3

a) Based on the total mass

b) Dried weight

c) Based on the total amount of styrene

d) Missing values given in section 5.7

Batch emulsion copolymerizations of styrene and butyl acrylate

All ingredients were de-aerated with nitrogen before introduction into the reaction medium. The reactor was initially loaded with distilled water and de-aerated with nitrogen for a 30 min period. After addition of the buffer and surfactant solutions, nitrogen flow was reduced to avoid foam formation. The monomer mixture (Sty, BA and NDM) were charged dropwise into the reactor while purging with nitrogen. The reaction temperature (T_r) was slowly raised to 55 °C; and after temperature stabilization, initiator solution (having about 10 h half-life at T_r) was added as a pulse. The general composition of the copolymerization systems is given in table 5.3. Samples were withdrawn from the reactor at regular time intervals. They were collected in small glass vials containing hydroquinone and immersed in an ice bath for few seconds to short stop the polymerization.

Table 5.3 The recipe used for the conventional and automated batch emulsion copolymerization

Ingredients	Composition
	(wt.-% total mass)
Water	85
Sty	3.6
BA	11
SDS	0.22
KPS	0.02
NaHCO ₃	0.01
NDM	0.15

Batch PMMA-seeded emulsion copolymerization of styrene and butyl acrylate

The same equipment and procedures were used as in previous reactions. The general composition of the polymerization system is given in Table 5.4.

Table 5.4 The composition (wt-%) of the recipes used for the PMMA-seeded batch emulsion copolymerization of styrene and butyl acrylate

Entry	Water ^a	PMMA latex ^{b, c}	Sty:BA ^d	CTA ^c	SDS ^c	KPS ^c
1 ^d	Variable ^e	25	Variable ^e	1	1.6	Variable ^e
2	56	25	30:30	1	1.6	0.46

^{a)} Based on the total mass

^{b)} Dried weight

^{c)} Based on the total amount of monomers

^{d)} Based on the water mass

^{e)} Value given in section 5.8

5.3.3 Automated emulsion polymerizations

Automated reactions were carried out with a Chemspeed Autoplant A100 equipped with four reactor blocks and a liquid handling system (4-needle head) containing four 10-mL syringe pumps, six reservoir bottles and two rinsing stations (c.f. Figures 5.3 and 5.4). The reactor blocks were equipped with stainless steel reactors with baffles, syringe pumps, and probes for temperature measurements. A reflux condenser (with a water/ethanol mixture as cooling liquid) was integrated into the reactor's head. Agitation of the reactor was performed with overhead triple blade stirrers at 800 rpm, and the reaction medium was heated by electrical cartridges. The robot's hood and the reactors were individually rendered inert by applying argon overpressure through some gas openings. It was not possible to de-oxygenate the 4-needle head because it was a hydraulic system whose operation required inlets free from gas bubbles. The recipe described in table 5.3 and the experimental conditions applied to conventional reactions were translated to the automated process by editing a computer program. This program controlled the preparation of monomer mixtures, dispensing the reagents in set quantities, switching on/off the reflux and stirring, the reaction temperature, sampling and rinsing of the 4-needle head. The 250-mL stock solutions of 0.2 M of SDS, 0.02 M of NaHCO₃, and 0.02 M of KPS in water were prepared with laboratory glassware.

Chapter 5

From the stock solutions, required amounts of reagents were dispensed automatically into the reactors. All reagents were deoxygenated with argon and charged in the reactor by using a 4-needle head. Sampling was performed automatically by withdrawing 100 μ L samples from reactors to GC vials containing 1 mL of 0.5% v/v toluene/THF mixture (GC solvent) and capped with silicone/PTFE septa.



Figure 5.3 A picture of the automated parallel synthesizer Autoplant A100 (Chemspeed) used in this study.

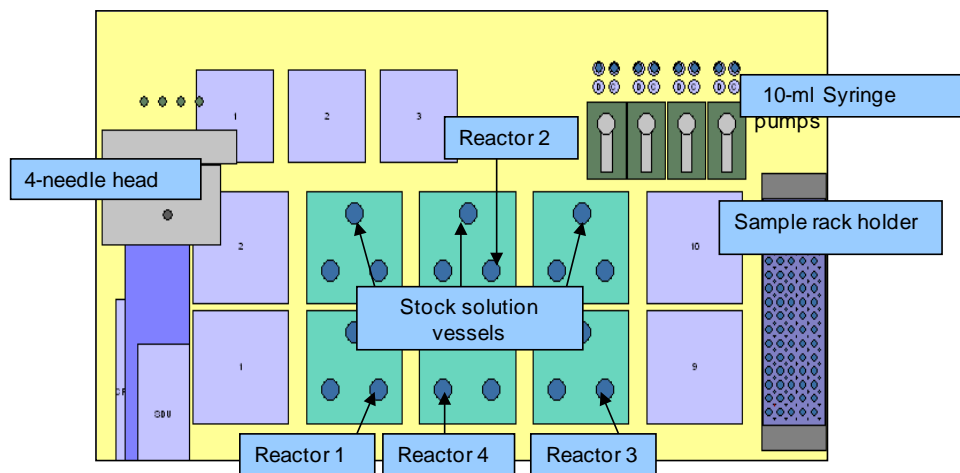


Figure 5.4 Schematic representation of the automated parallel synthesizer Autoplant A100 (Chemspeed) used in this study.

Determination of the liquid dispensing accuracy

Before performing the experiments, it was important to ensure that the transfer of reagents was not prone to significant errors. For this purpose, after flushing the system with distilled water (priming), the liquid dispensing accuracy was determined by transferring with the 4-needle head, from separate reactors to sample vials, the following solutions: 1 mL of GC solvent, 100 μL of latex, and 100 μL of water. Delivery rate was set to 10 mL min^{-1} . Volumes and weights of the sample vials were then recorded.

Calibration of the sample rack holder and verification of the reactor sealing

A blank experiment (without initiator) was carried out in order to optimize the setting of the sample rack holder position for proper sampling. This blank experiment also permitted to check whether the reactors were properly tightened during reaction. The recipe of the blank experiment is described in Table 5.5; inhibitor and oxygen were not removed from the monomer before the experiments. Reactors 1 and 4 were used: Reactor 1 was kept at room temperature and Reactor 4 was heated at 55 $^{\circ}\text{C}$. A volume of 100 μL samples were withdrawn from the

Chapter 5

reactors (while stirring at 800 rpm) to the sample vials every 10 min for 2 h; the weights of the sample vials were then recorded.

Table 5.5 The blank experiment recipe for the calibration of the sample rack position

Ingredients	Composition
	wt % total mass
Water	95.7
Sty	4.03
SDS	0.26
NaHCO ₃	0.01

5.3.4 Characterizations

Overall monomer conversion

The overall monomer conversion was determined via gravimetry. At regular time intervals, samples of about 2.5-3.5 g were withdrawn and poured in previously weighed aluminum dishes containing a small amount of solid hydroquinone (HQ), to quench the polymerization, and weighed. The polymers were dried to constant weight in an oven at 40°C all night to evaporate the volatile components. The dried polymers were weighed to determine the instantaneous monomer conversion simply using mass balance equations.⁹

Chapter 5

Partial monomer conversion

At regular time intervals, samples of about 0.2-0.4mL were withdrawn and poured in vials containing HQ. The vials were immediately submerged into an ice bath for a few seconds to quickly quench the reaction. From these samples, 100 μ L of latex were transferred in vials containing 1mL of a solution of THF and butyl acetate (BuAc) used as internal standard.

Determination of individual partial monomer conversion was performed by use of a GC450 chromatograph equipped with a CP – Wax 52CB capillary column (length: 25 m; diameter: 0.4 μ m) and with a glass PEG pre-column. Analyses were carried out with the following operating conditions:

- Injection temperature: 250 °C,
- Temperature: 50°C for 1 min , 15°C/min to 100°C, then 25°C/min to 200°C
- Carrier gas: Helium, flow rate: 3 ml min⁻¹,
- Detector temperature: 300°C.

It should be noted that a sample was withdrawn at time t_0 from the reaction medium immediately after addition of the initiator. The monomer concentration of this sample was set as the initial monomer concentration before polymerization. The monomer conversion at time t_0 was therefore arbitrarily set with a value of 0 %.

Average particle diameters

Determination of average particle diameters was performed by the use of a Malvern Zetasizer Nano ZS dynamic light scattering apparatus, with a He-Ne laser as the light source (at a fixed wavelength of 633 nm). This apparatus was used at a scattering angle of 173 ° and at a temperature of 25 °C. The measurements were done after dilution of the samples with de-ionized water. An indication of the particle size distribution (PSD) was determined with the same equipment. Analysis of the PSD was based on the intensity distribution pattern generated by DLS, assuming that the particles are spherical in shape.

Chapter 5

Weight-average molar masses

Determination of molar mass distributions and derived weight-average molar masses was done by size exclusion chromatography (Waters 2695) using right angle light scattering (Viscotek) and refractive index (Waters 2414) as dual detectors. Two mixed bed columns (Mixed-C, Polymer Laboratories, 30 cm, 40 °C) were used and calibrated with narrow molar mass polystyrene standards (range = 580 - 7.5×10^6 g mol⁻¹). Elution was performed with THF; the flow rate was 1 mL min⁻¹. Concentration of polymer solutions and corresponding injected volumes were 1 mg mL⁻¹ and 50 µL, respectively. Data analysis was performed by using the software Empower Pro version 2 from the Waters Corporation.

Raman spectroscopy

The Raman spectrometer AvaRaman-2048TEC (Avantes) was used for our experiments. The instrument was equipped with a solid state 785 nm diode laser (maximum power of 500 mW), a 5/8" focusing immersible fibers probe (with a 100 µm excitation fiber and a 200 µm read fiber) allowing *in-situ* measurements and a thermo-regulated cooled CCD detector. The spectral coverage was from 1.4 to 2226.4cm⁻¹ with a resolution of 5 cm⁻¹.

A spectrum corresponded to an average of 100 scans acquired with an integration time of 1200 ms The Panorama software (LabCognition) was used for data acquisition and, if necessary, for preprocessing the spectra.

PLSR modeling

The PLSR analyses were performed using the Unscrambler software version X (CAMO ASA). Before modeling, all spectral datasets were standardized and mean-centered. The PLSR models were built using Martens uncertainty test¹⁰ in order to eliminate any non-significant variables (spectral data) from the model.

Then, the percentage of explained variations in the monomer conversion (Y-variance) was plotted as a function of the number of PCs. The optimal number of principal components (PC) corresponded to a maximum explained variance with a minimum noise in the design of the model. The noise of the model was estimated

by the root mean square error of prediction (RMSEP) which was calculated using the segment leave-one-out cross validation method.¹⁰ Finally, the calibration model used for further experiments was chosen according to an optimum number of PCs and a minimum RMSEP.

Analysis of variance (ANOVA)

The analysis of variance was performed using the software Statgraphics Centurion XV version 15.2.00 from StatPoint.¹¹

5.4 OPTIMIZATION OF THE AUTOMATED REACTIONS

To achieve good reproducibility of the 4-needle head, the automated liquid transfer method had to be optimized. This optimization consisted of the choice of the dispensing/aspiration rate and the mode of the 4-needle head. The chosen dispensing/aspiration rate was thus at least 10 mL min⁻¹ to minimize contact of (sticky) latex samples with the tubing wall. Liquid from reactors or vessels was withdrawn by the 4-needle head in three steps: (i) formation of 20 µL of air (air gap) in the 4-needle-head tubing, (ii) withdrawing of 2 mL extra-volume of the targeted solution, then of (iii) the required amount of the latter [the air gap and the extra-volume of liquid permitted to physically buffer the latter from the system fluid (distilled water)]. After dispensing of reagents/samples into reactors/ vials, air gap and extra-volume were discharged into the waste. The reproducibility of the 4-needle head was further improved when the system tubing was regularly flushed with distilled water. Moreover, to avoid cross-contaminations, rigorous rinsing with distilled water of the needles and tubing was necessary after each transfer. After optimization of the system, the automated liquid dispensing accuracy and precision was then determined by transferring a pre-set amount of different samples from reactors to 2-mL vials (c.f. Table 5.6). As can be seen in Table 5.6, the 4-needle head had an acceptable accuracy and precision range; the lowest accuracy observed for latex samples is due to adherence of a small amount of latex onto the tubing wall during transfer.

In emulsion polymerization, the presence of oxygen in the reaction medium is known to retard or even to inhibit the polymerization.¹² Unlike in previously

Chapter 5

reported automated RAFT polymerizations,¹³ it was necessary to continuously purge the individual robotic reactors with argon during the reaction. Incoherent results were obtained when the argon flow rate, adjusted manually before the reactions, was too low. For instance, in Figure 5.5, the partial conversion-time plots of butyl acrylate and styrene of an automated batch emulsion copolymerization (c.f. recipe in Table 5.3) exhibited different profiles depending on the investigated reactor. For Reactors 1 and 2, conversions of the two monomers leveled off after 30 min of reaction, whereas for Reactors 3 and 4, the copolymerizations seemed to proceed normally. In fact, at the beginning of the polymerization process (c.f. arrow (1) in Figure 5.5), argon flushing of Reactors 1 and 2 was found to be rather inefficient. This was due to a leakage of the argon-carrying tubing. The tubing was then immediately sealed without interrupting the polymerization process, and an increase of the polymerization rate could be observed in the graphs at a later stage of the reaction (c.f. arrow (2) in Figure 5.5). The latter observation shows that a poor argon pressure over the reactors can strongly enhance the inhibition of the polymerization by oxygen.

Table 5.6 Accuracy and precision of the 4-needle head

Samples	Set quantity (μL)	Experimental quantity ^{a)} (μL)
Toluene/THF ^{a)}	1000	962 \pm 7
Latex ^{c)}	100	90 \pm 5
Water ^{c)}	100	97 \pm 2

^{a)} Measured as the ratio mass to density

^{b)} Volume ratio of toluene/THF is 0.5 % v/v

^{c)} Density of water and latex is assumed to be equal to 1 g cm⁻³

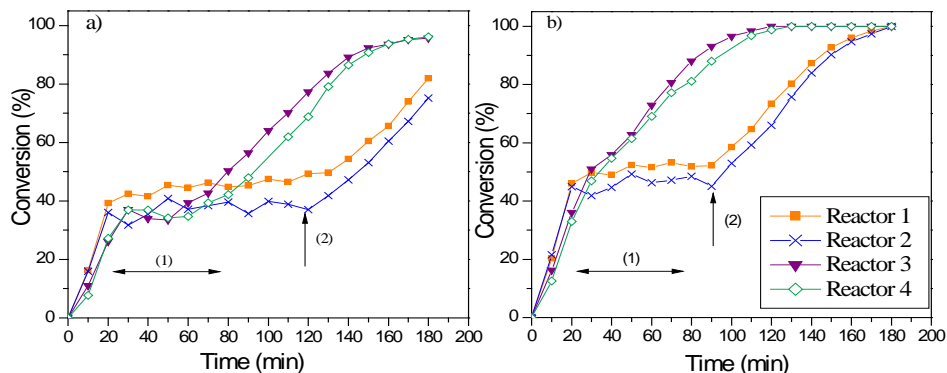


Figure 5.5 Irreproducible automated reaction course due to poor inertization efficiency: a) butyl acrylate; b) styrene; (1) poor argon flow for reactors 1 and 2; (2) argon flow restored for reactors 1 and 2.

The major challenge was the automated sampling step. Initially, the reaction medium consisted of monomer emulsions in an aqueous surfactant solution and a headspace saturated with gas phase reactants. As the polymerization proceeded, latex particles were formed and the relative amount of monomers partitioned in the different phases varied. Thus, one of the challenges was to withdraw liquid samples automatically from the reactors without affecting the course of the reaction.

The samples also had to be representative of the heterogeneity of the reaction medium. Because of the small size of the reactors, high speed mixing was required to obtain a proper emulsion polymerization. However, the high agitation rate of the reactor often led to some vortex formation and foaming in the vicinity of the stirrers. These phenomena had dramatic effects on the sampling efficiency since gas/liquid mixed samples were collected. To circumvent this difficulty, agitation of the reactor was stopped during sampling for a short time. The samples were then collected at the bottom of the reactors where components are optimally mixed.

Chapter 5

In addition, the calibration of the sample rack holder position was of significant importance. For proper setting of the rack holder, blank experiments were carried out during which samples were periodically transferred from the reactors to the sample vials. During blank experiments, the reactors were respectively heat treated and at room temperature. Table 5.7 gives the sample mass recorded after one of those experiments. This is an example of a bad setting of the rack holder position: less than 80% of the theoretical sample mass was obtained experimentally. Therefore, the correct position of the rack holder was set, so that the needles of the 4-needle head were properly immersed into the solvent contained in the sample vials before dispensing. In that case, the sample mass reached more than 90% of their theoretical value. Moreover, it seems that the reactors were well sealed during application, because the sample weights of the reactors without and with heating are not significantly different in the absence of initiator.

Table 5.7 Mass of the samples measured after the blank experiment carried out on reactors 1 and 4

Treatment of the reactors	Sample mass ^a mg
Reactor 1 without heating	81 ± 9
Reactor 4 with heating	76 ± 6

^{a)} Theoretical value of the sample mass is 99.7 mg

5.5 REPRODUCIBILITY OF THE AUTOMATED REACTIONS

Gas chromatography combined with an automated sampling was the technique used in the current study to determine the partial monomer conversions of the polymerizations. Such technique can be less accurate in the presence of polymers, as previously reported by Petrak and Pitts.¹² Therefore, before the experiments were performed, the reproducibility of the measurement procedure was checked by performing five injections of each sample withdrawn from a reactor, during an automated reaction. Errors were found to be at most 2 and 3% for styrene and butyl acrylate respectively, even in the presence of polymers. Therefore, we can

conclude that systematic quantitative GC errors were insignificant. For all experiments, typical partial monomer conversion-time profiles of styrene and butyl acrylate are depicted in Figure 5.6. Distinct stages of the reaction are clearly visible for both monomers represented by time intervals I to IV. The partial conversions for styrene and butyl acrylate follow the typical conversion-time profiles known for this emulsion copolymerization.¹³ Initially, styrene is preferentially incorporated in the copolymer (I, II). After almost complete consumption of styrene, homopolymerization of butyl acrylate occurs with a higher rate than the copolymerization (III). In stage IV both monomers are reaching full conversion. Actually, differences of partial conversion-time profiles of styrene and butyl acrylate are translated by a drift in the copolymer composition, which is basically due to the differences in the relative reactivity ratio of the monomers ($r_{\text{Sty}} = 0.75$; $r_{\text{BA}} = 0.2$)¹⁴ and their water solubility ($s_{\text{Sty}} = 0.025 \text{ mol L}^{-1}$; $s_{\text{BA}} = 0.029 \text{ mol L}^{-1}$, at $60 \text{ }^\circ\text{C}$).¹⁵

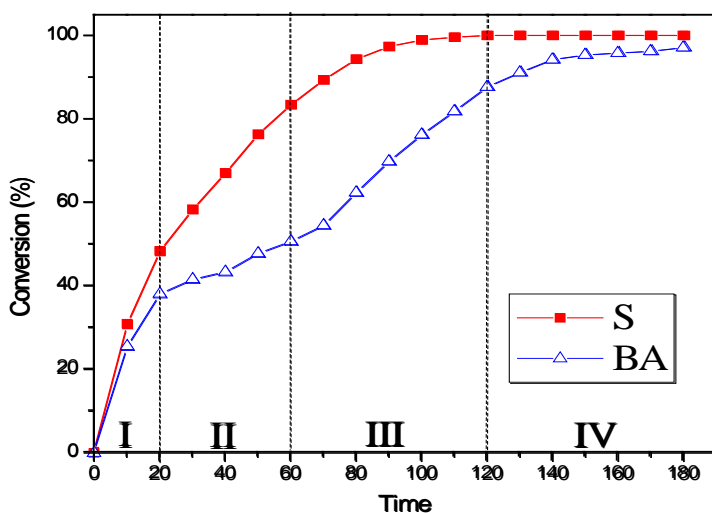


Figure 5.6 The typical partial conversions of styrene and butyl acrylate of an automated batch emulsion copolymerization. Recipe composition in wt.-% of the total mass: water: 85 ; Sty: 3.6; BA: 11; SDS: 0.22; KPS: 0.02; NaHCO_3 : 0.01; NDM: 0.15; $T_r = 55 \text{ }^\circ\text{C}$.

Chapter 5

The partial conversions of styrene and butyl acrylate are respectively given in Figures 5.7 and 5.8 for different experiments on different days (numbered in a chronological order) and in Figures 5.9 and 5.10 sorted by reactor number. At first glance, the reactions look very reproducible, with no significant differences between the reactors (Figures 5.7 and 5.8). Furthermore, day-by-day variation seems to be small, except perhaps for the reactions performed on Day 1 (Figures 5.9 and 5.10). In order to quantify the reproducibility better, the conversion rates at intermediate conversion are compared with Tables III.1 and III.2 in Appendix III. These rates correspond to the slopes of straight lines drawn between 50 and 80% conversion. Except on Day 1, the intermediate conversion rates are more or less similar. This latter observation was further evidenced by an analysis of variance of the intermediate conversion rates (c.f. Table I.2 in Appendix I). Neither the experimental day nor the reactor type on which the experiments were performed was found to have a significant effect on this variance. Values of intermediate conversion rates of butyl acrylate and styrene can thus be expressed as $0.69 \pm 0.06 \text{ min}^{-1}$ and $0.88 \pm 0.10 \text{ min}^{-1}$, respectively. In a closer analysis of the graphs (c.f. Figures 5.8 – 5.10), one can observe that a given monomer conversion can be obtained at different times depending on either the experimental day or the observed reactor on which the experiments were performed. For instance, in Day 2, 20% of butyl acrylate is converted within 15 min in Reactor 1, whereas about 7 more minutes are required in Reactor 2 to reach the same conversion (c.f. Figure 5.9). Such variability of the conversion-time plots would represent the occurrence of inhibition period during which no reaction takes place. Sources of inhibition can be the presence of impurities in the reaction medium. Oxygen could be one of those impurities since the 4-needle head was not flushed with argon during application.

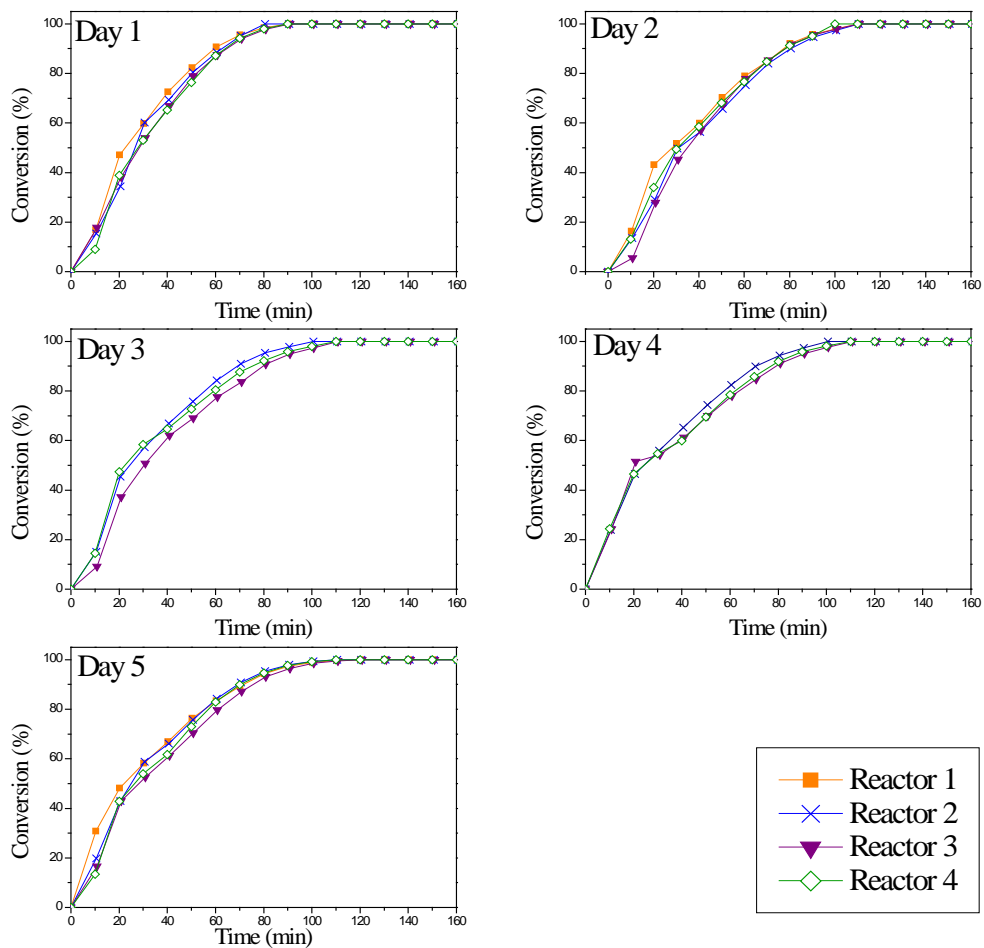


Figure 5.7 Reproducibility of the automated reactions over days of experimentation for the partial conversion of styrene.

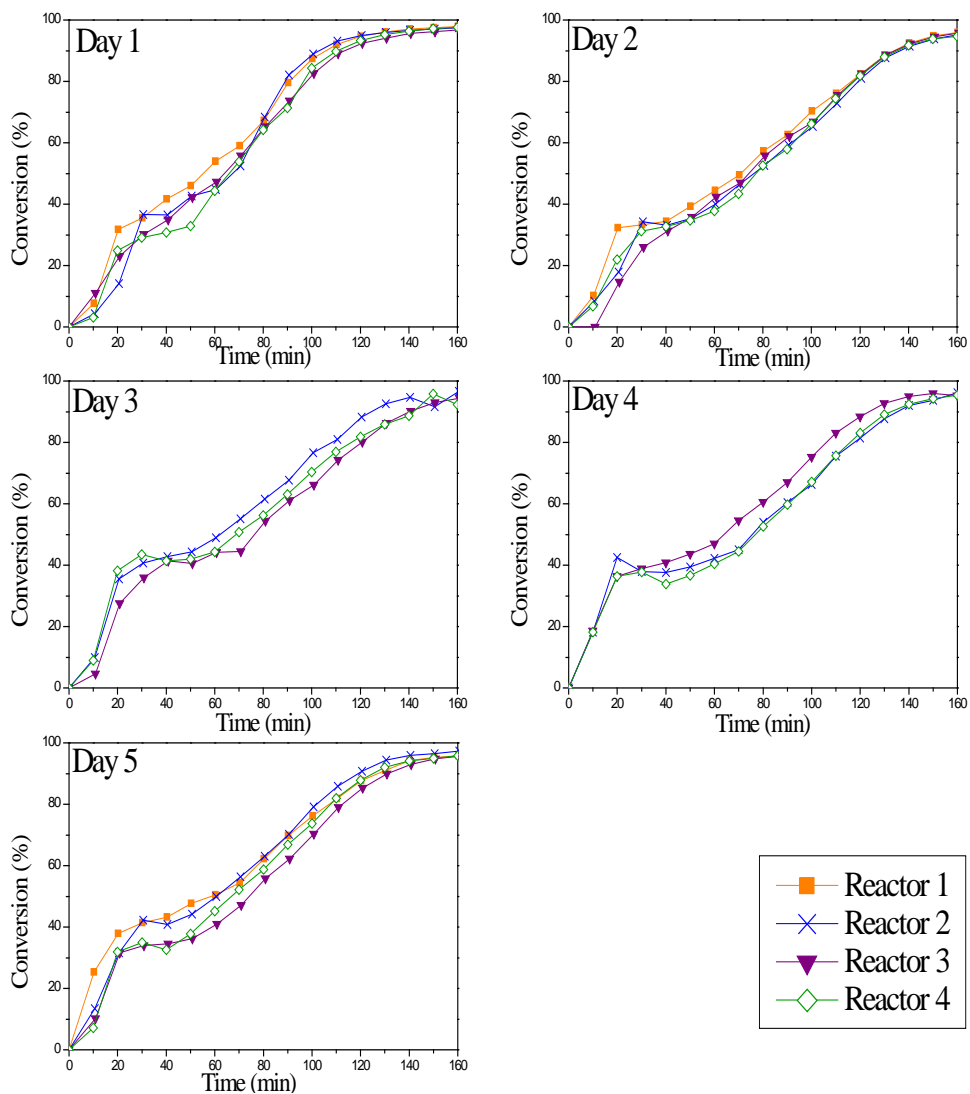


Figure 5.8 Reproducibility of the automated reactions over days of experimentation for the partial conversion of butyl acrylate.

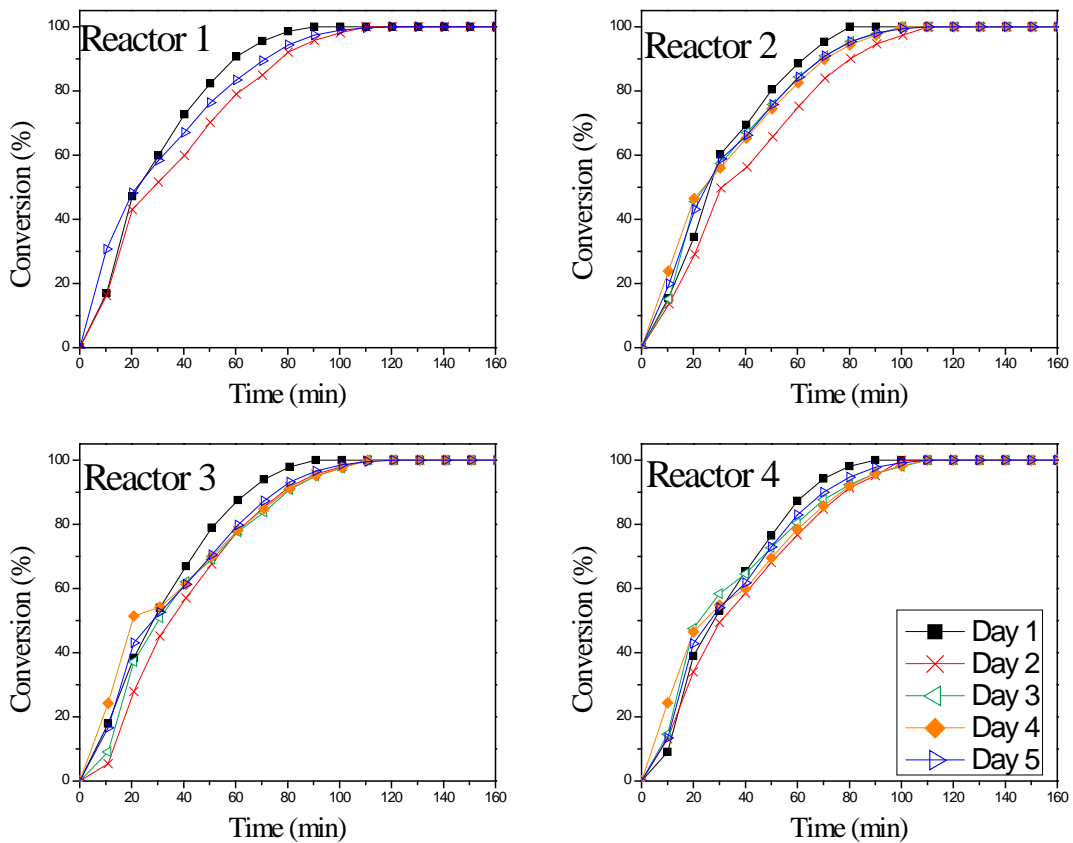


Figure 5.9 Reproducibility of the automated reactions in the reactors 1, 2, 3 and 4 for the partial conversion of styrene.

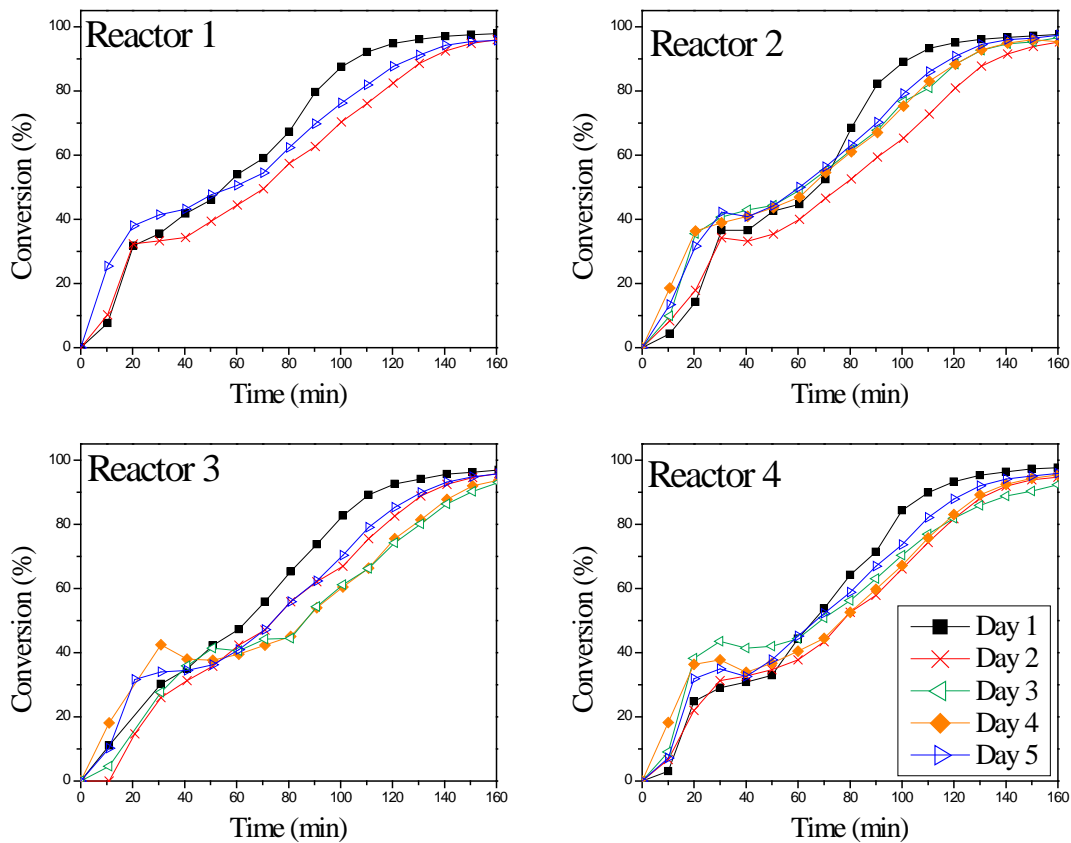


Figure 5.10 Reproducibility of the automated reactions in the reactors 1, 2, 3 and 4 for the partial conversion of butyl acrylate.

Chapter 5

The effect of inhibition on the variability in the reaction rates was verified by shifting the curves horizontally as shown in Figures 5.11 and 5.12. It has to be taken into consideration that after removal of any inhibition effects, the polymerization rates should be identical if there are no other sources of variability. For most of the transposed graphs, a good overlapping of the curves is observed, which confirms the occurrence of inhibition for the corresponding reactions. These inhibition periods might be within a few seconds or several minutes. This was impossible to be graphically determined because the time interval between first and second samples was restricted to 10 min; it was hardly possible to decrease the sampling time interval because of the thorough rinsing step of the needles after each sample transfer. Impact of inhibition was thus qualitatively studied by comparing the errors at 20% and 80% monomer conversion before and after an exact overlapping of the curves at 50% conversion (c.f. Tables III.3 – III.6). After correction of the inhibition effect, it was observed a general decrease of the errors due to inhibition could be observed (c.f. Tables III.5 and III.6). Sources of inhibition, namely systematic or random experimental errors, were investigated by performing an ANOVA¹⁵ of the different times observed at 50% monomer conversion (t_{50}) (c.f. Table I.3 in Appendix I). It was found that neither experimental day nor reactor significantly affects the variance of t_{50} at a 95% confidence level, which is equal to 70 ± 4 min and 24 ± 4 min for butyl acrylate and styrene, respectively. We can thus conclude that inhibition effects can be treated as random experimental errors.

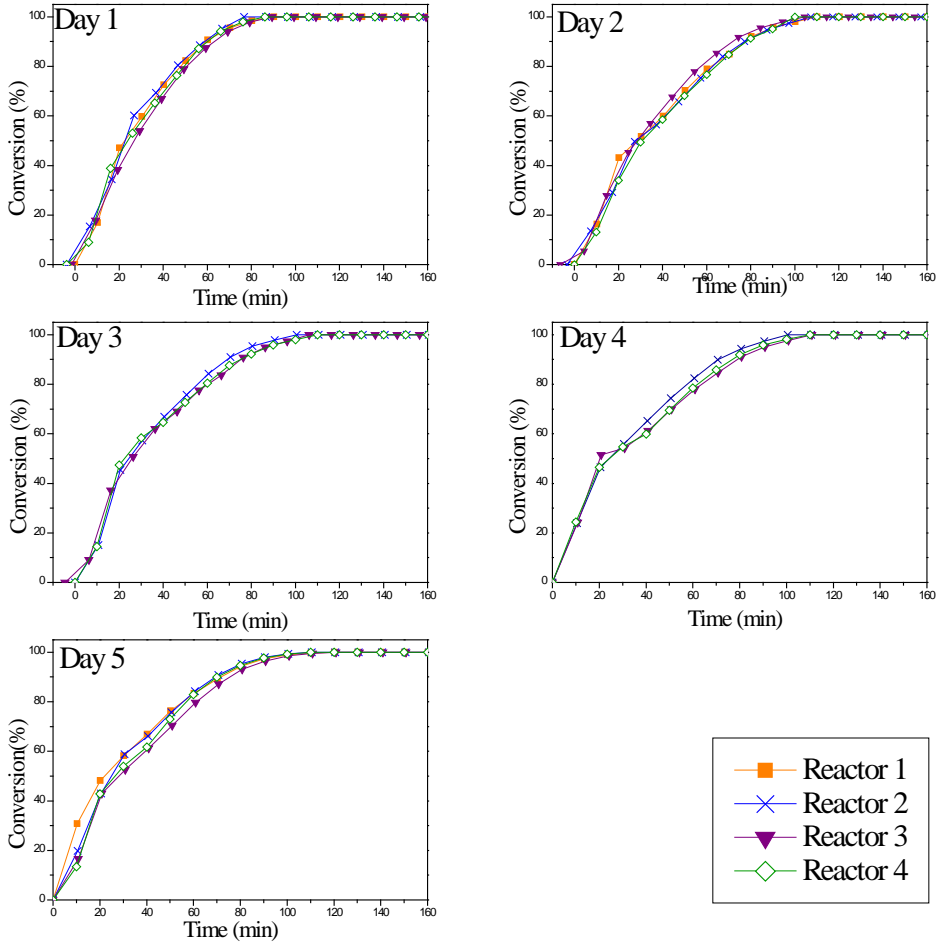


Figure 5.11 Minimization of the inhibition effect from the conversion-time plots of styrene by exact overlapping of the curves at 50% monomer conversion (no transposition was performed on Day 4).

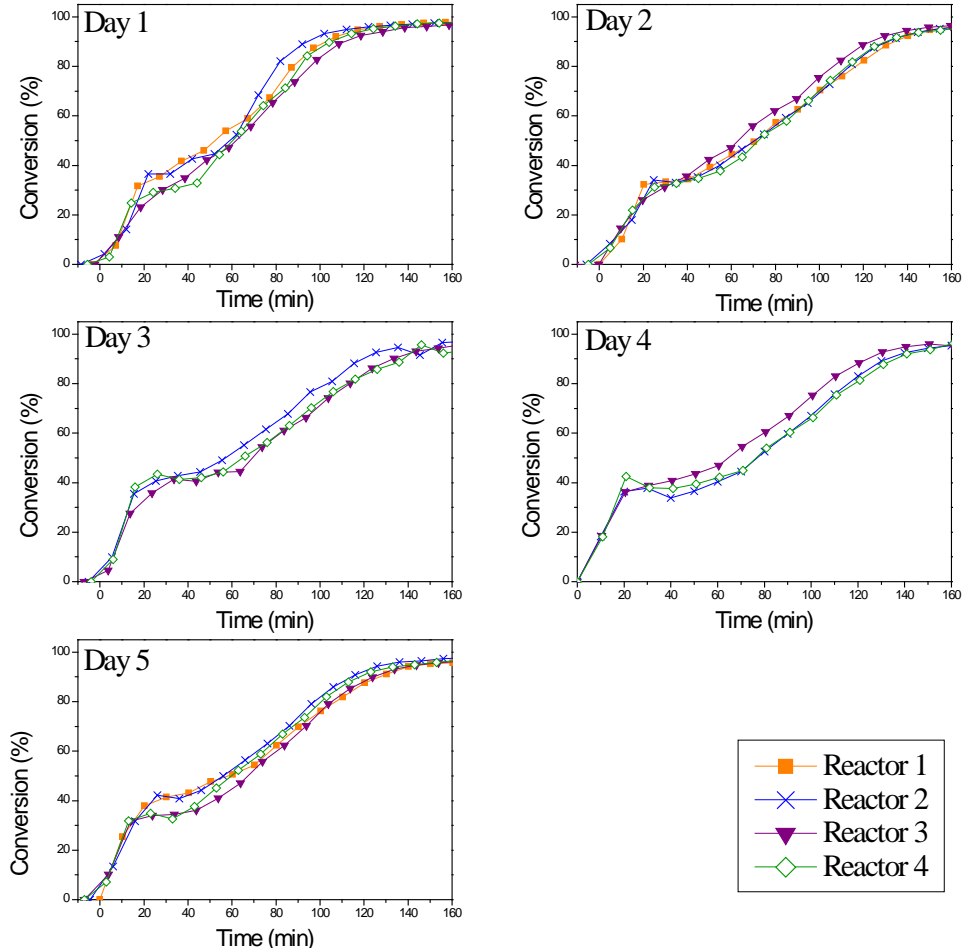


Figure 5.12 Minimization of the inhibition effect from the conversion-time plots of butyl acrylate by exact overlapping of the curves at 50% monomer conversion (no transposition was performed on Day 4).

Chapter 5

The full picture of the reproducibility of the automated reactions cannot be visualized by a sole comparison of the monomer conversion plots. In fact, the overall polymerization kinetics is governed by the particle nucleation mechanism, which leads to a specific particle size distribution of the final latex product. As can be seen in Figure 5.13, particle size distributions of all reactions are similarly narrow and monomodal. Also, from Tables 5.8 and 5.9, we can observe that mean particle diameters of all runs are similar within the experimental error. Therefore, the rates of the reactions in the automated reactors, inversely proportional to particle diameter, are all the same. This is in agreement with our previous conclusion, which stated that inhibition is the main source of variability of the monomer conversion plots. We can thus conclude with confidence that the automated reactions has a good reproducibility. Analysis of molar mass further confirmed the reproducibility of the final latex product properties. In Table 5.8, we can observe similar molar mass on days 2 to 5 within the experimental error. In Table 5.9, latex particles characteristics are presented for each reactor by only considering reactions carried out on days 2 to 5. It seems that the automated reactions were highly reproducible. Reactors 2, 3, and 4 yield molar masses within experimental error, with Reactor 1 yielding only slightly higher molar masses.

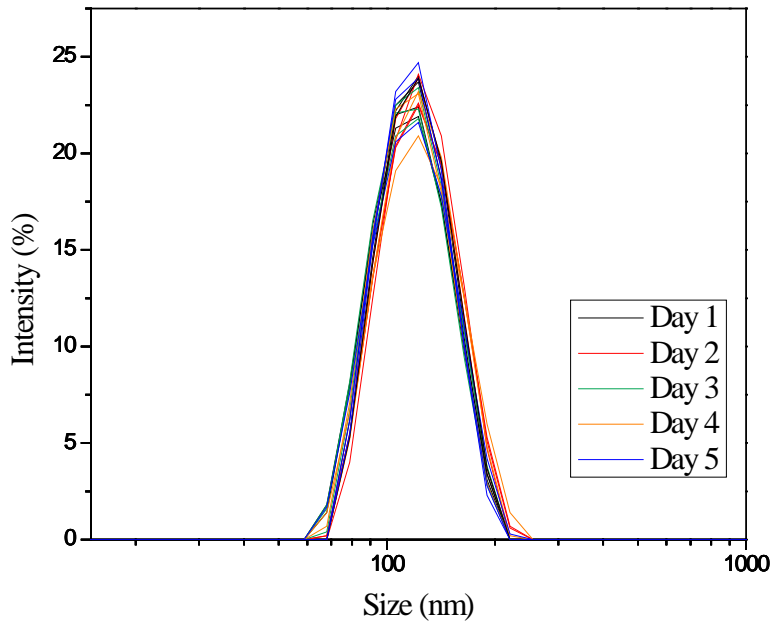


Figure 5.13 Reproducibility of the particle size distribution in the automated reactors.

Chapter 5

Table 5.8 Final product properties measured on different days

Days	Mean particle diameter		$\overline{M}_w \times 10^{-3}$ g·mol ⁻¹
	D _z nm	PDI	
1	117 ± 4	0.02 ± 0.01	153 ± 7
2	120 ± 1	0.02 ± 0.02	211 ± 34
3	114 ± 2	0.02 ± 0.02	194 ± 10
4	118 ± 3	0.02 ± 0.02	193 ± 8
5	116 ± 1	0.01 ± 0.02	211 ± 16

Table 5.9 Final product properties in several reactors

Reactors	Mean particle diameter		$\overline{M}_w \times 10^{-3}$ g·mol ⁻¹
	D _z nm	PDI	
1	118 ± 4	0.009 ± 0.002	237 ± 18
2	116 ± 2	0.01 ± 0.01	205 ± 11
3	118 ± 2	0.02 ± 0.02	186 ± 13
4	116 ± 3	0.03 ± 0.01	203 ± 16

5.6 BATCH EMULSION COPOLYMERIZATION: COMPARISON BETWEEN AUTOMATED AND CONVENTIONAL OPERATIONS

An automated reaction is considered reliable if the results obtained with such a synthetic method are comparable with the ones of conventional operation, which represents a well-established process. Therefore, conversion rates of conventional and automated reactions were compared. For this purpose, conventional reactions were repeated three times on different days. The monomer conversion-time plots obtained are presented in Figure 5.14. As performed in the previous section, a correction of the inhibition effect, due to random experimental errors, shows a clear overlapping of the curves (cf. Figure 5.15). For all reactions, reaction at 50% conversion was then determined and is equal to 51 ± 2 min and 23 ± 1 min for butyl acrylate and styrene, respectively. This result shows that the magnitude of random errors of conventional and automated reaction is comparable. Table 5.14 summarizes the conversion rates at intermediate monomer conversion. We can observe that a similar range of rates was found for the automated reactions, with a polymerization of styrene only slightly faster compared to the conventional reactions. A matching of the curves of conventional and automated reactions was subsequently performed at intermediate conversion (c.f. Figure 5.16). Despite this transpose, important scattering of the plots is observed at the early stage of the reaction. Again, such scattering might be due to important sampling errors because the PSD of latex particles from conventional and from automated reactions are similar (c.f. Figure 5.17). As a consequence, despite different physical characteristics between conventional and automated reactors, a similar reproducibility of the polymerization rates can be obtained.

Chapter 5

Table 5.10 Conversion rates x at intermediate monomer conversion of the conventional reactions

Monomer	Day	dx/dt (min^{-1})
Butyl acrylate	1	0.77
	2	0.67
	3	0.83
Styrene	1	1.30
	2	1.20
	3	1.30

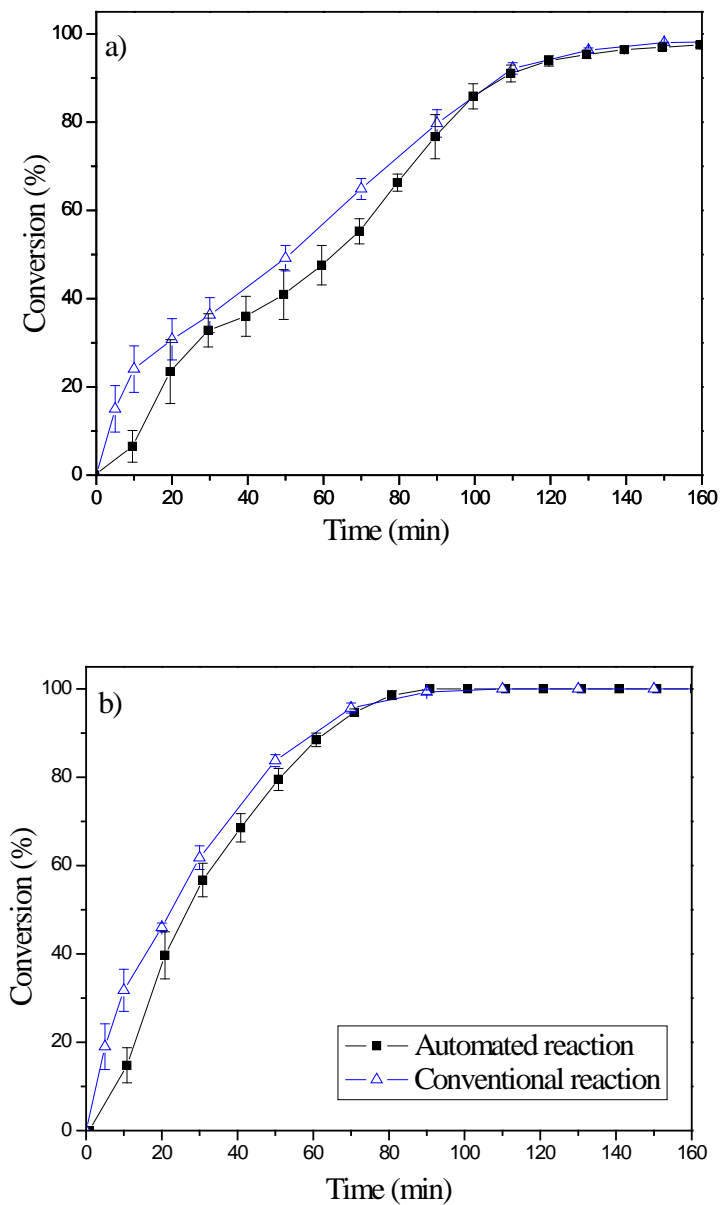


Figure 5.14 Partial conversion-time histories for conventional operation and automated reactors (a) butyl acrylate and (b) styrene.

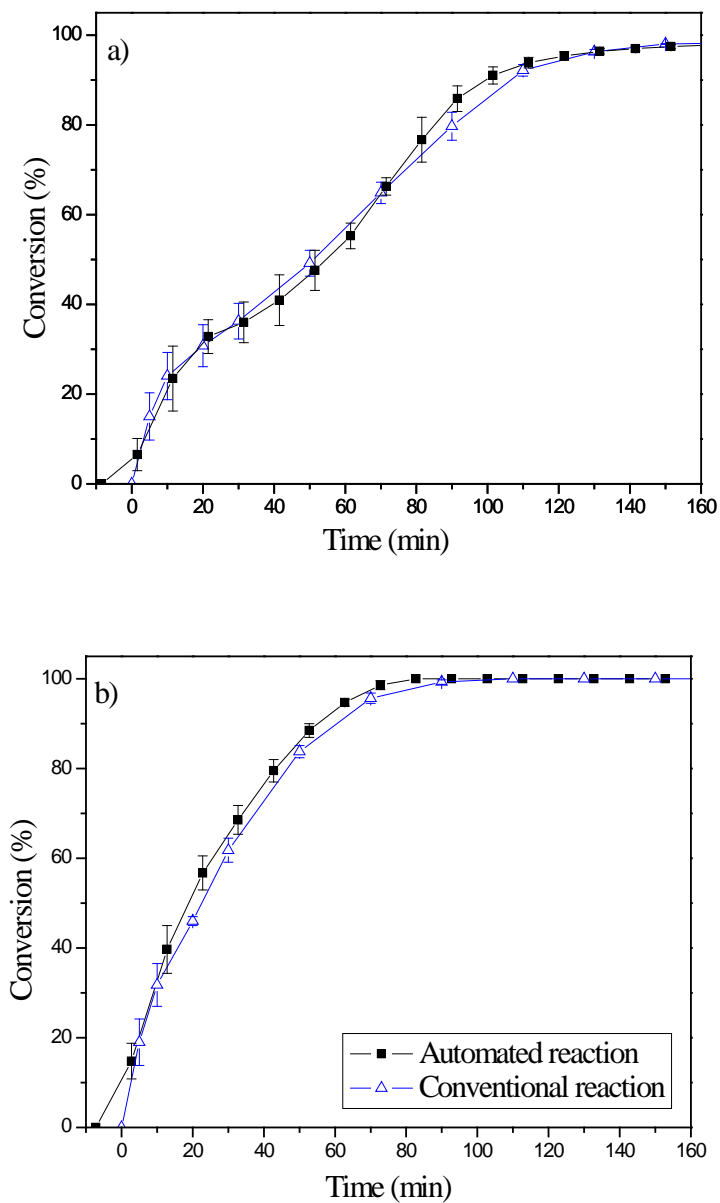


Figure 5.15 Minimization of the inhibition effect from the conversion-time plots for the conventional batch operation by exact overlapping of the curves at 50% monomer conversion: (a) butyl acrylate and (b) styrene.

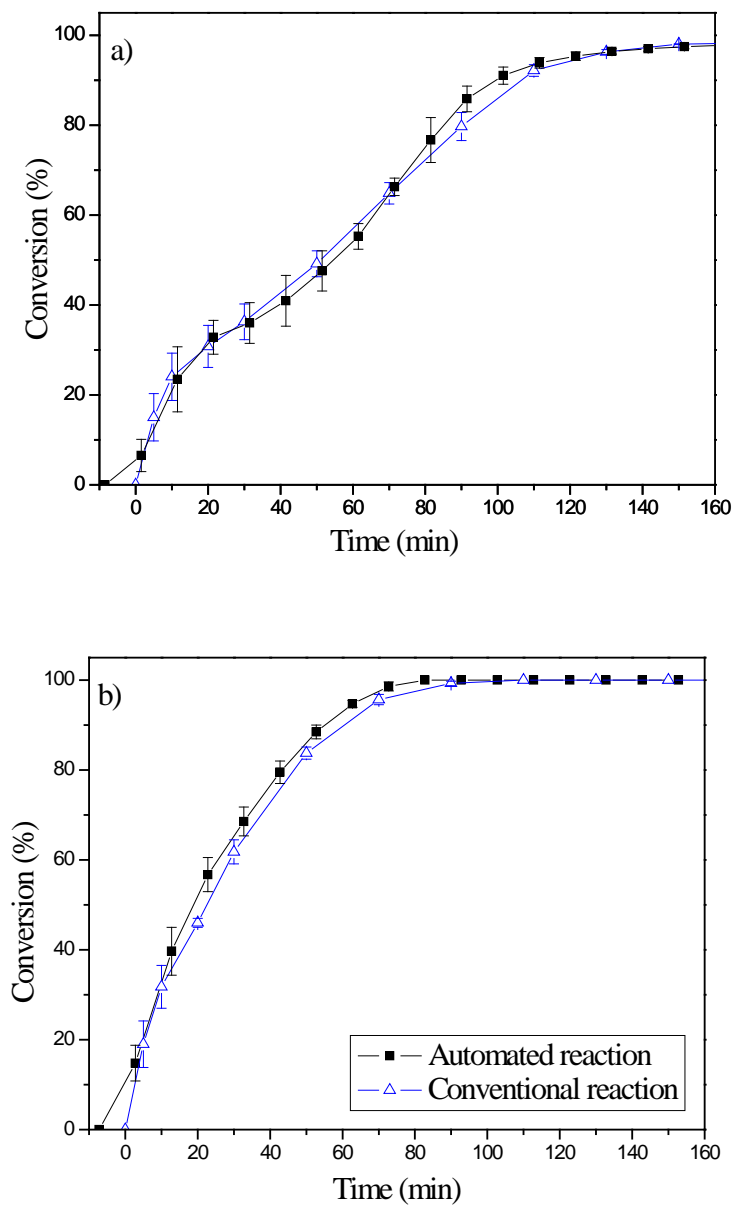


Figure 5.16 Overlapping of the conversion-time plots for conventional batch operation and automated reactions at intermediate monomer conversion: (a) butyl acrylate and (b) styrene.

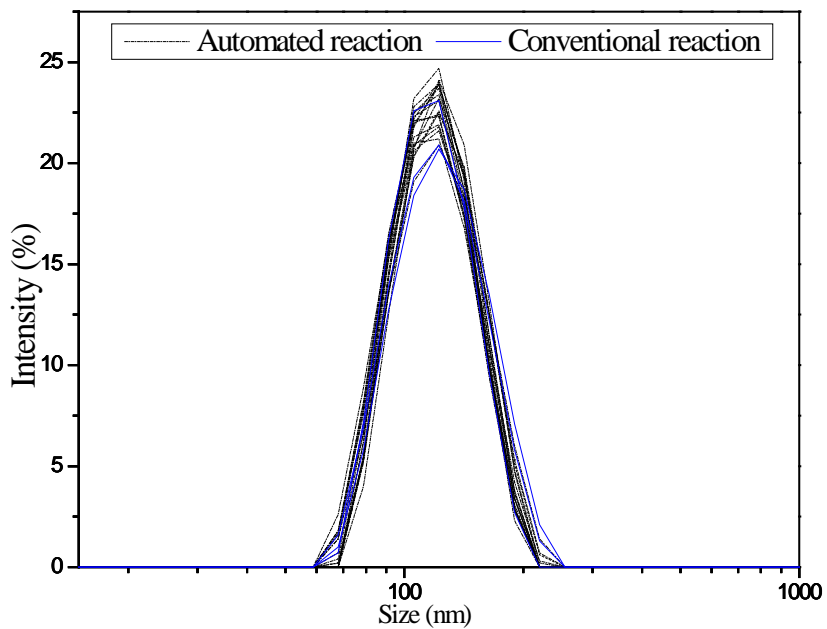


Figure 5.17 Comparison of the particle size distribution between automated and conventional reaction.

Chapter 5

In the previous sections, it was demonstrated that sampling can be an important source of errors in the determination of monomer conversion-time histories via gas chromatography. Raman spectroscopy can be an excellent alternative to the chromatographic method due the fact that there is no need to take samples for analysis. The application of such a technique in a combinatorial fashion requires several instruments which could be simultaneously used and easily integrated in a robotic platform. A low-cost low-resolution portable (LCLR-P) Raman spectrometer as a potential candidate is the topic of the following sections.

5.7 ON-LINE MONITORING OF PMMA-SEEDED EMULSION HOMOPOLYMERIZATIONS OF STYRENE USING A LOW-COST LOW-RESOLUTION RAMAN SPECTROMETER

The present section investigates whether the LCLR-P Raman spectrometer in combination with partial least square regression (PLSR) could be potentially used for the on-line monitoring of PMMA-seeded batch emulsion homopolymerization of styrene.

A set of five reactions (Entries C.1 – C.5 in Table 5.11) were used to build the calibration model. Three principal components were chosen to build the calibration model so that 95.15 % of variations in the monomer conversion dataset were explained by the model with a RMSEP of around 6.7 %.

\

Table 5.11 Recipes used for the calibration modeling of PMMA-seeded batch emulsion homopolymerizations of styrene and for its external validation. ^a

Entry	Water ^b	Sty ^b (%)	KPS ^c (%)	Solid content (%)	Number of spectra ^d
C.1	69	15	0.32	30	20
C.2	59	20	0.32	40	20
C.3	52	24	0.32	45	20
C.4	74	13	0.32	25	20
C.5	74	13	0.16	25	23
V.1	66	17	0.16	30	25

^{a)} Other ingredients are (composition %-wt based on monomers): PMMA-latexes (dried weight, 100), NDM (1) and SDS (1.6)

^{b)} Based on the total mass

^{c)} Based on the total amount of styrene

^{d)} Number of spectra used to build the calibration models and to perform its external validation

The recipe of the experiment used to check the reliability of the calibration model is given in Table 5.11 (Entry V.1.). The spectra recorded at regular time intervals Δt during the polymerization formed the “new” X-data matrix of the calibration model. The instantaneous monomer conversions at time t were calculated from the calibration model with 2 PCs: 3 PCs brought more noises than useful information. The RMSEP was around 10 %.

Figure 5.18 shows the results given by the calibration model to describe the styrene conversion-time profiles. A fairly good agreement between the Raman and the gravimetric technique can be observed.

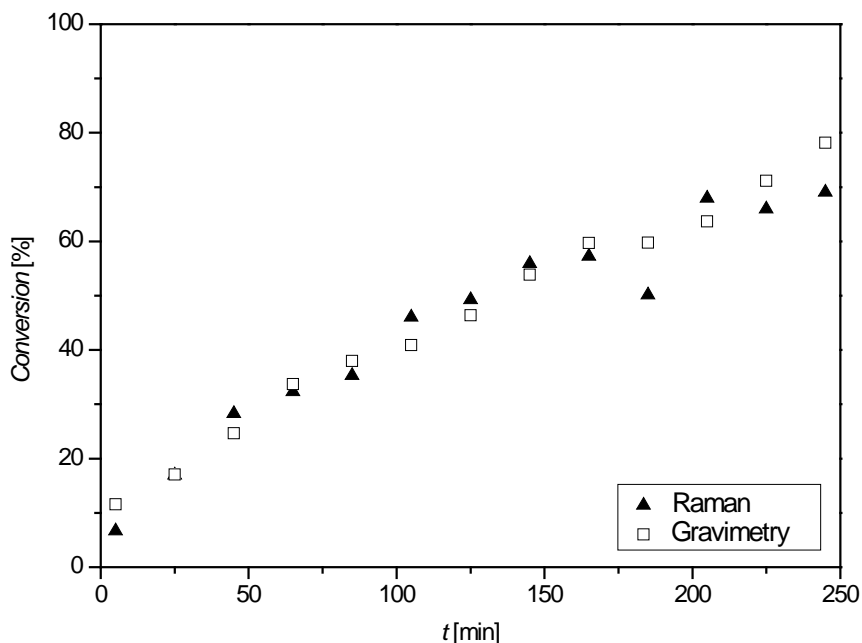


Figure 5.18 Conversion-time profiles of styrene as determined via (▲) Raman and (□) gas chromatography during a PMMA-seeded batch emulsion polymerization of the monomer. Experimental conditions (wt-% based on total mass): H₂O (74), PMMA-latexes (dried weight, 13), Sty (13), NDM (0.13), KPS (0.02), SDS (0.20) and NaHCO₃ (0.006).

5.8 ON-LINE MONITORING OF PMMA-SEEDED EMULSION COPOLYMERIZATIONS OF STYRENE AND BUTYL ACRYLATE USING A LOW-COST LOW-RESOLUTION RAMAN SPECTROMETER

Table 5.12 shows the set of experiments (Entries D.1 – D.5) used to construct the Raman calibration model for the determination of the instantaneous conversion of styrene and butyl acrylate during a batch seeded-emulsion copolymerization of the monomers. The model was built with 2 PCs with a RMSEP of about 6 % for the determination of the instantaneous conversion of styrene. 3 PCs were necessary to

Chapter 5

design the Raman calibration model for following the consumption of BA; the RMSEP of the corresponding model was about 5 %.

Table 5.12 Recipes used for the calibration modeling of PMMA-seeded batch emulsion copolymerizations of styrene and butyl acrylate and for its external validation. ^{a)}

Entry	Water ^b	Sty:BA ^c (%)	KPS ^c (%)	Solid content (%)	Number of spectra ^d
D.1	58	20:30	0.32	40	21
D.2	56	30:30	0.46	42	22
D.3	49	40:40	0.63	50	24
D.4	57	30:30	0.32	42	25
D.5	64	18:18	0.30	35	20
W.1	56	30:30	0.46	42	23

^{a)} Other ingredients are (composition %-wt based on monomers): PMMA-latexes (dried weight, 25), NDM (1) and SDS (1.6)

^{b)} Based on the total mass

^{c)} Based on the total amount of monomers

^{d)} Number of spectra used to build the calibration models and to perform its external validation

The performance of these calibration models was checked by following the instantaneous conversion of styrene and butyl acrylate with Raman and GC during a seeded batch emulsion (co)polymerization of the monomers (c.f. Entry W.1 in Table 5.12). From Figure 5.19, it can be observed that there are significant discrepancies between GC and the Raman techniques at the beginning of the reaction and beyond 50 % of conversion. A much better matching between the Raman and the chromatographic technique is, however, observed in the intermediate region.

Chapter 5

In fact, it is a loss of the Raman signals observed at the beginning of the reaction which probably led to incoherent results between the Raman and the chromatographic technique. At higher conversions, some unknown experimental errors might have also altered the quality of the spectra.

From this unique experiment, it is somehow difficult to conclude on the performance of the Raman calibration models due to the poor quality of the spectra recorded.

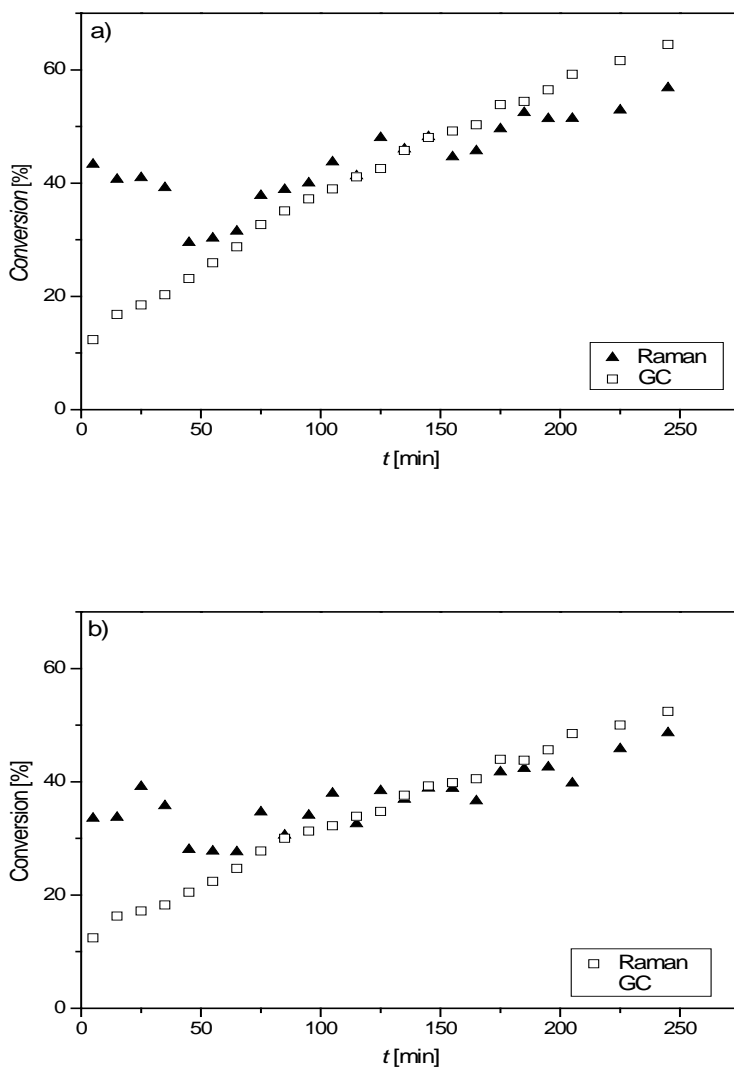


Figure 5.19 Conversion-time profiles of (a) styrene and (b) butyl acrylate as determined via (\blacktriangle) Raman and (\square) gravimetry during a PMMA-seeded batch emulsion copolymerization of the monomers. Experimental conditions (wt-% based on total mass): H₂O (56), PMMA-latexes (dried weight, 8.7), Sty (17), BA (17), NDM (0.43), KPS (0.16), SDS (0.54) and SBC (0.04).

5.9 EFFECT OF CLAY ON RAMAN SPECTRA

Raman spectroscopy could be used for the monitoring of clay encapsulation via emulsion polymerization. It was therefore interesting to see how Raman signals could be related to the presence of clay particles during encapsulation.

A Raman spectrum was recorded from an aqueous emulsion of styrene monomers (25 % w/w) under vigorous mixing (see Figure 5.20). The addition of 2 % (based on monomers) of montmorillonite clay particles in the monomer dispersion significantly decreased the Raman signal of styrene by a factor of 3. This change in the Raman signal, likely to depend on the clay concentration, could be used as a response variable in the Raman calibration modeling allowing detection of bare clay during encapsulation. It is clear, however, that in the presence of clay only emulsion homopolymerization can be monitored with this instrument.

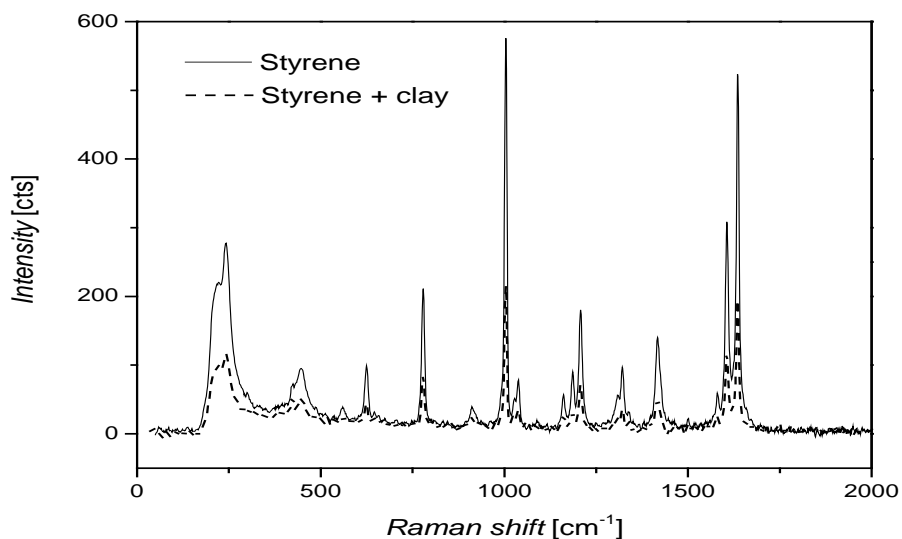


Figure 5.20 The Raman spectrum of (solid line) an aqueous emulsion of styrene (25 % w/w). The dashed line corresponds to the Raman spectrum of the same styrene dispersion in the presence of montmorillonite clay particles (2 % based on monomers).

5.10 CONCLUDING REMARKS

For the first time, a methodology to conduct successful batch emulsion copolymerization with a parallel stirred automated synthesizer has been presented. Among others, sampling was the most challenging step for the optimization of the automated reactions. Sampling and inhibition were the main source of errors of the partial monomer conversion-time plots. Therefore, the comparison of the conversion rates, which do not depend on inhibition, was the chosen method for the investigation of the reaction kinetics reproducibility. Further analysis of the particle size distributions and the final product properties clearly showed that the automated reactions were highly reproducible.

Moreover, it was found that automated and conventional reactions have similar reproducibility. Indeed, the amplitude of random experimental errors was the same for both synthesis methods.

This chapter also clearly demonstrated the potential of a low-cost-low-resolution portable Raman spectrometer to monitor emulsion polymerizations. The Raman spectroscopy method required, however, time-consuming calibration steps in order to gather large and representative data sets. In addition, because of its high sensitivity to small variation in the reaction medium, the spectroscopic technique suffered from important measurement errors.

REFERENCES

1. Voorn D.-J.; Fijten M.W.M.; Meuldijk J.; Schubert U.S.; van Herk A. M. *Macromol. Rapid Commun.* 24: 320 (2003).
2. Van den Brink M.; Pepers M.; Van Herk A. M.; German A. L. *Macromol. Symp.* 150: 121 (2000).
3. McCaffery T.R.; Durant Y. G. *J Appl. Polym. Sci.* 86: 1507 (2002).
4. Elizalde O.; Leiza J. R.; Asua J. M. *Macromol. Symp.* 206: 135 (2004).
5. Reis M. M.; Araújo P. H. H.; Sayer C.; Giudici R. *Macromol. Symp.* 206 : 165 (2004)
6. Reis M. M.; Araújo P. H. H.; Sayer C.; Giudici R. *Anal. Chim. Acta* 595: 257 (2007).
7. Pepers M.L.H. *On-line monitoring and control of copolymerizations*. Eindhoven University of Technology, PhD thesis (2004).
8. Geladi P.; Kowalski B. *Anal. Chim. Acta* 185: 1 (1988).
9. Esbensen K.H.; Guyot D.; Westad F.; Houmã I.L.P. *Multivariate Data Analysis– In Practice*, 5th ed. Camo Process AS, Esbjerg (2005).
10. STATGRAPHICSV Centurion XVI User Manual (2009).
11. Petrak K. L.; Pitts E. *Polymer* 24: 729 (1983).
12. Guerrero-Sanchez C.; Paulus R.M.; Fijten M.W.M.; de la Mar M.J.; Hoogenboom R.; Schubert U.S. *Appl. Surf. Sci.* 252: 2555 (2006).
13. Zoco N.; Lopez de Arbina L.; Leiza J.R.; Asua J.M.; Arzamendi G. *J. Appl. Polym. Sci.* 87: 1918 (2003).

Chapter 5

14. Chai X.-S.; Schork F.J.; DeCinque A.; Wilson K. *Ind. Eng. Chem. Res.* 44: 5256 (2005).
15. Montgomery D.C.; Runger G.C.; Hubele N.F. *Engineering Statistics*, 2nd ed. John Wiley and Sons Inc., Chichester (2001).

Summary

In-situ control of the morphology of multiphase latex/clay nanocomposites

The key objective of this thesis is the morphology control of latex/clay nanocomposites (LCN) which are of particular interest to water-based coating and adhesive applications. Indeed, the incorporation of inorganic fillers into a polymer matrix generally leads to better performing materials. However, a good dispersion and an alignment of the clay layers as single platelets into the polymer matrix are the prerequisites for the largest property enhancement. Such requirements have been the driving force for the development of many LCN synthetic routes. The inorganic encapsulation technique, using conventional emulsion polymerization was employed in this thesis. The natural occurring montmorillonite clay particles were used as the inorganic fillers. The primary goal was to make a start in fine tuning the dispersion and orientation of the clay into the polymer matrix by controlling the morphology of the clay-encapsulated latex particles. We realized that with so many parameters involved the potentials of high-throughput experimentation (HTE) and on-line Raman spectroscopy should be explored, so some first attempts in this direction were made. Furthermore this thesis investigated the influence of clay on the morphology of multiphase latex particles.

Clay particles are hydrophilic inorganic compounds and must be rendered (partially) hydrophobic in order to be more compatible with the *in-situ* synthesized polymer. In this thesis, the organic modification of clay was performed using two kinds of titanate coupling agents, titanium IV, (2-propanolato)tris(2-propenoata-O), 2-(2-methoxy-ethoxy) ethanol(KR39DS) and titanium IV, 2-propanolato, tris isooctadecanoato-0 (KRTTS), where the former is unsaturated and the second contains saturated alkyl groups. In Chapter 3, a study of the hydrolytic stability of the organoclays thus synthesized showed that the titanate modifiers used were highly susceptible to hydrolysis in the emulsion polymerization conditions. From the results obtained, it was concluded that successful clay encapsulation does not

Summary

require the use of unsaturated organic modifiers as previously believed. Furthermore, emulsion polymerizations carried out with pristine clay also led to successful clay encapsulation showing that the modification step could be completely omitted.

In addition to the organic modification, the influence of monomer feed composition, i.e. monomer mixtures consisting of different weight ratios of methyl methacrylate/ butyl acrylate, and the process type on the morphology of two-phase LCN was studied. It was shown that the monomer feed composition added under starved conditions strongly influenced the morphology of the LCN. Indeed, when the T_g of the encapsulating (co)polymer was well above the reaction temperature (hard polymer), anisotropic latex particles containing single clay platelets were mainly observed. In contrast, the use of a soft encapsulating polymer led to armored-like latex particles. Furthermore, only starved-feed monomer addition led to successful encapsulation: a batch process generated larger aggregates of clay particles and only a few armored-like latex particles. A heat treatment of the encapsulated clay particles showed that the clay encapsulation process was mainly kinetically controlled: after the heat treatment the clay was again on the outside of the latex particles. A mechanism of encapsulation was proposed, where the clay particles act as seed in the process (polymerization carried out from the surface of the inorganic particle).

A systematic study of the effects of clay loading, surfactant concentration and surfactant type on the clay/polymer interaction was performed via a design of experiments. All three parameters were found to have significant effects on the clay/polymer interaction.

In Chapter 4, three-phase PMMA/PS/MMT latex particles were synthesized from clay-containing PMMA seeds via (semi-)batch emulsion polymerization of styrene. For the interpretations of the morphologies obtained, the established theories to understand the morphology development of two-phase latex particles could be applied. An interesting observation was that clay platelets could act as physical barriers preventing diffusion of second stage polymers within the seed latex particles. A methodology to successfully conduct batch emulsion copolymerization using a parallel stirred automated synthesizer is described in Chapter 5. The most

Summary

challenging step for such automated reactions was sampling. Sampling operations and inhibition were found to be the main source of errors in the determination of the partial monomer conversion-time histories. A comparison of the conversion rates of the automated reactions and the analyses of the particle size distributions and the molar mass distributions of the latexes synthesized clearly showed that the automated reactions were highly reproducible.

A methodology to successfully conduct batch emulsion copolymerization using an automated parallel synthesizer is described in Chapter 5. The most challenging step for such automated reactions was sampling. Sampling operations and inhibition were found to be the main source of errors in the determination of the partial monomer conversion-time histories. A comparison of the conversion rates of the automated reactions and the analyses of the particle size distributions and the molar mass distributions of the latexes synthesized clearly showed that the automated reactions were highly reproducible.

Chapter 5 also clearly demonstrated the potential of a low-cost-low-resolution portable Raman spectrometer to monitor emulsion homopolymerizations. The Raman spectroscopy technique in combination with partial least regression methods requires extensive calibration steps in order to gather large and representative data sets. Low-cost low-resolution portable Raman can be used as a conversion monitoring device and might be easy to integrate in the robotic platform.

Epilogue

In this epilogue, I seek to highlight the directions for future research work in the field of control of latex/clay particle morphologies.

In this thesis, several experimental parameters were identified as crucial factors for successfully encapsulating clay platelets via conventional emulsion polymerization. Questions remain about the exact role of these factors in the mechanism of the particle morphology development. Through my research studies, only the final morphologies of the hybrid latex particles were investigated, which made it difficult to fully understand the mechanisms operating during the reactions. Future research work should focus on describing the morphological changes occurring during the clay encapsulation process in order to gain insight into basic aspects of particle morphology development.

An appealing outcome of my research was the synthesis of hybrid multiphase latex particles exhibiting unusual morphologies. Besides changing the properties of the latex particles, the clay platelets could be used as a morphology modifier giving the opportunity to create new properties via well-established chemistry. For this reason we did not apply controlled radical polymerization mechanisms but only applied free – radical polymerization in emulsion. From an industrial point of view, this new possibility is very interesting because it should enable ongoing product innovation without performing costly testing of new chemicals as required by the REACH regulation.

In the preceding chapter, the potential of high-throughput experimentation (HTE) for systematic studies in controlling the morphology of latex/clay particles is emphasized. Although the challenges of translating conventional reactions into a complex robotic platform have clearly been tackled, the scalability to industrial applications of the chemistry created with HTE tools is highly questionable. Moreover, several issues still need to be overcome before achieving fast and

Epilogue

efficient analysis of the large amount of data generated by HTE instruments. On-line partial conversion measurements are essential in morphology control in (clay-containing) emulsion copolymerization. Compact machines able to do so might be the portable Raman spectrometers investigated in this thesis.

This thesis showed the possibilities and limits of such a low-cost low-resolution (LCLR-P) portable Raman spectrometer in providing reliable spectral data for emulsion copolymerizations and for clay-containing monomer emulsions. The answer on the question whether LCLR-P Raman spectroscopy methods are ready to be applied for the on-line monitoring of clay encapsulation processes is likely to be negative. However, it will not be surprising that, within the next couple of years, new generations of these portable Raman devices with greatly enhanced resolution will enable accurate monitoring of emulsion polymerization kinetics.

A quantitative determination of the particle morphology requires the use of microscopic methods and other complementary techniques which can be very time-consuming and greatly dependent on the technical skills of the operator. Such drawbacks, prone to human errors, may bring many uncertainties in the prediction of the particle morphology. I hope that the development of automated microscopy and image analysis will gradually help in resolving such issues.

I also hope that the findings reported in this thesis will contribute to the development of strategies to gain a deeper knowledge in the control of the morphology of latex/clay particles and will be beneficial for researchers, active in this topic area, using other synthetic approaches such as RAFT-based (mini)emulsion polymerization.

Appendix I

Table I.1 Analysis of variance of the glass transition temperatures of dried film latex/clay nanocomposites synthesized in this study

Source of variance	Sum of Squares ^{a)}	Df ^{b)}	Mean Square ^{c)}	F-ratio ^{d)}	p-Value ^{e)}
Surfactant type (A)	55	1	55	49.00	0.0903
[Surfactant] (B)	91	1	91	81.00	0.0704
Clay loading (C)	10	1	10	9.00	0.2048
AB	3	1	3	2.78	0.3440
AC	21	1	21	18.78	0.1444
BC	78	1	78	69.44	0.0760
Random Errors ^{f)}	1	1	1		

a) Sum of squares is given by where $SS = \sum_{i=1}^N (X_i - \bar{X})^2$ where X_i is the i th data point, \bar{X} the estimated mean and N the number of data.

b) Df, the degree of freedom is defined as the number of levels minus 1.

c) Mean square is given by $MS = \frac{SS}{Df}$

d) F-ratio is given by $F\text{-ratio} = \frac{MS_{\text{factor}}}{MSE}$ where factor is the source of variance and MSE the mean square of random errors

e) If $p\text{-value} < 0.05$, the factors have a significant effect on the variance of the data studied at 95 % confidence level.

f) The random errors correspond to the interaction effect ABC

Appendix I

Table I.2 Analysis of variance of conversion rates at intermediate monomer conversion of the automated reactions ^{a)}

Monomer	Source	Sum of Squares ^{b)}	Df ^{c)}	Mean Square ^{d)}	F-Ratio ^{e)}	P-Value ^{f)}
Butyl acrylate	Days	0.02	3	0.006	1.67	0.26
	Reactors	0.03	3	0.010	2.53	0.14
	Random errors	0.03	7	0.004		
Styrene	Days	0.05	3	0.020	1.58	0.28
	Reactors	0.01	3	0.004	0.40	0.76
	Random errors	0.07	7	0.010		

^{a)} The results of Day 1 were not taken into account in the ANOVA

^{b)} Sum of squares is given by where $SS = \sum_{i=1}^N (X_i - \bar{X}_i)^2$ where X_i is the i th data point, \bar{x} the estimated mean and N the number of data.

^{c)} Df, the degree of freedom is defined as the number of levels minus 1.

^{d)} Mean square is given by $MS = \frac{SS}{Df}$

^{e)} F-ratio is given by $F\text{-ratio} = \frac{MS_{\text{factor}}}{MSE}$ where factor is the source of variance and MSE the mean square of random errors

^{f)} If p-value < 0.05, the factors have a significant effect on the variance of the data studied at 95 % confidence level.

Appendix I

Table I.3 Analysis of variance of time at 50% monomer conversion of the automated Reactions

Monomer	Source	Sum of Squares ^{a)}	Df ^{b)}	Mean Square ^{c)}	F-Ratio ^{d)}	P-Value ^{e)}
Butyl acrylate	Days	192	3	64	3.39	0.0831
	Reactors	235	3	78	4.15	0.0552
	Random errors	132	7	19		
Styrene	Days	23	2	11	0.80	0.5096
	Reactors	17	3	6	0.40	0.7635
	Random errors	57	4	14		

a) Sum of squares is given by where $SS = \sum_{i=1}^N (X_i - \bar{X})^2$ where X_i is the i th data point, \bar{X} the estimated mean and N the number of data.

b) Df, the degree of freedom is defined as the number of levels minus 1.

c) Mean square is given by $MS = \frac{SS}{Df}$

d) F-ratio is given by $F - \text{ratio} = \frac{MS_{\text{factor}}}{MSE}$ where factor is the source of variance and MSE the mean square of random errors

e) If p-value < 0.05, the factors have a significant effect on the variance of the data studied at 95 % confidence level.

Appendix II

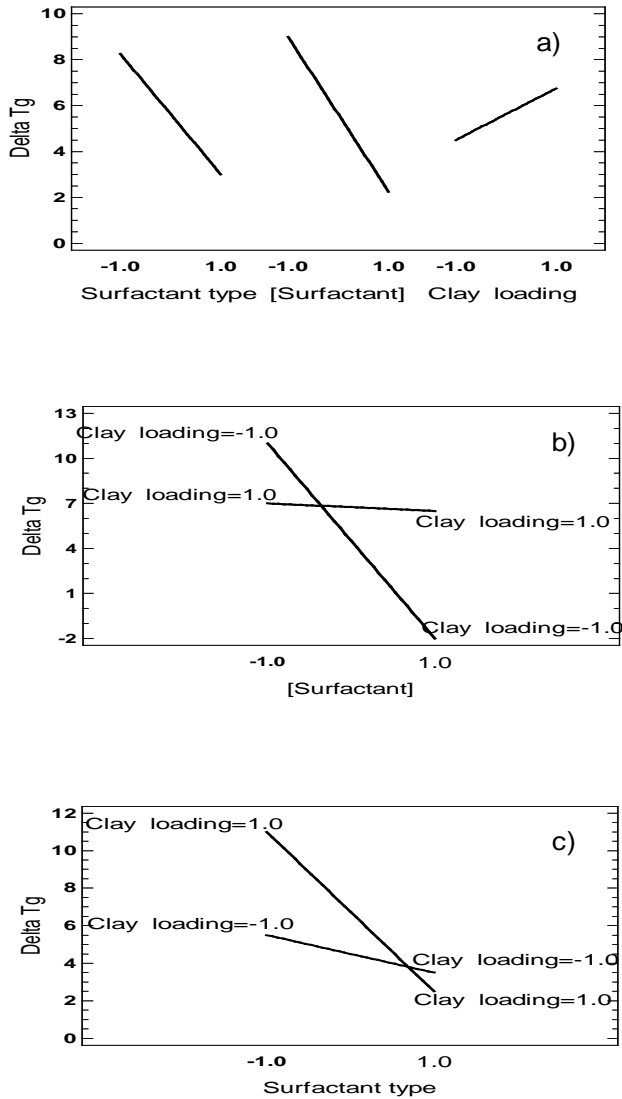


Figure II Plots of (a) the main effects and the interaction effects (b) surfactant concentration/clay loading and (c) surfactant type /clay loading

Appendix III

Table III.1 Dependence of the observed conversion rates on the performed day of the experiments of the automated reactions at intermediate monomer conversion

Monomer	Day	Mean (min ⁻¹)	σ_M ^{a)} (min ⁻¹)
Butyl acrylate	1	0.90	0.04
	2	0.70	0.02
	3	0.65	0.02
	4	0.73	0.02
	5	0.73	0.06
Styrene	1	1.20	0.04
	2	0.93	0.04
	3	0.88	0.05
	4	0.80	0.07
	5	0.93	0.04

a) The standard error of the mean σ_M is given by: $\sigma_M = \frac{\sigma}{\sqrt{N}}$ where σ is the standard deviation of the original mean, and N the number of points considered in the calculation of the mean

Appendix III

Table III.2 Reactor dependence of the conversion rates of the automated reactions at intermediate monomer conversion

Monomer	Day	Mean (min ⁻¹)	σ_M ^{a)} (min ⁻¹)
Butyl acrylate	1	0.70	0.07
	2	0.70	0.02
	3	0.73	0.04
	4	0.80	0.06
Styrene	1	0.98	0.09
	2	0.99	0.07
	3	0.95	0.10
	4	0.94	0.07

Table III.3 Days dependence of the mean time values (min) at 20 % (t_{20}), 50 % (t_{50}) and 80 % (t_{80}) monomer conversion and their standard errors σ .

Monomer	Day	t_{20}	$\sigma_{t_{20}}$	t_{50}	$\sigma_{t_{50}}$	t_{80}	$\sigma_{t_{80}}$
BA	2	19	2	75	25	118	1
	3	16	2	73	4	119	2
	4	11	0	77	0	118	2
	5	12	2	65	5	105	2
Sty	2	14	1	32	1	64	1
	3	13	1	26	3	60	3
	4	9	0	23	1	61	2
	5	10	1	25	1	58	1

Appendix III

Table III.4 Reactor dependence of the mean time values (min) at 20 % (t_{20}), 50 % (t_{50}) and 80 % (t_{80}) monomer conversion and their standard errors σ .

Monomer	Reactor	t_{20}	$\sigma_{t_{20}}$	t_{50}	$\sigma_{t_{50}}$	t_{80}	$\sigma_{t_{80}}$
BA	1	12	4	65	6	118	5
	2	17	3	66	5	109	5
	3	17	2	72	5	117	5
	4	15	2	72	2	112	2
Sty	1	10	2	26	2	59	4
	2	12	1	26	1	59	6
	3	13	1	28	3	64	2
	4	12	1	27	2	61	2

Appendix III

Table III.5 Days dependence of the mean time values (min) at 20 % (t_{20}) and 80 % (t_{80}) monomer conversion and their standard errors σ after exact overlapping of the curves at t_{50} .

Monomer	Day	t_{20}	$\sigma_{t_{20}}$	t_{80}	$\sigma_{t_{80}}$
BA	2 ^{a)}	17	1	114	2
	3 ^{b)}	12	2	115	2
	4 ^{c)}	11	0	118	2
	5 ^{a)}	10	2	106	2
Sty	2 ^{a)}	10	2	62	0
	3 ^{b)}	10	1	57	2
	4 ^{c)}	9	1	61	2
	5 ^{a)}	11	1	54	1

a) Reactor 1 as reference

b) Reactor 4 as reference

c) No transposition of the curves on Day 4

Appendix III

Table III.6 Reactor dependence of the mean time values (min) at 20 % (t_{20}) and 80 % (t_{80}) monomer conversion and their standard errors σ after exact overlapping of the curves at t_{50} .^{a)}

Monomer	Reactor	t_{20}	$\sigma_{t_{20}}$	t_{80}	$\sigma_{t_{80}}$
BA	1	6	3	106	1
	2	10	3	103	1
	3	13	2	115	3
	4	14	2	114	2
Sty	1	10	2	55	4
	2	10	1	51	6
	3	9	1	58	2
	4	11	1	58	2

^{a)} Day 5 as reference for all transposition

Abbreviations

ANOVA	Analysis of variance
APS	Ammonium persulfate
BA	Butyl acrylate
CMC	Critical micelle concentration
DSC	Differential scanning calorimetry
FTIR	Fourier transform infrared
KPS	Potassium persulfate
KR39DS	Titanium IV, (2-propanolato)tris(2-propanoata-O),2-(2-methoxy,ethoxy ethanol)
KRTTS	Titanium IV, 2-propenoato, tris isooctadecanoato-O
LCN	Latex/clay nanocomposite
MMA	Methyl methacrylate
MMT	Montmorillonite
PMMA	Poly(methyl methacrylate)
PS	Poly(styrene)
SDBS	Sodium dodecyl benzene sulfonate
SDS	Sodium dodecyl sulfate
SEM	Scanning electron microscopy
Sty	Styrene
TGA	Thermal gravimetry analysis
TEM	Transmission electron microscopy
TMEDA	N,N,N',N'-tetramethylethylenediamine
TX-100	Triton X-100

Abbreviations

VA-086 2,2'-Azobis[2-methyl-N-(2-hydroxyethyl)propionamide]

XRD X-ray diffraction

Acknowledgments

First, I would like to thank every supportive people around me without whom it would have not been possible to write this thesis. Here, I only mention a few of them.

Above all, I would like to thank my parents, sister and brothers for their unconditional support. I also thank Billy for his great kindness and support throughout the most stressful time of my doctoral studies.

This thesis would not have been possible without the help, support and trust of my principal supervisor, Alex van Herk, not to mention his indispensable advice both in a personal and an academic level. I am deeply grateful to my second supervisor, Hans Heuts, for his advice and friendly support. I must particularly acknowledge the fact that Hans has inspired me to be more meticulous in my approach of work.

I would like to acknowledge the Dutch Polymer Institute (DPI) for the financial support of my research project. I particularly thank Ulrich Schubert for giving me the opportunity to work within the DPI High-Throughput Experimentation Technology Area.

I would like to thank all the members of my dissertation committee especially Jan Meuldijk, José Asua and Elodie Bourgeat-Lami for their helpful advice and comments.

The good support and friendship of my paranympths, Yingyuan Li and Rafaël Sablong, for which I am very grateful, have been constant throughout my doctoral studies.

I would like to thank my trainees Vincent Clerc, Vincent Beugeard and Nevin Yilmaz who made tangible contributions in my research project.

I am grateful to Cor Koning for warmly welcoming me into the Laboratory of Polymer Chemistry and Rob Duchateau for his cheerful encouragements. I would like to thank Jos Laven and Gerben Mooiweer for their helpful suggestions and discussions.

I am very grateful to Ingeborg Schreur-Piet and Roxana Albu for showing me the way of working within our laboratory in the early stage of my research experience. I also thank Paul Bomans, Anne Spoelstra, Rinske Knoop, Marco

Acknowledgements

Hendrix, Mark Berix, Neomy Zaquen and Martin Fijten for their advice and technical support.

Amongst my fellow mates in our laboratory, I am extremely grateful to Lidia Jasinska, Syed Ali and Ece Koç for their friendly and unequivocal support. My warm gratitude goes to Elena Miloskovska and Jérôme Garnier who used to listened to my complaints and “success stories” with great care and patience.

Last, but by no means least, I would like to thank all my colleagues of the Laboratory of Polymer Chemistry and friends in the Netherlands and elsewhere for their support and encouragements throughout the time it has taken to complete my research doctorate. *Mèsi!*

Curriculum Vitae

Monique A. Mballa Mballa was born on September 21st in 1983 in Paris (France). After completing her high school education in 2001 at Lycée Général et Technologique des Droits de l'Homme in Petit-Bourg (Guadeloupe) and undertaking intensive undergraduate preparatory program in mathematics, physics and chemistry, she started an engineering curriculum at the National Graduate School of Engineering Chemistry of Lille in France. She obtained her Master's Degree in Chemistry in 2007 after finishing her graduation project within the Laboratory of Non-Aqueous Corrosion Study in the French Atomic Energy Commission (Gif-sur-Yvette). From 2007, she started a PhD project at the Eindhoven University of Technology in the Netherlands of which the results are presented in this dissertation.

